

Inflation and Higgs Phenomenology in a Model Unifying the DFSZ Axion with the Majoron

Michael Matlis^a, Juhi Dutta^b, Gudrid Moortgat-Pick^{a,c}, Andreas Ringwald^a

^a*Deutsches Elektronen-Synchrotron DESY,
Notkestr. 85, 22607 Hamburg, Germany*

^b*Homer L. Dodge Department of Physics and Astronomy, University of Oklahoma,
Norman, OK 73019, USA*

^c*II. Institut für Theoretische Physik, Universität Hamburg,
Luruper Chaussee 149, 22761 Hamburg, Germany*

Abstract

The Two-Higgs-Doublet-Standard Model-Axion-Seesaw-Higgs-Portal inflation (2hdSMASH) model consisting of two Higgs doublets, a Standard Model (SM) singlet complex scalar and three SM singlet right-handed neutrinos can embed axion dark matter, neutrino masses and address inflation. We report on an investigation of the inflationary aspects of 2hdSMASH and its subsequent impact on low energy phenomenology. In particular, we identify inflationary directions for which the parameter values required for successful inflation do not violate perturbative unitarity and boundedness-from-below conditions. By analyzing the renormalization-group flow of the parameters we identify the necessary and sufficient constraints for running all parameters perturbatively and maintaining stability from the electroweak to the PLANCK scale. We observe that stringent constraints arise on the singlet scalar self coupling from inflationary constraints, i.e., $\lambda_S \sim 10^{-10}$. Further, we find that all theoretical and experimental constraints are satisfied if the portal couplings are typically in the range $(\frac{v}{v_S})$ and $(\frac{v}{v_S})^2$ (where v, v_S refer to the electroweak and singlet scalar vacuum expectation value respectively). As a consequence, inflation is realized in a variety of field space directions in the effective single field regime. Finally we provide testable benchmark scenarios at colliders.

E-mail: michael.maxim.matlis@gmx.de, juhi.dutta@ou.edu,
gudrid.moortgat-pick@desy.de, andreas.ringwald@desy.de

Contents

1	Introduction	2
2	The 2hdSMASH Model	4
2.1	Field content and PQ symmetry	4
2.2	Vacuum structure, particle content and masses	5
2.3	Theoretical constraints	7
3	Characteristics of the Scalar Mass Spectrum	8
4	Inflation in 2hdSMASH	10
4.1	PQ- and PQ-2HDM-inflation in 2hdSMASH	13
5	Connecting Inflation with TeV Scale Particle Physics	22
5.1	Stability analysis of λ_S	24
5.2	RG-Analysis with BAU and thermal leptogenesis	25
5.3	Interconnection of portal couplings	28
5.4	Stability analysis	31
5.5	Benchmark points	37
6	Allowed Parameter Space	39
7	Summary and Conclusions	41
A	Derivation of CP-even/odd Scalar Masses	45
B	Constraints on the Axion Decay Constant	49
C	Theoretical Constraints	50
C.1	Bounded from below conditions	50
C.2	Perturbative unitarity bounds	51
D	Renormalisation Group Equations	53
E	2HDM inflation in 2hdSMASH	54
F	2hdSMASH at the Matching Scale	63
G	Coleman-Weinberg Potential	65

1 Introduction

The discovery by the ATLAS and CMS collaborations in the year 2012 of a new particle that is, within the current theoretical and experimental uncertainties, consistent with predictions of the Higgs boson in the Standard Model (SM) of particle physics is by no means a completion of the SM. In fact, the discovered Higgs particle is still compatible with a wide range of Beyond Standard Model (BSM) physics models that are addressing in addition a number of facts for which the SM is lacking an explanation: *i*) the non-observation of strong CP-violation, *ii*) the evidence for non-baryonic dark matter (DM),

iii) the evidence for neutrino masses and mixing, *iv)* the evidence for a baryon asymmetry of the universe (BAU), and *v)* the circumstantial evidence for an era of inflationary expansion of the universe before the hot thermal radiation dominated era.

Remarkably, all five shortcomings can be solved in one smash [1, 2] in a minimal extension of the SM by three SM singlet right-handed neutrinos and a Kim-Shifman-Vainshtein-Zakharov (KSZV) type axion model [3, 4] involving an exotic quark and a complex SM singlet scalar. The model, dubbed SM-Axion-Seesaw-Higgs Portal inflation (SMASH), solves *i)* by the Peccei-Quinn (PQ) mechanism [5], *ii)* by axion dark matter [6–8], *iii)* by the seesaw mechanism [9–12], *iv)* by thermal leptogenesis [13], and *v)* by Higgs portal inflation [14, 15]. SMASH is very predictive and constitutes a kind of minimal, but complete model of particle physics, up to the PLANCK scale, and of cosmology, back to inflation.

Possible variants of SMASH have been discussed superficially in Ref. [16]. In this paper, we concentrate on one of them, namely, the Two-Higgs-Doublet-SM-Axion-Seesaw-Higgs-Portal inflation (2hdSMASH) [17] model¹. The 2hdSMASH model consists of two Higgs doublets, a complex SM singlet PQ scalar and three SM singlet right-handed Majorana neutrinos. It differs from SMASH by replacing in the latter the KSVZ axion model by a Dine-Fischler-Srednicki-Zhitnitsky (DFSZ) axion model [20, 21] and does not feature an exotic quark. The field content of the 2hdSMASH model was originally proposed in refs. [22, 23] in order to explain neutrino masses, baryogenesis, the strong CP problem, and dark matter. It has been dubbed ‘Neutrino-DFSZ’ (ν DFSZ) model in Ref. [23] where the authors discuss the high scale validity and the technical naturalness of the model, while Ref. [24] focuses on the low energy phenomenology of the Higgs sector but does not account for the impact of inflationary constraints on the model nor does it involve high scale validity of the model. In this paper, we combine both directions to study the impact of inflationary constraints on low-energy Higgs phenomenology.

Recent work, Ref. [25], also extends the ν DFSZ model to address inflationary directions. Our work has several differences from theirs. Ref. [25] addresses inflation in a similar model (VISH ν) but with a trilinear U(1) breaking term for non-minimal couplings in the large regime ($\xi_1, \xi_2 \gg 1$) and hierarchical regime ($\xi_S \gg \xi_1, \xi_2$) while neglecting the U(1) breaking coupling. It also addresses the domain wall problem by having only the top quark carrying PQ charge, resulting in a domain wall number $N_{DW} = 1$, rendering domain walls cosmologically unstable. In our work on 2hdSMASH, we discuss the inflationary directions in the presence of a quartic U(1) breaking term (ν DFSZ) consistent with all theoretical constraints (including perturbative unitarity, boundedness-from-below, high scale validity). Our main focus is on the hierarchical regime including the effect of small portal couplings ($\lambda_{1S}, \lambda_{2S}$ and λ_{12S}) thereby allowing for inflation in the effective singlet field directions including singlet and singlet-doublet directions as discussed in sec.4.1 (see Ref. [17] for more details). For completeness, the 2HDM directions are discussed in the appendix E. We address the domain wall issue by assuming that the Peccei-Quinn symmetry arises as an accidental symmetry from an exact discrete Z_N symmetry for large $N \geq 9$. This in turn also addresses the axion quality problem (see appendix B).

Further, we also investigate the connection between inflation its impact on BAU, thermal leptogenesis and its influence on the low-energy Higgs phenomenology and provide suitable benchmark points for future collider studies. While Ref. [25] also deals with a top-specific model where the second Higgs doublet couples only to the top quarks, we

¹For some supersymmetric models addressing inflation see [18, 19].

Field	S	Φ_1	Φ_2	q_L	u_R	d_R	l_L	N_R	e_R
Charge	X_S	X_1	X_2	X_q	X_u	X_d	X_l	X_N	X_e
Value	1	$-\frac{2x}{x-1}$	$\frac{2}{1-x}$	0	$\frac{2}{1-x}$	$\frac{2x}{x-1}$	$\frac{3}{2} - \frac{2}{1-x}$	$-\frac{1}{2}$	$\frac{7}{2} - \frac{4}{1-x}$

Table 1: Charges of fields under the PQ symmetry [23]. Here $x \neq 1$.

make no such specifications but focus on the phenomenology of the full flavour sector and no FCNC decays are allowed by construction at tree-level from the Z_2 conserving Type II 2HDM-like Higgs potential structure. Therefore, 2hdSMASH [17] yields another viable complete model for particle physics and cosmology, complementary to SMASH and VISH ν .

The paper is structured as follows: in section 2 and 3 we introduce the field content of 2hdSMASH, its theoretical constraints and its scalar mass spectrum. In section 4 we describe inflation in 2hdSMASH and its theoretical predictions for inflationary observables. In section 5 we discuss the connection of the inflationary epoch with particle phenomenology by investigating whether all relevant constraints are fulfilled to accommodate successful inflation while remaining perturbative and stable. In particular, we discuss in this context the stability of the renormalization-group-flow of the PQ-scalar self-coupling λ_S and its implications for successful inflation, generation of the BAU via thermal leptogenesis, the interconnection of portal couplings, stability analysis on the effective low energy theory and benchmark points acquired from the accumulated analysis. In section 6 we present the parameter space regions allowed by both theoretical and experimental constraints and summarise our main conclusions in section 7.

2 The 2hdSMASH Model

In this section, we introduce the 2hdSMASH model by specifying its field content, its theoretical constraints and its scalar mass spectrum.

2.1 Field content and PQ symmetry

In the 2hdSMASH model, one adds to the SM three right-handed neutrinos $N_{R,i}$ and a complex SM-singlet scalar field S . Furthermore, one extends the Higgs sector to a Type-II 2HDM, involving two $SU(2)_L$ Higgs doublets Φ_i , $i = 1, 2$, and imposes a global $U(1)_{\text{PQ}}$ -symmetry, whose charges are distributed among the fields as shown in table 1. The most general renormalizable scalar potential invariant under this symmetry is then given by [23]:

$$\begin{aligned}
V(\Phi_1, \Phi_2, S) = & M_{11}^2 \Phi_1^\dagger \Phi_1 + M_{22}^2 \Phi_2^\dagger \Phi_2 + M_{SS}^2 S^* S \\
& + \frac{\lambda_1}{2} (\Phi_1^\dagger \Phi_1)^2 + \frac{\lambda_2}{2} (\Phi_2^\dagger \Phi_2)^2 + \frac{\lambda_S}{2} (S^* S)^2 \\
& + \lambda_3 (\Phi_1^\dagger \Phi_1) (\Phi_2^\dagger \Phi_2) + \lambda_4 (\Phi_1^\dagger \Phi_2) (\Phi_2^\dagger \Phi_1) \\
& + \lambda_{1S} (\Phi_1^\dagger \Phi_1) (S^* S) + \lambda_{2S} (\Phi_2^\dagger \Phi_2) (S^* S) - \lambda_{12S} (\Phi_2^\dagger \Phi_1 S^2 + h.c.) ,
\end{aligned} \tag{2.1}$$

while the most general Yukawa interactions of the fermions in the model read [23]:

$$-\mathcal{L}_Y = Y_u \bar{q}_L \tilde{\Phi}_2 u_R + Y_d \bar{q}_L \Phi_1 d_R + Y_e \bar{l}_L \Phi_1 e_R + Y_\nu \bar{l}_L \tilde{\Phi}_1 N_R + \frac{1}{2} y_N (\bar{N}_R)^c S N_R + \text{h.c.}, \quad (2.2)$$

where family indices are implied and $\tilde{\Phi}_i \equiv i\tau_2 \Phi_i^*$. These Yukawa interactions correspond to the ones of a Type-II 2HDM extended by Majorana and Dirac neutrino interactions².

2.2 Vacuum structure, particle content and masses

It is assumed that the parameters in the scalar potential are such that its minimum is attained at the vacuum expectation values (VEVs) $\langle \Phi_i \rangle \equiv (0, v_i/\sqrt{2})^T$ and $\langle S \rangle \equiv v_S/\sqrt{2}$, where $\sqrt{v_1^2 + v_2^2} \equiv v \simeq 246$ GeV and $v_S \gg v$.

After symmetry breaking, the model features two $SU(2)_L$ doublets and a complex scalar singlet, so a total of $4 + 4 + 2 = 10$ spin-zero particle excitations around the vacuum. Three of these excitations are eaten by the W^\pm and Z bosons and 7 of them are left in the spectrum: two charged Higgses, H^\pm , two CP-odd states, a and A , and three neutral CP-even states, h , H , and s . We defer the calculation of their masses at tree-level to appendix A (see also refs. [22, 24]). Here we just quote the results.

2.2.1 Mass of charged Higgs bosons

The tree-level masses of the charged Higgs bosons are obtained as

$$m_{H^\pm}^2 = \frac{1}{2} \left(\frac{(t_\beta^2 + 1) \lambda_{12S}}{t_\beta} - \frac{\lambda_4 v^2}{v_S^2} \right) v_S^2, \quad (2.3)$$

where $t_\beta \equiv \tan \beta = v_2/v_1$.

2.2.2 Masses of CP-odd scalars

One of the two CP-odd scalars is massless at tree level. It is the axion, a , the Nambu-Goldstone boson from the breaking of the $U(1)_{\text{PQ}}$ symmetry³ [27, 28]. Non-perturbatively, it acquires a small mass through mixing with the neutral pion,

$$m_a \simeq \frac{\sqrt{z}}{1+z} \frac{m_\pi f_\pi}{f_a} \simeq 0.57 \text{ meV} \left(\frac{10^{10} \text{ GeV}}{f_a} \right), \quad (2.4)$$

where $z = m_u/m_d$ is the ratio of the masses of the up and the down quark, and m_π and f_π are the mass and the decay constant of the neutral pion, respectively, and f_a is the axion decay constant:

$$f_a = \frac{\sqrt{v_S^2 + 4 \frac{v_1^2 v_2^2}{v^2}}}{6}. \quad (2.5)$$

²Choosing another charge assignment to the right-handed charged leptons, e_R , one may also realise a Flipped 2HDM in 2hdSMASH [23].

³In 2hdSMASH, the PQ symmetry is at the same time a lepton symmetry (cf. table 1). Correspondingly, the axion is at the same time also the majoron, see also [26].

Important constraints on the axion decay constant, f_a , and therefore on the PQ scale, $v_S \simeq 6f_a$, come from astrophysics and cosmology. A lower bound arises from the measured duration of the neutrino signal of the supernova 1987A and an upper bound from the requirement that there is not too much dark matter. In appendix B we argue that the PQ scale in 2hdSMASH lies preferably in the range

$$\begin{aligned} 3.1 \times 10^9 \text{ GeV} &\lesssim v_S \lesssim 5.9 \times 10^{10} \text{ GeV}, \text{ for } \tan \beta \lesssim 0.5, \\ 5.9 \times 10^9 \text{ GeV} &\lesssim v_S \lesssim 5.9 \times 10^{10} \text{ GeV}, \text{ for } \tan \beta \gtrsim 5. \end{aligned} \quad (2.6)$$

The second CP-odd scalar boson, A , has the tree-level mass

$$m_A^2 = \frac{2\lambda_{12S}}{1+t_\beta^2} \left(\frac{(1+t_\beta^2)^2}{4t_\beta} + \frac{v^2}{v_S^2} t_\beta \right) v_S^2. \quad (2.7)$$

To avoid a tachyonic mass for m_A , we require

$$\lambda_{12S} \geq 0. \quad (2.8)$$

2.2.3 Masses of CP-even scalars

The analytic form of the expression for the masses of the three CP-even scalars is not very enlightening. Here, we give the mass squares, in units of v_S^2 , as power series in $v/v_S \ll 1$:

$$\frac{m_h^2}{v_S^2} = \frac{1}{(1+t_\beta^2)^2} \left[\lambda_1 + t_\beta^4 \lambda_2 + 2t_\beta^2 \lambda_{34} - \frac{(\lambda_{1S} + t_\beta^2 \lambda_{2S} - 2t_\beta \lambda_{12S})^2}{\lambda_S} \right] \left(\frac{v}{v_S} \right)^2 + \mathcal{O} \left(\left(\frac{v}{v_S} \right)^4 \right), \quad (2.9)$$

$$\begin{aligned} \frac{m_H^2}{v_S^2} &= \frac{(1+t_\beta^2) \lambda_{12S}}{2t_\beta} + \frac{t_\beta}{(1+t_\beta^2)^2} \left[\frac{2((\lambda_{1S} - \lambda_{2S}) t_\beta + \lambda_{12S} (1 - t_\beta^2))^2}{\lambda_{12S} (1 + t_\beta^2) - 2t_\beta \lambda_S} \right. \\ &\quad \left. + (\lambda_1 + \lambda_2 - 2\lambda_{34}) t_\beta \right] \left(\frac{v}{v_S} \right)^2 + \mathcal{O} \left(\left(\frac{v}{v_S} \right)^4 \right), \end{aligned} \quad (2.10)$$

$$\begin{aligned} \frac{m_s^2}{v_S^2} &= \lambda_S + \frac{t_\beta}{(1+t_\beta^2)^2} \left[\frac{(\lambda_{1S} + \lambda_{2S} t_\beta^2 - 2t_\beta \lambda_{12S})^2}{\lambda_S} \right. \\ &\quad \left. - \frac{2t_\beta^2 ((\lambda_{1S} - \lambda_{2S}) t_\beta + \lambda_{12S} (1 - t_\beta^2))^2}{\lambda_{12S} (1 + t_\beta^2) - 2t_\beta \lambda_S} \right] \left(\frac{v}{v_S} \right)^2 + \mathcal{O} \left(\left(\frac{v}{v_S} \right)^4 \right). \end{aligned} \quad (2.11)$$

In the series for m_h^2/v_S^2 , the leading contribution, $\mathcal{O}((v/v_S)^0)$, vanishes, while the latter is present for m_H^2/v_S^2 and m_s^2/v_S^2 . Correspondingly, m_h is $\mathcal{O}(v)$, and we can associate h with the SM-like Higgs Boson which is constrained by collider searches to 125.25 ± 0.17 GeV [29], while the masses of H and s are of order v_S . We defer the discussion of the characteristics of the scalar mass spectrum in 2hdSMASH to sec. 3.

2.2.4 Masses of neutrinos

After symmetry breaking, the last two terms in eq. (2.2) give rise to the aforementioned Majorana- and Dirac neutrino mass terms, realizing the Type I seesaw mechanism [9–12].

The neutrino mass matrix reads:

$$M_\nu = \begin{pmatrix} \mathbf{0}_{3 \times 3} & M_D \\ M_D^T & M_M \end{pmatrix} = \frac{1}{\sqrt{2}} \begin{pmatrix} \mathbf{0}_{3 \times 3} & Y_\nu v_1 \\ Y_\nu^T v_1 & \frac{1}{2} Y_N v_S \end{pmatrix}, \quad (2.12)$$

where M_M represents the Majorana neutrino mass matrix and M_D represents the Dirac neutrino mass matrix. The smallness of the masses of the SM active neutrinos is thus explained by the hierarchy $v_S \gg v_1$:

$$m_\nu = -M_D M_M^{-1} M_D^T = -\frac{Y_\nu Y_N^{-1} Y_\nu^T}{\sqrt{2}} \frac{v_1^2}{v_S}. \quad (2.13)$$

2.3 Theoretical constraints

In this subsection, we give theoretical constraints regarding vacuum stability by considering the Boundedness-from-Below (BfB) conditions and perturbative unitarity conditions.

The BfB conditions guarantee that the scalar potential remains positive in all field directions for large field values. This prevents unphysical lower minima to develop and keeps the vacuum stable. The necessary and sufficient Boundedness-from-Below conditions (BfB) are based on copositivity criteria⁴. We start with the necessary BfB conditions:

$$\begin{aligned} \lambda_1 &> 0, \quad \lambda_2 > 0, \quad \lambda_3 > -\sqrt{\lambda_1 \lambda_2}, \quad \lambda_{34} > -\sqrt{\lambda_1 \lambda_2}, \\ \lambda_S &> 0, \quad \sqrt{\lambda_1 \lambda_S} > \lambda_{1S} > -\sqrt{\lambda_1 \lambda_S}, \quad \sqrt{\lambda_2 \lambda_S} > \lambda_{2S} > -\sqrt{\lambda_2 \lambda_S}, \\ \lambda_S \lambda_{34} - \lambda_{1S} \lambda_{2S} + \sqrt{(\lambda_1 \lambda_S - \lambda_{1S}^2)(\lambda_2 \lambda_S - \lambda_{2S}^2)} &> 0, \\ \lambda_{1S} + \lambda_{2S} &> 0, \quad \lambda_{1S} \lambda_{2S} - \lambda_{12S}^2 > 0, \end{aligned} \quad (2.14)$$

where $\lambda_{34} \equiv \lambda_3 + \lambda_4$. And the sufficient BfB conditions are given by:

$$\lambda_{1S} > 0, \quad \lambda_{2S} > 0, \quad \lambda_{1S} \lambda_{2S} - \lambda_{12S}^2 > 0. \quad (2.15)$$

The sufficient BfB conditions are very restrictive and can be softened. This is done by using the **Mathematica** package **BFB** [30] where the BfB conditions are solved numerically by using the Resultants method. If a parameter point is positive (semi-)definite then it is allowed, otherwise, it is dismissed. This will be useful when considering inflation in section 4.

The perturbativity conditions on the quartic couplings for 2hdSMASH ensure that our theory remains finite and perturbative at low- and high energies. This avoids divergencies that make the theory unpredictable as for any finite quantum field theory. The perturbative unitarity conditions for 2hdSMASH are given by⁵:

$$|\lambda_{1,2,1s,2s}| < 8\pi, \quad (2.16)$$

$$|\lambda_3 \pm \lambda_4| < 8\pi, \quad (2.17)$$

$$\left| \frac{1}{2} \left(\lambda_1 + \lambda_2 + \sqrt{(\lambda_1 - \lambda_2)^2 + 4\lambda_4^2} \right) \right| < 8\pi, \quad (2.18)$$

$$\left| \frac{1}{2} \left(\lambda_{1s} + \lambda_{2s} + \sqrt{16\lambda_{12S}^2 + (\lambda_{1s} - \lambda_{2s})^2} \right) \right| < 8\pi, \quad (2.19)$$

⁴The derivation of the necessary & sufficient BfB conditions is given in Appendix C.1.

⁵The conditions on perturbative unitarity are derived in Appendix C.2.

$$\left| \frac{1}{2} \left(\lambda_3 + 2\lambda_4 + \lambda_s \pm \sqrt{16\lambda_{12S}^2 + (\lambda_3 + 2\lambda_4 - \lambda_s)^2} \right) \right| < 8\pi, \quad (2.20)$$

$$\frac{1}{2} |a_{1,2,3}| < 8\pi. \quad (2.21)$$

The ratio of VEVs $\tan \beta \equiv v_2/v_1$ is bounded by perturbative unitarity of the Yukawa couplings $y_{u,d,e}$ given for any Type-II 2HDM by [31]:

$$0.28 \lesssim \tan \beta \lesssim 140. \quad (2.22)$$

3 Characteristics of the Scalar Mass Spectrum

The hierarchy of scales, $v/v_S \ll 1$, required to satisfy astrophysical and cosmological constraints, cf. eq. (2.6), implies a hierarchical scalar spectrum: *i*) the very light axion, a , with $m_a \propto 1/v_S$, *ii*) the CP-even Higgs h , to be identified with the Higgs boson detected at the LHC, with $m_h \propto v$, and *iii*) the CP-odd Higgs boson A , the CP-even Higgs H , the charged Higgses H^\pm , and the PQ scalar boson s , with masses proportional to the PQ scale v_S .

The 2HDM quartic couplings λ_i , $i = 1, 2, 3, 4$, the Higgs portal couplings λ_{iS} , $i = 1, 2, 12$, the PQ scalar quartic coupling λ_S , and $\tan \beta$, all appearing in (2.9), have to be chosen such that they result in an m_h which is within 2σ of its measured value. The spectrum of the remaining scalars, on the other hand, grossly depends only on the value of $\tan \beta$, λ_{12S} , v_S , and λ_S (see also ref. [24]). This is seen by observing that in a huge range of parameter space, namely for

$$\lambda_{12S}, \lambda_S \gg (v/v_S)^2 \simeq 6 \times 10^{-16} \left(\frac{10^{10} \text{ GeV}}{v_S} \right)^2, \quad (3.1)$$

the leading terms on the right-hand sides of Eqs. (2.3), (2.7), (2.10), (2.11) proportional to v_S^2 dominate over the next-to-leading terms. This results in an almost degenerate mass spectrum for the scalars A , H^\pm and H , whose masses are determined mainly by $\tan \beta$, λ_{12S} and v_S , while the mass of the s is determined by λ_S and v_S :

$$m_A^2 \approx m_{H^\pm}^2 \approx m_H^2 \approx \frac{1}{2} \frac{t_\beta^2 + 1}{t_\beta} \lambda_{12S} v_S^2; \quad m_s^2 \approx \lambda_S v_S^2. \quad (3.2)$$

For illustration, we present in table 2 four benchmark examples illustrating the cross features of the scalar mass spectrum for different values of λ_{12S} and λ_S . For these examples, the masses have been calculated using the full tree level expressions, going beyond the expansion in v/v_S . Moreover, the parameters have been chosen to obey the BfB and perturbative unitarity constraints. The mass spectrum (3.2) seems to reproduce nicely the numerical results, even in the case when λ_{12S} is approaching the boundary value $\lambda_{12S} \sim (v/v_S)^2$ behind the approximate relation (3.2).

Benchmark point 1 (**BP1**) illustrates that for $\lambda_{12S}, \lambda_S = \mathcal{O}(1)$ one obtains the extreme decoupling limit where all extra Higgses are at the PQ-symmetry breaking scale and decoupled from the SM. In this region of parameter space, 2hdSMASH cannot be tested at the LHC or future colliders.

BP2 shows that for $\lambda_{12S} \sim (v/v_S) \sim 10^{-8}$ and $\lambda_S \sim 1$, the extra Higgses have a mass in the range $\sim 10^3 - 10^4$ TeV. Only the PQ-scalar s is still decoupled and has a mass around the PQ-symmetry breaking scale.

Parameters	BP1	BP2	BP3	BP4
λ_1	0.1	0.1	0.1	0.1
λ_2	0.258	0.258	0.258	0.258
λ_3	0.54	0.54	0.54	0.54
λ_4	-0.14	-0.14	-0.14	-0.14
λ_S	1.0	1.0	1.0	10^{-10}
λ_{1S}	10^{-15}	10^{-15}	10^{-15}	10^{-15}
λ_{2S}	10^{-15}	10^{-15}	10^{-15}	10^{-15}
λ_{12S}	0.1	2.5×10^{-8}	2.5×10^{-16}	2.5×10^{-16}
$\tan \beta$	26	26	26	26
v_S	3.0×10^{10}	3.0×10^{10}	3.0×10^{10}	3.0×10^{10}
m_h (GeV)	125.1	125.1	125.1	125.1
m_H (GeV)	3.4×10^{10}	1.7×10^7	1711.5	1711.5
m_s (GeV)	3.0×10^{10}	3.0×10^{10}	3.0×10^{10}	3.0×10^5
m_A (GeV)	3.4×10^{10}	1.7×10^7	1711.5	1711.5
m_{H^\pm} (GeV)	3.4×10^{10}	1.7×10^7	1712.8	1712.8

Table 2: List of benchmarks considering cases a)-d).

BP3 is phenomenologically more interesting. It illustrates that a portal coupling as low as $\lambda_{12S} \sim (v/v_S)^2 \sim 10^{-16}$ pushes the masses of the extra Higgses all the way down to the electroweak scale [22, 24]. Observable effects at the HL-LHC and future colliders may be a result of this case [24].

In **BP4** we present a case where $\lambda_S \sim 10^{-10}$, in addition to $\lambda_{12S} \sim (v/v_S)^2 \sim 10^{-16}$. In this case, the mass of the s is pushed to intermediate scales between the electroweak and the PQ scale. Such a tiny PQ self-coupling is required for inflation, as we will see in the next section.

Intriguingly, portal couplings in the range exploited in **BP3** and **BP4**, leading to possible signatures at colliders, are also favored by theoretical considerations. In fact, tiny values of the portal couplings can be motivated by the fact that they provide a technically natural stabilisation of the required hierarchy between the electroweak and the PQ scale, $v/v_S \gg 1$ [22, 23, 32].

The argument goes as follows: The portal couplings are responsible for the communication between the electroweak sector and the PQ sector,

$$-\mathcal{L}_{\text{portal}} = \lambda_{1S} \left(\Phi_1^\dagger \Phi_1 \right) (S^* S) + \lambda_{2S} \left(\Phi_2^\dagger \Phi_2 \right) (S^* S) - \lambda_{12S} \left(\Phi_2^\dagger \Phi_1 S^2 + h.c. \right). \quad (3.3)$$

Clearly, the hierarchy $v/v_S \gg 1$ is preserved at tree level, if the portal couplings are parametrically suppressed,

$$|\lambda_{1S}|, |\lambda_{2S}|, |\lambda_{12S}| \lesssim \left(\frac{v}{v_S} \right)^2 \simeq 6 \times 10^{-16} \left(\frac{10^{10} \text{ GeV}}{v_S} \right)^2 \ll 1. \quad (3.4)$$

Tiny values for the portal couplings are technically natural because the 2HDM sector and the PQ sector decouple from each other in this limit, giving an enhanced Poincare symmetry. The portal couplings are also controlling the radiative corrections to the masses of the electroweak mass scalars from the PQ sector. Correspondingly, their masses are also

not destabilized by radiative corrections, if the portal couplings are in the range (3.4). In addition, this ensures that tiny values of λ_S , as required from inflation, are also technically natural as will be shown in sec 5.1.

4 Inflation in 2hdSMASH

Inflation in 2hdSMASH is described by chaotic inflation. Any theory with a plateau-like scalar potential at sufficiently high field values which hosts a slow-roll regime for the fields involved can give rise to chaotic inflation. This idea was first introduced by Andrei Linde in Ref.[33]. In 2hdSMASH chaotic inflation is an automatic feature where the Higgs doublets Φ_1 , Φ_2 and the PQ-singlet S are non-minimally coupled to the Ricci scalar R [14, 34–37]. At operator mass dimension four we show the action of 2hdSMASH in Jordan frame:

$$S_{\text{2hdSMASH}} \supset - \int d^4x \sqrt{-g} \left(\frac{M^2}{2} + \xi_1 |\Phi_1|^2 + \xi_2 |\Phi_2|^2 + \xi_S |S|^2 \right) R, \quad (4.1)$$

where ξ_i , $i = 1, 2, S$, are the dimensionless non-minimal couplings and M is the mass which is related to the reduced Planck mass, $M_p \equiv 1/\sqrt{8\pi G}$, given by

$$M^2 = M_p^2 + \xi_1 v_1^2 + \xi_2 v_2^2 + \xi_S v_S^2. \quad (4.2)$$

By means of metric- and scalar field transformation via the so-called Weyl transformation, we transform the action of eq. (4.1) from Jordan to Einstein frame. In Einstein frame the non-minimal couplings cause the quartic potential to be asymptotically flat and convex such that a plateau-like region is created suitable for inflation. This is true for any quartic potential and is preferred by current cosmic microwave background (CMB) measurements [38]. We restrict ourselves to the neutral part of the two $SU(2)_L$ doublets $\Phi_{1,2}$ and define the scalar fields involved in inflation as:

$$\Phi_1^0 = \frac{h_1}{\sqrt{2}} e^{i\theta_1}, \quad \Phi_2^0 = \frac{h_2}{\sqrt{2}} e^{i\theta_2}, \quad S = \frac{s}{\sqrt{2}} e^{i\theta_S}, \quad (4.3)$$

where the angular fields are expressed by $\theta_i \equiv a_i/v_i$. The Weyl transformation is given by the frame function

$$\Omega^2(x) = 1 + \frac{\xi_1 h_1^2(x) + \xi_2 h_2^2(x) + \xi_S s^2(x)}{M_p^2}. \quad (4.4)$$

Thus, we transform the metric into Einstein frame via

$$\tilde{g}_{\mu\nu}(x) = \Omega^2(h_1(x), h_2(x), s(x)) g_{\mu\nu}(x), \quad (4.5)$$

for which we obtain the action in Einstein frame relevant for inflation

$$S_{\text{2hdSMASH}}^{(\text{E})} \supset \int d^4x \sqrt{-\tilde{g}} \left[-\frac{M_p^2}{2} \tilde{R} + \frac{1}{2} \sum_{i,j} \mathcal{G}_{ij} \tilde{g}^{\mu\nu} \partial_\mu \phi_i \partial_\nu \phi_j - \tilde{V}(\phi_i) \right], \quad (4.6)$$

with fields $\phi = (\phi_1, \phi_2, \phi_3, \phi_4, \phi_5, \phi_6) = (h_1, h_2, s, \theta_1, \theta_2, \theta_S)$, Weyl-transformed metric $\tilde{g}^{\mu\nu}(x) = \Omega^2(x) g^{\mu\nu}(x)$, canonical Einstein-Hilbert action given by the gravitational term

$\frac{M_P^2}{2}\tilde{R}$, induced field space metric \mathcal{G}_{ij} and scalar potential $\tilde{V}(\phi_i)$. The scalar potential is transformed under Weyl transformation as follows

$$\tilde{V}(\phi_i) = \frac{1}{\Omega^4(\phi_i)} V(\phi_i), \quad (4.7)$$

where a field-dependent factor of Ω^{-4} rescales the Jordan frame scalar potential into the Einstein frame and makes it flat for large field values. Therefore, we neglect the quadratic part and only consider the quartic part of the scalar potential at large field values

$$\begin{aligned} \tilde{V}_{\text{quartic}}(h_1, h_2, s, \tilde{\theta}_1) \\ = \frac{\lambda_1 h_1^4 + \lambda_2 h_2^4 + \lambda_S s^4 + 2 \left(\lambda_{34} h_1^2 h_2^2 + \lambda_{1S} h_1^2 s^2 + \lambda_{2S} h_2^2 s^2 - 2\lambda_{12S} h_1 h_2 s^2 \cos(\tilde{\theta}) \right)}{8 \left(1 + \frac{\xi_1 h_1^2 + \xi_2 h_2^2 + \xi_S s^2}{M_p^2} \right)^2}, \end{aligned} \quad (4.8)$$

where $\lambda_{34} \equiv \lambda_3 + \lambda_4$. We note that we have four dynamical fields, namely h_1 , h_2 , s and an effective angle $\tilde{\theta}$ which is defined as follows

$$\tilde{\theta} \equiv 2\theta_S + \theta_1 - \theta_2, \quad (4.9)$$

where orthogonal directions to $\tilde{\theta}$ are omitted since they correspond to flat directions. The cosine of the λ_{12S} -term can take extrema in the interval $[-1, 1]$. We make the restriction $\tilde{\theta} \in [0, \pi]$ and determine the extrema by taking the partial derivative of $\tilde{V}_{\text{quartic}}$ w.r.t. $\tilde{\theta}$:

$$\frac{\partial \tilde{V}_{\text{quartic}}}{\partial \tilde{\theta}} \stackrel{!}{=} 0 \quad \Rightarrow \quad \tilde{\theta}_0 = \{0, \pi\}. \quad (4.10)$$

The sufficient conditions for $\tilde{\theta}$ at its extrema are calculated by taking the second partial derivative of $\tilde{V}_{\text{quartic}}$ w.r.t. $\tilde{\theta}$

$$\frac{\partial^2 \tilde{V}_{\text{quartic}}}{\partial \tilde{\theta}^2} = \begin{cases} \frac{\lambda_{12S} h_1 h_2 s^2 M_p^4}{8 (M_p^2 + \xi_1 h_1^2 + \xi_2 h_2^2 + \xi_S s^2)^2} \geq 0 & , \quad \tilde{\theta}_0 = 0 \\ \frac{-\lambda_{12S} h_1 h_2 s^2 M_p^4}{8 (M_p^2 + \xi_1 h_1^2 + \xi_2 h_2^2 + \xi_S s^2)^2} \leq 0 & , \quad \tilde{\theta}_0 = \pi \end{cases}. \quad (4.11)$$

Since $\lambda_{12S} \geq 0$ and the product $h_1 h_2 s^2$ is rotation invariant, $\tilde{\theta}$ is stabilized in its minimum at $\tilde{\theta}_0 = 0$. Hence, the potential reads:

$$\tilde{V}_{\text{quartic}}(h_1, h_2, s) = \frac{\lambda_1 h_1^4 + \lambda_2 h_2^4 + \lambda_S s^4 + 2 \left(\lambda_{34} h_1^2 h_2^2 + \lambda_{1S} h_1^2 s^2 + \lambda_{2S} h_2^2 s^2 - 2\lambda_{12S} h_1 h_2 s^2 \right)}{8 \left(1 + \frac{\xi_1 h_1^2(x) + \xi_2 h_2^2(x) + \xi_S s^2(x)}{M_p^2} \right)^2}. \quad (4.12)$$

There is now a three-dimensional induced field space metric in Einstein frame spanned by $\phi = (h_1, h_2, s)$ which is calculated via:

$$\mathcal{G}_{ij} = \frac{\delta_{ij}}{\Omega^2} + \frac{3}{2} M_p^2 \frac{\partial \log \Omega^2}{\partial \phi_i} \frac{\partial \log \Omega^2}{\partial \phi_j},$$

$$= \frac{1}{\Omega^2} \begin{pmatrix} 1 + 6\xi_1^2 \frac{h_1^2}{\Omega^2 M_p^2} & 6\xi_1 \xi_2 \frac{h_1 h_2}{\Omega^2 M_p^2} & 6\xi_1 \xi_S \frac{h_1 s}{\Omega^2 M_p^2} \\ 6\xi_1 \xi_2 \frac{h_1 h_2}{\Omega^2 M_p^2} & 1 + 6\xi_2^2 \frac{h_2^2}{\Omega^2 M_p^2} & 6\xi_2 \xi_S \frac{h_2 s}{\Omega^2 M_p^2} \\ 6\xi_1 \xi_S \frac{h_1 s}{\Omega^2 M_p^2} & 6\xi_2 \xi_S \frac{h_2 s}{\Omega^2 M_p^2} & 1 + 6\xi_S^2 \frac{s^2}{\Omega^2 M_p^2} \end{pmatrix}.$$

The scalar potential is thus symmetric under $h_1 \rightarrow -h_1$, $h_2 \rightarrow -h_2$, and $s \rightarrow -s$. Therefore, we use spherical field space coordinates as parametrization for h_1 , h_2 and s :

$$h_1(x) = \phi(x) \cos \vartheta \sin \gamma, \quad h_2(x) = \phi(x) \sin \vartheta \sin \gamma, \quad s(x) = \phi(x) \cos \gamma. \quad (4.13)$$

During inflation the scalar potential given in eq. (4.12) becomes a constant by cancellation since the numerator and denominator scale as ϕ^4 . Hence, we can make the following approximation

$$\phi^2(x) \gg \frac{M_p^2}{(\xi_1 \cos^2 \vartheta \sin^2 \gamma + \xi_2 \sin^2 \vartheta \sin^2 \gamma + \xi_S \cos^2 \gamma)}, \quad (4.14)$$

which allows us to express the scalar potential solely by angles ϑ and γ :

$$\begin{aligned} \tilde{V}_{\text{quartic}}(\vartheta, \gamma) &\simeq \\ M_p^4 &\frac{t_\gamma^4 (\lambda_1 + \lambda_2 t_\vartheta^4 + 2\lambda_{34} t_\vartheta^2) + 2t_\gamma^2 (t_\vartheta^2 + 1) (\lambda_{1S} + \lambda_{2S} t_\vartheta^2 - 2\lambda_{12S} t_\vartheta) + \lambda_S (t_\vartheta^2 + 1)^2}{8 (t_\gamma^2 (\xi_1 + \xi_2 t_\vartheta^2) + \xi_S (1 + t_\vartheta^2))^2}, \end{aligned} \quad (4.15)$$

where $t_x \equiv \tan x$. Furthermore, we require the portal couplings to be tiny in order to avoid large radiative corrections which is technically natural and associated with an enhanced Poincaré symmetry⁶ [23]. Therefore we consider two portal coupling regimes

$$\lambda_{12S} \ll \lambda_{1,2,34,1S,2S,S}, \quad (\text{I})$$

$$\lambda_{12S} \lesssim \lambda_{1S} \sim \lambda_{2S} \ll \lambda_{1,2,34,S}, \quad (\text{II})$$

where cases with $\lambda_{12S} \gg \lambda_{iS}$ are neglected due to scale-invariance, and cases with $\lambda_{1S,2S} \ll \lambda_{2S,1S}$ are neglected due to the intricacies of RG running⁷. Case (I) is the most general case to consider, whereas case (II) can be understood as the limit $\lambda_{1S,2S} \rightarrow 0$ by going from (I) to (II). In (II), all of the portal couplings are tiny, so that the PQ-sector decouples completely from the 2HDM sector. In order to find the most general description, we will focus on (I) and note when (II) can be applied. The scalar potential for case (I) is therefore given by

$$\begin{aligned} \tilde{V}_{\text{quartic}}(\vartheta, \gamma) &\simeq \\ M_p^4 &\frac{t_\gamma^4 (\lambda_1 + \lambda_2 t_\vartheta^4 + 2\lambda_{34} t_\vartheta^2) + 2t_\gamma^2 (t_\vartheta^2 + 1) (\lambda_{1S} + \lambda_{2S} t_\vartheta^2) + \lambda_S (t_\vartheta^2 + 1)^2}{8 (t_\gamma^2 (\xi_1 + \xi_2 t_\vartheta^2) + \xi_S (1 + t_\vartheta^2))^2}. \end{aligned} \quad (4.16)$$

From this expression, we are able to determine the minima and thus the effective single-field trajectories. This is done by considering the Jacobian of eq. (4.16) in two-dimensional field space :

$$J(\vartheta, \gamma) = \left(\frac{\partial \tilde{V}_{\text{quartic}}(\vartheta, \gamma)}{\partial \vartheta} \quad \frac{\partial \tilde{V}_{\text{quartic}}(\vartheta, \gamma)}{\partial \gamma} \right)^2. \quad (4.17)$$

⁶This was introduced by Ref. [23] in the context of the ν DFSZ model which we adopted for 2hdSMASH and discussed in section 3.

⁷We comment on the features of RG running with portal couplings in section 5.

With $J_2 \equiv \frac{\partial \tilde{V}_{\text{quartic}}}{\partial \gamma} = 0$ we determine the extrema of γ :

$$\gamma_{0,i} = \begin{cases} \gamma_{\text{THI}} = \frac{\pi}{2} \\ \gamma_{\text{PQI}} = 0 \\ \gamma_{\text{PQTHI}} = \gamma_{\text{PQTHI}}(\vartheta) \end{cases}, \quad (4.18)$$

which correspond to the three coarse field space directions for inflation, i.e. 2HDM-inflation denoted by THI, PQ-inflation denoted by PQI and mixed PQ-2HDM-inflation denoted by PQTHI. We have omitted for now the detailed expression of γ_{PQTHI} which will be mentioned in section 4.1. There are in principle seven inflationary directions, namely three 2HDM-field directions (h_1, h_2, h_{12}), one PQ-field direction s and three mixed PQ-2HDM directions (sh_1, sh_2, sh_{12}). All of these field directions are effective single-field trajectories that omit multi-field effects. As mentioned above, we will use case (I) as the most general description and take the limit to case (II) for THI and PQI since both sectors decouple from each other and are thus technically natural [23]. In the following, we will start the discussion on PQI and PQTHI (see appendix E for the discussion on THI). This is done by considering the γ -directions given by γ_{THI} , γ_{PQ} and $\gamma_{\text{PQTHI}}(\vartheta)$, respectively.

4.1 PQ- and PQ-2HDM-inflation in 2hdSMASH

In this section, we discuss inflation in the PQ- and PQ-2HDM directions. This corresponds to the field directions determined by γ_{PQI} and γ_{PQTHI} respectively. These types of inflationary field directions have been discussed in the context of a KSVZ-type model, dubbed SMASH [2], where the number of field directions is drastically reduced compared to 2hdSMASH. In the context of the DFSZ-type model, inflation has been previously discussed in the 2HDM direction where quartic self-couplings were taken to be of order $\mathcal{O}(1)$ (see Ref. [39]) and recently in an extension of the ν DFSZ model with a trilinear $U(1)$ breaking term, VISH ν [25]. Ref. [25] has considered inflation along all possible directions including the 2HDM, singlet and mixed directions for non-minimal couplings in the large regime ($\xi_1, \xi_2 \gg 1$) and hierarchical regime ($\xi_S \gg \xi_1, \xi_2$) while neglecting the $U(1)$ breaking coupling. Since both studies differ in the structure of the scalar potential, it is instructive to study the inflationary conditions for the quartic $U(1)$ breaking case. In this work, we focus on the hierarchical regime including the effect of small portal couplings ($\lambda_{1S}, \lambda_{2S}$ and λ_{12S}) that contribute to the singlet and singlet-doublet mixed inflation directions. For completeness, the 2HDM directions are discussed in the appendix E for which THI requires $\lambda_i^{\text{THI}} \lesssim 10^{-10}$ for $\xi_{1,2} \lesssim 1$ [2, 40, 41]. According to our naturalness philosophy non-minimal couplings should be radiatively generated and are thus an automatic feature in the very early universe. Accounting for RG running of the 2HDM self-couplings, i.e. β_{λ_1} and β_{λ_2} , this would spoil the picture since either coupling would make the other one large in order to satisfy Higgs phenomenology. Hence, we consider PQI and PQTHI for which we implement a hierarchy of non-minimal couplings, i.e. $\xi_S \gg \xi_{1,2}$, in order to effectively decouple the PQ- from the 2HDM-sector. This makes PQTHI parametrically close to the PQI which results in the suppression of large self-coupling contributions from the 2HDM-sector at the Planck scale. Therefore, we require at the Planck scale $\xi_S \lesssim 1$ and thus $\lambda_{\text{PQI}, \text{PQTHI}} \lesssim 10^{-10}$. These small self-couplings can be generated quite naturally for PQI and PQTHI since their RGE's are effectively decoupled from the 2HDM-sector and thus hidden from low energy phenomenology. We

discuss these intricacies in section 5 and explain in the following our naturalness philosophy regarding the portal couplings and which role they play for decoupling.

We consider for PQI and PQTHI case (I) but note for PQI the limit to case (II). This consideration can be understood by the decoupling of the 2HDM- from the PQ- sector by going from case (I) to (II). For PQTHI, however, the mixing between these two sectors is allowed to a certain extend. In fact, the mixing is sufficiently suppressed which refines case (I) by

$$\lambda_{12S} \ll \lambda_S \lesssim \lambda_{1S,2S} \ll \lambda_{1,2,34} \quad \text{with} \quad \lambda_{iS}^2/\lambda_S \ll \lambda_{1,2,34} \quad (\text{I}')$$

and denotes a mild decoupling compared to case (II). Therefore, case (I') decouples the two sectors as well, which corresponds to an enhanced Poincaré symmetry, i.e. $\mathcal{G}_P^{2\text{HDM}} \times \mathcal{G}_P^{\text{PQ}}$. This is due to the fact, that all 2HDM couplings are much greater than the portal couplings which accounts to a technically natural limit where radiative corrections are negligible to low energy physics.

Hence, we will start with the mixed PQ-2HDM directions before we proceed with the PQ-direction. As mentioned in section 4, we will keep the discussion on PQI as general as possible, i.e. use case (I), but mention the limiting case by going from (I) to (II).

Thus, we obtain the following scalar potential

$$\tilde{V}(\vartheta, \gamma) \simeq M_p^4 \frac{t_\gamma^4 (\lambda_1 + \lambda_2 t_\vartheta^4 + 2\lambda_{34} t_\vartheta^2) + 2t_\gamma^2 (t_\vartheta^2 + 1) (\lambda_{1S} + \lambda_{2S} t_\vartheta^2) + \lambda_S (t_\vartheta^2 + 1)^2}{8\xi_S^2 (1 + t_\vartheta^2)^2}. \quad (4.19)$$

The Jacobian for the PQTHI is given by

$$\begin{aligned} J(\vartheta, \gamma_{\text{PQTHI}}) &= \left(\frac{\partial \tilde{V}_{\text{quartic}}}{\partial \vartheta} \quad \frac{\partial \tilde{V}_{\text{quartic}}}{\partial \gamma} \right)^T, \\ &= \begin{pmatrix} \frac{(t_\vartheta^3 + t_\vartheta)(\lambda_{1S} + \lambda_{2S} t_\vartheta^2)(-\lambda_1 \lambda_{2S} + \lambda_{1S} \lambda_{34} + t_\vartheta^2(\lambda_{1S} \lambda_2 - \lambda_{2S} \lambda_{34}))}{2\xi_S^2 (\lambda_1 + \lambda_2 t_\vartheta^4 + 2\lambda_{34} t_\vartheta^2)^2} \\ 0 \end{pmatrix}, \end{aligned} \quad (4.20)$$

where we used $\gamma_{\text{PQTHI}}(\vartheta)$ for the PQ-2HDM direction which is given by

$$\gamma_{\text{PQTHI}}(\vartheta) = \arctan \left(\sqrt{\frac{(t_\vartheta^2 + 1)(-\lambda_{1S} - \lambda_{2S} t_\vartheta^2)}{\lambda_1 + \lambda_2 t_\vartheta^4 + 2\lambda_{34} t_\vartheta^2}} \right). \quad (4.21)$$

The extrema for ϑ are thus obtained via $J_1(\vartheta, \gamma_{\text{PQTHI}}) \stackrel{!}{=} 0$

$$\vartheta_{\text{PQTHI}} = \begin{cases} \vartheta_{sh_1} = 0 \\ \vartheta_{sh_2} = \frac{\pi}{2} \\ \vartheta_{sh_{12}} = \arctan \left(\sqrt{\frac{\lambda_1 \lambda_{2S} - \lambda_{1S} \lambda_{34}}{\lambda_{1S} \lambda_2 - \lambda_{2S} \lambda_{34}}} \right) \end{cases}, \quad (4.22)$$

which corresponds to the following γ_{PQTHI} -values

$$\gamma_{\text{PQTHI}} = \begin{cases} \gamma_{sh_1} = \arctan\left(\sqrt{-\frac{\lambda_{1S}}{\lambda_1}}\right) \\ \gamma_{sh_2} = \arctan\left(\sqrt{-\frac{\lambda_{2S}}{\lambda_2}}\right) \\ \gamma_{sh_{12}} = \arctan\left(\sqrt{-\frac{\lambda_{1S}(\lambda_2 - \lambda_{34}) + \lambda_{2S}(\lambda_1 - \lambda_{34})}{\lambda_1 \lambda_2 - \lambda_{34}^2}}\right) \end{cases} \quad (4.23)$$

for the three possible field directions, i.e. sh_1 , sh_2 and sh_{12} . We can now determine the inflationary vacuum energies in the PQ-2HDM direction which need to be positive in order to avoid tachyonic vacuum states

$$V_0^{\text{PQTHI}} \geq 0 \quad \Leftrightarrow \quad \frac{1}{8\xi_S^2} \begin{cases} \lambda_S - \frac{\lambda_{1S}^2}{\lambda_1} \geq 0 \\ \lambda_S - \frac{\lambda_{2S}^2}{\lambda_2} \geq 0 \\ \lambda_S - \frac{\lambda_1 \lambda_{2S}^2 + \lambda_{1S}^2 \lambda_2 - 2\lambda_{1S} \lambda_{2S} \lambda_{34}}{\lambda_1 \lambda_2 - \lambda_{34}^2} \geq 0 \end{cases} . \quad (4.24)$$

In the following, we give the minimum conditions for the PQ-2HDM direction, i.e. for $sh_{1,2,12}$, in order to determine whether the extrema correspond to inflationary valleys while other directions correspond to inflationary ridges. As in section E, the minima conditions are determined via the hessian and obey the conditions given by eq. (E.7) for the PQ-2HDM direction, i.e. $sh_{1,2,12}$.

PQTHI- (sh_1) :

$$\begin{aligned} \kappa_{1s} &\equiv \lambda_{1S} \leq 0, \\ \kappa_{s1} &\equiv \lambda_{2S} \lambda_1 - \lambda_{1S} \lambda_{34} \geq 0. \end{aligned}$$

PQTHI- (sh_2) :

$$\begin{aligned} \kappa_{2s} &\equiv \lambda_{2S} \leq 0, \\ \kappa_{s2} &\equiv \lambda_{1S} \lambda_2 - \lambda_{2S} \lambda_{34} \geq 0. \end{aligned}$$

PQTHI- (sh_{12}) :

$$\begin{aligned} \kappa_{s1} \kappa_{s2} (\kappa_{s1} + \kappa_{s2}) &\leq 0, \\ (\kappa_{s1} + \kappa_{s2}) (\lambda_{1S} \kappa_{s2} + \lambda_{2S} \kappa_{s1}) &\leq 0. \end{aligned}$$

Most importantly, the inflationary conditions are given by the minimum conditions which are supplemented by the maximum conditions of other field directions in order to classify inflationary valleys and ridges accordingly. Similar to our discussion for 2HDM field space directions of appendix E, the PQTHI- sh_{12} direction already contains this feature automatically since PQTHI- sh_{12} is a mixture of all three fields. However, the conditions of the PQTHI- sh_{12} direction need some refining. The first of the two conditions state

$$\kappa_{s1} \leq 0 \quad , \quad \kappa_{s2} \leq 0. \quad (4.25)$$

This leads to the second condition to become

$$\kappa_{1s} \equiv \lambda_{1S} > 0 \quad , \quad \kappa_{2s} \equiv \lambda_{2S} > 0. \quad (4.26)$$

We list the complete set of inflationary conditions for the 2HDM- h_{12} direction in Table 3.

Considering that PQTHI is composed of two or three field directions, i.e. $sh_{1,2,12}$, we need to examine whether orthogonal field directions contribute to inflation. Therefore, we provide the field space metric in these three inflationary directions

$$\mathcal{G}_{ij}^{sh_i} \simeq \frac{b_i}{\Omega_{sh_i}^2} \begin{pmatrix} 1 & 0 & 0 \\ 0 & 1 & 0 \\ 0 & 0 & \frac{\Omega_{sh_i}^2 + 6\xi_S^2 \frac{\phi^2}{M_p^2}}{\Omega_{sh_i}^2} \end{pmatrix}, \quad (4.27)$$

where b_i are the mixing parameters determined via $\sin^2 \gamma_{sh_i} = 1 - b_i^{-1}$,

$$b_1 \equiv 1 + \left| \frac{\lambda_{1S}}{\lambda_1} \right|, \quad (4.28)$$

$$b_2 \equiv 1 + \left| \frac{\lambda_{2S}}{\lambda_2} \right|, \quad (4.29)$$

$$b_{12} \equiv 1 + \left| \frac{\lambda_{2S}(\lambda_1 - \lambda_{34}) + \lambda_{1S}(\lambda_2 - \lambda_{34})}{\lambda_1 \lambda_2 - \lambda_{34}^2} \right| \quad (4.30)$$

and $\Omega_{sh_i}^2$ are the frame functions given by

$$\Omega_{sh_i}^2 = b_i + 6\xi_S \frac{s^2}{M_p^2}. \quad (4.31)$$

We can see from the field space metric and its corresponding frame functions that the mixing parameter determine whether inflation occurs in the PQ-2HDM ($b_i \neq 1$) or in the PQ direction ($b_i = 1$) resembling case (II). In order to examine whether the orthogonal field space directions contribute to PQTHI, we compute the instantaneous masses

$$m_{\phi_i}^2 \Big|_{\substack{\vartheta=\vartheta_{sh_i} \\ \gamma=\gamma_{sh_i}}} \simeq \begin{cases} \begin{pmatrix} -\frac{\lambda_{1S}}{\xi_S} & , & \frac{\kappa_{s2}}{2\lambda_2\xi_S} & , & -\frac{\kappa_{s2}\lambda_1}{\xi_S(\lambda_1\lambda_2-\lambda_{34}^2)} \end{pmatrix} & (h_1) \\ \begin{pmatrix} -\frac{\lambda_{2S}}{\xi_S} & , & \frac{\kappa_{s1}}{2\lambda_1\xi_S} & , & -\frac{\kappa_{s1}\lambda_2}{\xi_S(\lambda_1\lambda_2-\lambda_{34}^2)} \end{pmatrix} & (h_2) \\ \begin{pmatrix} \frac{\lambda_{1S}^2}{\lambda_1\xi_S(1+6\xi_S)} & , & \frac{\lambda_{2S}^2}{\lambda_2\xi_S(1+6\xi_S)} & , & \frac{\kappa_{s1}\lambda_{2S}+\kappa_{s2}\lambda_{1S}}{\xi_S(6\xi_S+1)(\lambda_1\lambda_2-\lambda_{34}^2)} \end{pmatrix} & (s) \end{cases} \quad (4.32)$$

where the masses are given for sh_1 , sh_2 and sh_{12} directions from left to right. These results are now related to the Hubble rate $\mathcal{H}^2 \approx \dot{V}/3M_p^2$

$$\frac{m_s^2}{\mathcal{H}^2} \Big|_{\substack{\vartheta=\vartheta_{sh_i} \\ \gamma=\gamma_{sh_i}}} \simeq \frac{24\xi_S}{1+6\xi_S} \frac{\delta\lambda_S}{\tilde{\lambda}} \lesssim 1, \quad (4.33)$$

$$\frac{m_{h_i}^2}{\mathcal{H}^2} \Big|_{\substack{\vartheta=\vartheta_{sh_i} \\ \gamma=\gamma_{sh_i}}} \simeq \frac{12\xi_S}{\tilde{\lambda}} \begin{cases} 2|\lambda_{iS}| \gtrsim 1 & (sh_i) \\ (\lambda_{iS} + (b_j - 1)\lambda_{34}) \gtrsim 1 & (sh_j) \\ \frac{2\lambda_1\lambda_2(\lambda_{iS} + (b_j - 1)\lambda_{34})}{\lambda_1\lambda_2 - \lambda_{34}^2} \gtrsim 1 & (sh_{12}) \end{cases} \quad (4.34)$$

with $\xi_S \sim 2 \times 10^4 \sqrt{\tilde{\lambda}}$ and $\tilde{\lambda} = \lambda_S - \delta\lambda_S \gtrsim 0$. This shows that all masses of orthogonal directions are stabilized while the inflaton remains dynamical at the inflationary valley.

For the PQ-direction, i.e. $\gamma_{\text{PQ}} = 0$, we acquire the following minimum condition given by the single component hessian

$$\frac{\xi_S (\lambda_{1S} + \lambda_{2S} t_\vartheta^2 - 2\lambda_{12S} t_\vartheta) - \lambda_S (\xi_1 + \xi_2 t_\vartheta^2)}{2\xi_S^3 (1 + t_\vartheta^2)} \geq 0. \quad (4.35)$$

In order to obtain minimum conditions w.r.t. all field directions, we simply apply the ϑ -extrema of the 2HDM- and PQ-2HDM directions, i.e. ϑ_{THI} and ϑ_{PQTHI} . This amounts to a total of four minimum condition for the PQ-direction:

PQI:

$$\begin{aligned} \kappa_{1s} &\equiv \lambda_{1S} \geq 0, \\ \kappa_{2s} &\equiv \lambda_{2S} \geq 0, \\ (\kappa_{s1} + \kappa_{s2}) (\lambda_{1S} \kappa_{s2} + \lambda_{2S} \kappa_{s1}) &\geq 0, \\ (\kappa_{s1} + \kappa_{s2}) (\lambda_1 + \lambda_2 - 2\lambda_{34}) &\geq 0, \end{aligned}$$

where the first two correspond to the 2HDM- $h_{1,2}$ directions and the last two conditions correspond to the PQTHI- sh_{12} direction and to the 2HDM- h_{12} direction, respectively. By considering the last two conditions, we cannot make a conclusive statement whether κ_{s1} and κ_{s2} are positive or negative. This can only be determined if either $\lambda_{1,2} \geq \lambda_{34}$ or $\lambda_{1,2} \leq \lambda_{34}$ is given. Thus, the last two conditions can be neglected. Moreover, we note that these conditions vanish by taking the limit to case (II). The absence of the portal couplings and the non-minimal coupling hierarchy, i.e. $\xi_S \gg \xi_{1,2}$, are mainly responsible for an inflationary valley to exist in the PQ-direction. For completeness we refer to the above minimum conditions as the inflationary conditions and add case (II) as a another condition in our model.

Since we are considering four inflationary trajectories, we need an adequate description of the inflaton field ϕ which we identify as the PQ-scalar s . Therefore, we canonically normalize the inflaton field s with the following field redefinitions for inflation in the s -, sh_1 -, sh_2 - and sh_{12} direction, respectively

$$\Omega^2 \frac{d\chi_s}{ds} = \sqrt{\Omega^2 + 6\xi_S^2 \frac{s^2}{M_p^2}}, \quad (4.36)$$

$$\Omega^2 \frac{d\chi_{sh_i}}{ds} = \sqrt{b_i \left(\Omega_i^2 + 6\xi_S^2 \frac{s^2}{M_p^2} \right)}. \quad (4.37)$$

By integration we obtain the canonically normalized fields $\chi_{s,sh_1,sh_2,sh_{12}}$

$$\frac{\sqrt{\xi_S}}{M_p} \chi_s = \sqrt{1 + 6\xi_S} \operatorname{arcsinh} \left(\sqrt{1 + 6\xi_S} u(s) \right) - \sqrt{6\xi_S} \operatorname{arctanh} \left(\frac{\sqrt{6\xi_S} u(s)}{\sqrt{1 + (1 + 6\xi_S) u^2(s)}} \right), \quad (4.38)$$

inflation along	Potential (4.19) minimized at	Inflationary conditions	Einstein frame slow roll potential
$s h_1$	$\gamma_0 = \arctan\left(\sqrt{-\frac{\lambda_{1S}}{\lambda_1}}\right)$ $\vartheta_0 = 0$	$\kappa_{s1} \geq 0, \kappa_{s2} \leq 0$ $\kappa_{1s} \leq 0, \kappa_{2s} \geq 0$	$\frac{\lambda_{sh_1}}{8} s^4 \left(1 + \xi_S \frac{s^2}{M_P^2}\right)^{-2}$
$s h_2$	$\gamma_0 = \arctan\left(\sqrt{-\frac{\lambda_{2S}}{\lambda_2}}\right)$ $\vartheta_0 = \frac{\pi}{2}$	$\kappa_{s1} \leq 0, \kappa_{s2} \geq 0$ $\kappa_{1s} \geq 0, \kappa_{2s} \leq 0$	$\frac{\lambda_{sh_2}}{8} s^4 \left(1 + \xi_S \frac{s^2}{M_P^2}\right)^{-2}$
$s h_{12}$	$\gamma_0 = \arctan\left(\sqrt{-\frac{\kappa_{s2} + \kappa_{s2}}{\lambda_1 \lambda_2 - \lambda_{34}^2}}\right)$ $\vartheta_0 = \arctan\left(\sqrt{\frac{\kappa_{s1}}{\kappa_{s2}}}\right)$	$\kappa_{s1} \leq 0, \kappa_{s2} \leq 0$ $\kappa_{1s} \leq 0, \kappa_{2s} \leq 0$	$\frac{\lambda_{sh_{12}}}{8} s^4 \left(1 + \xi_S \frac{s^2}{M_P^2}\right)^{-2}$
s	$\gamma_0 = 0$ $\vartheta_0 = \{0, \frac{\pi}{2}\}$	$\kappa_{1s} \geq 0, \kappa_{2s} \geq 0$ $\vee \lambda_{1S,2S} \ll \lambda_S$	$\frac{\lambda_S}{8} s^4 \left(1 + \xi_S \frac{s^2}{M_P^2}\right)^{-2}$

Table 3: Conditions and characteristics for PQI and PQTHI, i.e. s - and $sh_{1,2,12}$ -inflation, with $\xi_S \gg \xi_{1,2}$.

$$\frac{1}{M_p} \sqrt{\frac{\xi_S}{b_i}} \chi_{sh_i} = \sqrt{1 + 6\xi_S} \operatorname{arcsinh} \left(\sqrt{\frac{1 + 6\xi_S}{b_i}} u(s) \right) - \sqrt{6\xi_S} \operatorname{arctanh} \left(\frac{\sqrt{6\xi_S} u(s)}{\sqrt{b_i + (1 + 6\xi_S) u^2(s)}} \right) \quad (4.39)$$

with $u(s) \equiv \sqrt{\xi_S} s / M_p$. By taking the inverse of the canonically normalized fields, we can write the inflationary scalar potential in Einstein frame for PQI and PQTHI in the usual form:

$$V_{s,sh_i}(\chi_i) = \frac{\tilde{\lambda}}{8} \frac{s^4(\chi_i)}{\left(1 + \xi_S \frac{s^2(\chi_i)}{M_P^2}\right)^2}, \quad (4.40)$$

where $\tilde{\lambda}$ is given by the following inflationary directions:

$$\tilde{\lambda} = \begin{cases} \lambda_S & \text{(PQI)} \\ \lambda_S - \frac{\lambda_{iS}^2}{\lambda_i} & \text{(PQTHI-} sh_i \text{)} \\ \lambda_S - \frac{\lambda_1 \lambda_{2S}^2 + \lambda_{1S}^2 \lambda_2 - 2\lambda_{1S} \lambda_{2S} \lambda_{34}}{\lambda_1 \lambda_2 - \lambda_{34}^2} & \text{(PQTHI-} sh_{12} \text{)} \end{cases}. \quad (4.41)$$

In Table 3 we summarize the extrema, inflationary conditions and Einstein frame slow-roll potential for PQI and PQTHI. We show the two inflationary scenarios in figure 1 which represents PQI (left) and PQTHI (right). As discussed in the appendix E, the inflationary predictions A_s , n_s and r are constrained by PLANCK/BICEP data [38, 42, 43]. According to our naturalness philosophy, we demand the non-minimal coupling to be constrained by $\xi_S \lesssim 1$ which is shown in figure 2. Thus, A_s sets the following limits to ξ_S and $\tilde{\lambda}$

$$8.5 \times 10^{-3} \lesssim \xi \lesssim 1 \text{ implying } 9 \times 10^{-10} \gtrsim \tilde{\lambda} \gtrsim 4.5 \times 10^{-13}. \quad (4.42)$$

In order to determine n_s and r we require the number of e-folds from some time t_* where

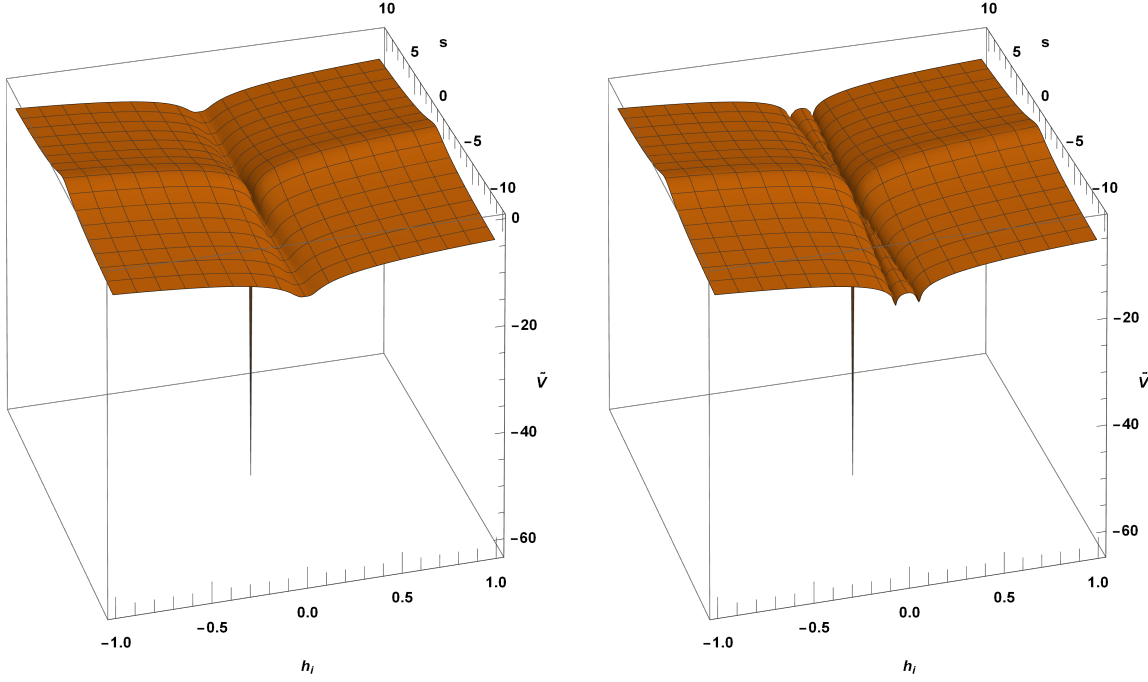


Figure 1: Decadic log Einstein frame scalar potential depicting PQI (left) and PQTHI (right) in units of M_p as a function of the PQ-scalar s and the two Higgs fields h_1 and h_2 .

the scale $k_* = a_* \mathcal{H}_*$ exited the horizon to the time where inflation ended denoted by $k_{\text{end}} = a_{\text{end}} \mathcal{H}_{\text{end}}$. This is defined by

$$N_* \equiv \log \left(\frac{a_{\text{end}}}{a_{k_*}} \right) = \int_{\chi_I}^{\chi_{\text{end}}} \frac{d\chi}{\sqrt{2\epsilon}}, \quad (4.43)$$

which can be solved exactly by the Klein-Gordon eq.

$$\frac{d^2 \chi}{dN^2} + 3 \frac{d\chi}{dN} - \frac{1}{2M_p^2} \left(\frac{d\chi}{dN} \right)^3 + \sqrt{2\epsilon} \left(3M_p - \frac{1}{2M_p} \left(\frac{d\chi}{dN} \right)^2 \right). \quad (4.44)$$

During inflation, the largest scales exit the horizon at k_* which re-enter the horizon at a later time, i.e. at matter or radiation domination, cf. Ref. [44]. In fact, the largest scales are the last to re-enter the horizon which corresponds to scales of our current horizon, i.e. $k_0 = a_0 \mathcal{H}_0$. The required amount of e-folds for solving the horizon problem is therefore related to the complete expansion history of the universe and is given by [45]

$$\frac{k_*}{k_0} \equiv \frac{k_*}{a_0 \mathcal{H}_0} = \frac{a_{k_*} \mathcal{H}_{k_*}}{a_0 \mathcal{H}_0} = \frac{a_{k_*}}{a_{\text{end}}} \frac{a_{\text{end}}}{a_{\text{eq}}} \frac{\mathcal{H}_{k_*}}{\mathcal{H}_{\text{eq}}} \frac{a_{\text{eq}} \mathcal{H}_{\text{eq}}}{a_0 \mathcal{H}_0}, \quad (4.45)$$

where the subscripts "eq" and "0" denote matter-radiation equality and the present time, respectively. With the ratio $a_{k_*}/a_{\text{end}} = \exp(-N_*)$, we identify the number of e-folds during inflation N_* by reformulating eq. (4.45) to find [45]

$$N_* = -\log \frac{k_*}{a_0 \mathcal{H}_0} + \log \frac{a_{\text{end}}}{a_{\text{eq}}} + \log \frac{\mathcal{H}_{k_*}}{\mathcal{H}_{\text{eq}}} + \log \frac{a_{\text{eq}} \mathcal{H}_{\text{eq}}}{a_0 \mathcal{H}_0}. \quad (4.46)$$

By using the slow-roll approximation for the Hubble rate during inflation, i.e.

$\mathcal{H}_{k_*} \simeq \sqrt{V_{k_*}/3 M_p^2}$, we obtain [45]

$$N_* = -\log \frac{k_*}{a_0 \mathcal{H}_0} + \log \frac{a_{\text{end}}}{a_{\text{eq}}} + \log \sqrt{\frac{V_{k_*}}{3 M_p^2}} \frac{1}{\mathcal{H}_{\text{eq}}} + \log \frac{a_{\text{eq}} \mathcal{H}_{\text{eq}}}{a_0 \mathcal{H}_0}. \quad (4.47)$$

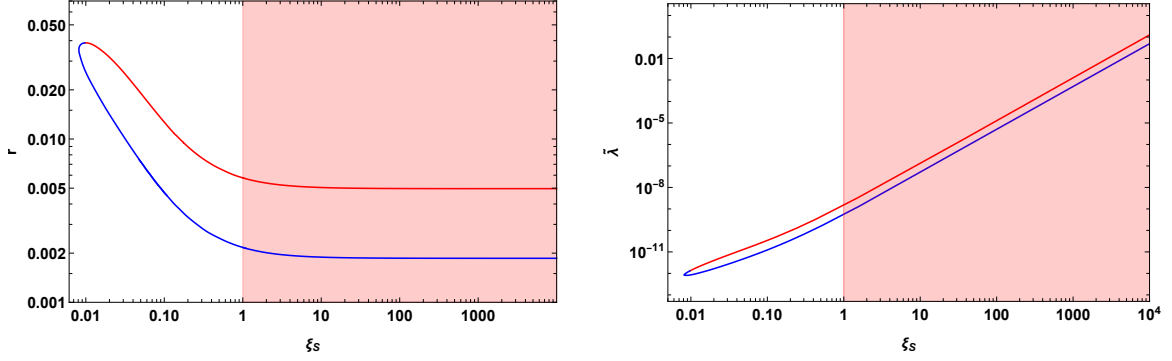


Figure 2: Shown are the 95% C.L. contours of r vs. ξ_S (left) and the effective quartic coupling for inflation $\tilde{\lambda}$ vs. ξ_S at the pivot scale $k_* = 0.002 \text{ Mpc}^{-1}$. The red shaded region given by $\xi_S > 1$ indicates the unnatural regime according to our naturalness philosophy. The red and blue curves indicate constraints given by the redder spectrum and the bluer spectrum of n_s [42, 43].

In 2hdSMASH we adopt the simplicity of the expansion history of the universe from SMASH [2]. Based on the smallness of the non-minimal couplings, they can be neglected by the end of inflation. Correspondingly, preheating and reheating occur in an approximate quartic potential, where the universe is radiation-dominated. This has been worked out for SMASH in detail by elaborate lattice simulations where it was shown that after a few oscillations the scalar potential is approximately quartic [2, 46].

By using the relation

$$\log \frac{a_{\text{end}}}{a_{\text{eq}}} = \log \frac{a_{\text{end}}}{a_0} + \log \frac{a_0}{a_{\text{eq}}} , \quad (4.48)$$

we can simplify the number of e-folds as follows

$$N_* = -\log \frac{k_*}{a_0 \mathcal{H}_0} + \log \frac{a_{\text{end}}}{a_0} + \log \sqrt{\frac{V_{k_*}}{3 M_p^2}} + \log \frac{1}{\mathcal{H}_0} . \quad (4.49)$$

The ratio a_{end}/a_0 relates the scale of the end of inflation with the scale of the present time which is given by [47]

$$\frac{a_{\text{end}}}{a_0} = \frac{a_{\text{end}}}{a_{\text{RD}}} \frac{a_{\text{RD}}}{a_{\text{end}}} = \left(\frac{g_{*,\text{RD}}}{g_{*,0}} \right)^{-1/3} \left(\frac{g_{*,\text{RD}}}{g_{*,0}} \right)^{1/4} \left(\frac{\rho_{0,\text{RD}}}{\rho_{\text{end}}} \right)^{1/4} \left(\frac{a_{\text{end}}}{a_{\text{RD}}} \right)^{(1-3w)} , \quad (4.50)$$

where the subscript "RD" denotes radiation domination, $g_{*,\rho}$ and $g_{*,s}$ denote the number of relativistic degrees of freedom for the energy density and entropy, respectively. Since the universe is radiation-dominated by the end of inflation, the energy of state parameter $w = p/\rho$ approaches $1/3$ instantaneously in the epoch of preheating for which we can approximate eq. (4.50)

$$\frac{a_{\text{end}}}{a_0} \simeq \left(\frac{g_{*,s}(T_R)}{g_{*,s}(T_0)} \right)^{-1/3} \left(\frac{g_{*,\rho}(T_R)}{g_{*,\rho}(T_0)} \right)^{1/4} \left(\frac{\rho_{0,\text{RD}}}{V_{\text{end}}} \right)^{1/4} , \quad (4.51)$$

where the subscript "R" denotes reheating. The corresponding number of relativistic degrees of freedom are given by [48]

$$g_{*,s}(T_0) \simeq 3.91 , \quad g_{*,\rho}(T_0) \simeq 2 , \quad g_{*,s}(T_R) \simeq g_{*,\rho}(T_R) \simeq 124.5 \quad (4.52)$$

and the present time energy density of radiation $\rho_{0,\text{RD}}$ is given by [48]

$$\rho_{0,\text{RD}} = \frac{\pi^2 T_0^4}{15} \simeq 2.02 \times 10^{-15} \text{ eV}^4. \quad (4.53)$$

Furthermore, we give the updated values of the present time Hubble parameter \mathcal{H}_0 and Hubble scale $k_0 = a_0 \mathcal{H}_0$ by Ref. [49]

$$\begin{aligned} \mathcal{H}_0 &\simeq 5.9 \times 10^{-61} h M_p \quad \text{with} \quad h \simeq 0.674, \\ a_0 \mathcal{H}_0 &\simeq 22.47 \times 10^{-5} \text{ Mpc}^{-1}, \end{aligned} \quad (4.54)$$

where h is the Hubble constant. The number of e-folds can now be approximated and reads [45, 50]

$$\begin{aligned} N_* &\simeq 61.25 - \log \frac{k_*}{a_0 \mathcal{H}_0} - \log \frac{10^{16} \text{ GeV}}{V_{k_*}^{1/4}} + \log \frac{V_{k_*}^{1/4}}{V_{\text{end}}^{1/4}} \\ &\simeq 59 - \log \left(\frac{k_*}{10^{-3} \text{ Mpc}^{-1}} \right) - \log \left(\frac{10^{-4} \text{ Mpc}^{-1}}{a_0 \mathcal{H}_0} \right) - \log \frac{10^{16} \text{ GeV}}{V_{k_*}^{1/4}} + \log \frac{V_{k_*}^{1/4}}{V_{\text{end}}^{1/4}}, \end{aligned} \quad (4.55)$$

where we included the maximum horizon of the observable universe given by the upper bound $V_{k_*}^{1/4} \lesssim 10^{16} \text{ GeV}$, cf. [1, 2, 48]. The scale of horizon exit is $k_* = 0.002 \text{ Mpc}^{-1}$ which corresponds to the largest observable scales in the CMB measured by Planck/BICEP [42, 43]. With the constants of eq. (4.54) we obtain

$$N_* \simeq 59.06 - \log \frac{10^{16} \text{ GeV}}{V_{k_*}^{1/4}} + \log \frac{V_{k_*}^{1/4}}{V_{\text{end}}^{1/4}}, \quad (4.56)$$

which illustrates that only the energy scales $V_{k_*}^{1/4}$ and $V_{\text{end}}^{1/4}$ are relevant. By utilizing the the Planck constraints to fit the quartic coupling $\tilde{\lambda}$ to A_s we can determine N_* of eq. (4.56) which must match the number of e-folds obtained from solving the inflaton's eom from eq. (4.44). Correspondingly, the energy scales $V_{k_*}^{1/4}$ and $V_{\text{end}}^{1/4}$ are determined. In figure 3 we show this correspondence of $V_{k_*}^{1/4}$ and $V_{\text{end}}^{1/4}$ as a function of the non-minimal coupling ξ_S where the solid black curve manifests this result. Typical values of $V_{k_*}^{1/4}$ and $V_{\text{end}}^{1/4}$ are in the range of

$$8 \times 10^{15} \text{ GeV} \lesssim V_{k_*}^{1/4} \lesssim 1.4 \times 10^{16} \text{ GeV}, \quad (4.57)$$

$$3.8 \times 10^{15} \text{ GeV} \lesssim V_{\text{end}}^{1/4} \lesssim 4.8 \times 10^{15} \text{ GeV} \quad (4.58)$$

for

$$1.35 \times 10^{-2} \lesssim \xi_S \lesssim 1 \quad \text{implying} \quad 9 \times 10^{-10} \gtrsim \tilde{\lambda} \gtrsim 2.2 \times 10^{-12}. \quad (4.59)$$

These ranges are indicated by the black dots in figure 3 for which we can compute the corresponding range of the number of e-folds N_* from eq. (4.56)

$$59.3 \lesssim N_* \lesssim 60.7. \quad (4.60)$$

We show our result in figure 4 where the thick red curve is obtained by eq. (4.56) which accounts for the numerically determined expansion history⁸. The black solid lines have been acquired by solving the Klein-Gordon equation (4.44) without taking the expansion history of our universe

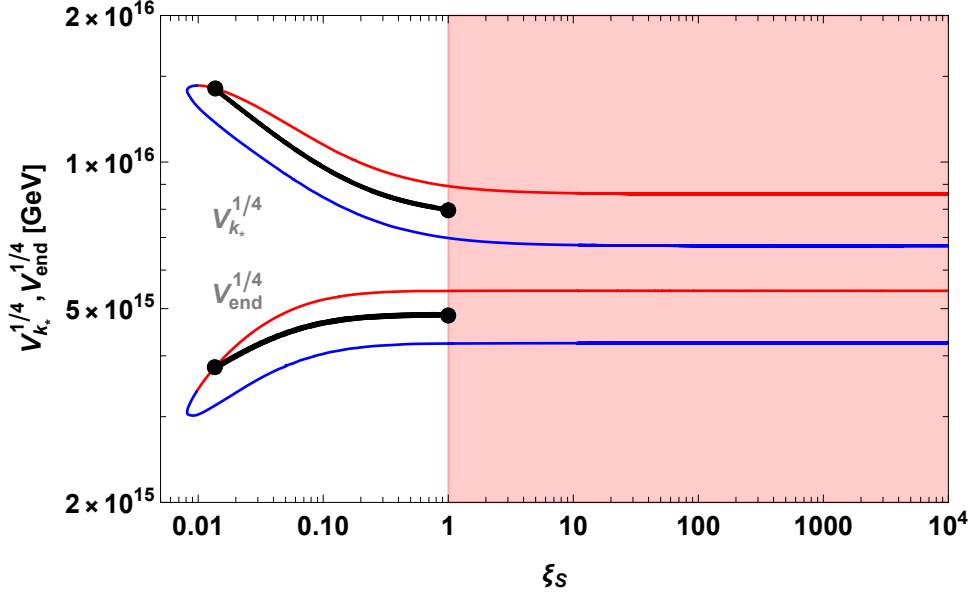


Figure 3: Shown are the 95% C.L. contours of $V_{k_*}^{1/4}$ and $V_{end}^{1/4}$ vs. ξ_S at the pivot scale $k_* = 0.002 \text{ Mpc}^{-1}$. The red shaded region given by $\xi_S > 1$ indicates the unnatural regime according to our naturalness philosophy. The red and blue curves indicate constraints given by the redder spectrum and the bluer spectrum of n_s [42, 43]. The black solid curves take the 2hdSMASH expansion history of our universe into account where inflation is followed by immediate radiation-domination. Correspondingly, the black dots specify the range of validity for a consistent expansion history.

into account. The red curve is close to $N = 60$ as indicated in eq. (4.60).

Correspondingly, we provide the range of n_s and r for PQI and PQTHI in 2hdSMASH

$$\xi_S \simeq 1 \Rightarrow \begin{cases} 0.9664 \lesssim n_s \lesssim 0.9668 \\ 0.0037 \gtrsim r \gtrsim 0.0036 \end{cases}, \quad \xi_S \simeq 1.35 \times 10^{-2} \Rightarrow \begin{cases} 0.9646 \lesssim n_s \lesssim 0.9651 \\ 0.037 \gtrsim r \gtrsim 0.036 \end{cases}. \quad (4.61)$$

5 Connecting Inflation with TeV Scale Particle Physics

This section is dedicated to make the connection between inflationary constraints and low energy constraints. For this reason, we consider the one-loop RGEs (see appendix D) which run the 2hdSMASH parameters from low- to high-scale and meet the constraints at their respective scales. In an effective field theory approach, the PQ-scalar s can be integrated out below the matching scale $m_s \sim \sqrt{\lambda_S} v_S$ where 2hdSMASH is matched to its low-energy theory, i.e. the ν 2HDM. Hence, the PQ self-coupling λ_S will determine the matching scale for fixed PQ-scale v_S .

In order to ensure successful inflation at the Planck scale, i.e. $\lambda_S(M_P) \lesssim 10^{-10}$, the parameters need to evolve stable from the matching scale to M_P . To this effect, constraints on the portal couplings and the neutrino Yukawa couplings ensure the required stability as we will see in sec. 5.1. Moreover, there are two inflationary scenarios realized in 2hdSMASH, namely PQI and PQTHI, which differ by sign and size of the portal couplings. These constraints must be met at the Planck scale. In order to account for thermal leptogenesis and BAU, we obtain further constraints on the neutrino Yukawa couplings Y_ν and Y_N affecting the RG evolution

⁸We utilized a numerical code from Ref. [2] to obtain the red curve shown in figure 4.

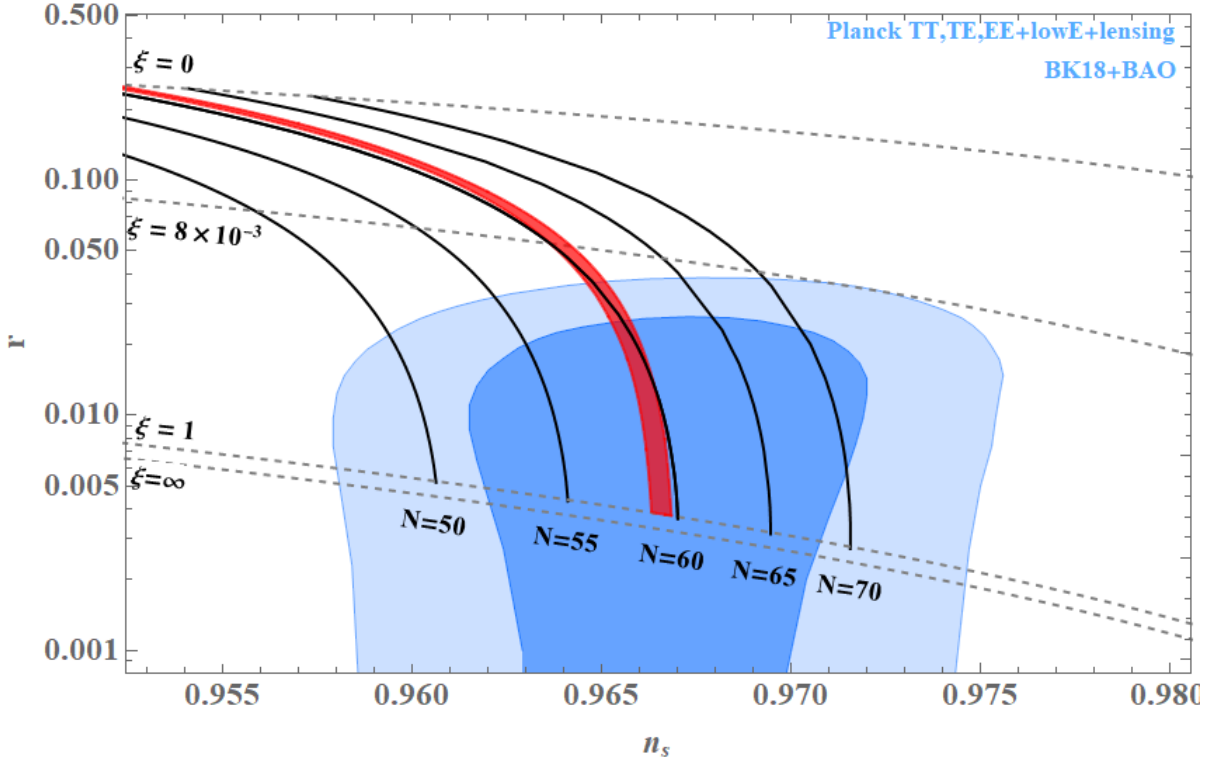


Figure 4: Shown are the 95% and 68% C.L. contours of r vs. n_s constrained by PLANCK/BICEP [38, 42, 43] (shaded blue), the isocontours of constant ξ (gray dashed), the isocontours of constant N (solid black) and the inflationary predictions by 2hdSMASH for PQI/PQTHI taking into account the numerically determined expansion history of the universe (thick red).

of the portal couplings. This effect will only consider PQI while PQTHI scenarios will face the challenge to run the portal couplings stable all the way up to the Planck scale. From a naturalness point of view, we further demand that the portal couplings do not impact Higgs phenomenology through large radiative corrections giving rise to an enhanced Poincaré symmetry $\mathcal{G}_P^{2HDM} \times \mathcal{G}_P^S$ (cf. sec. 3) where $\lambda_{1S,2S,12S}, Y_N \rightarrow 0$ [22, 23]. Hence, the portal couplings underlie tight constraints for connecting inflation with particle phenomenology. Along these lines, all parameters need to run stable and perturbative accounted by the vacuum stability and perturbative unitarity conditions (see sec. 2.3). High-scale validity is ensured by obeying the BfB and perturbative unitarity conditions for all energy scales until the Planck scale. By breaking perturbative unitarity, Landau poles emerge which lead to a breakdown of predictivity. If vacuum stability is not guaranteed, our universe would not correspond to the universe we know today. We will discuss these intricacies in the following subsections.

We structure the sections as follows: In section 5.1 we will discuss the stability requirements for λ_S by considering the RG running effects of the right handed neutrino Yukawa and portal couplings. In section 5.2 we discuss the constraints from thermal leptogenesis and BAU and their impact on RG running. In section 5.3 we will analyze the running of the portal couplings and give conditions which motivate PQI and PQTHI. Therefore, we give three benchmark points which underline our considerations and illustrate the interconnection of inflation and Higgs phenomenology. In section 5.4 we discuss vacuum-stability, perturbativity and high-scale validity by identifying the effective 2HDM model in our RG-analysis. Since all other couplings are fixed, i.e. portal couplings $\lambda_{1S,2S,12S}$, neutrino Yukawa couplings $Y_{\nu,N}$ and PQ self-coupling λ_S , we consider the remaining 2HDM couplings $\lambda_{1,2}$ and λ_{34} . In particular we pay attention to

the stability of λ_2 which tends to run negative. We will argue that λ_3 and λ_{34} can cure this instability while keeping λ_1 fixed. This is illustrated by representative benchmarks. In section 5.5 we accumulate all of the analysis and provide benchmark points which accommodate inflation, theoretical and experimental constraints while presenting interesting Higgs phenomenology relevant for HL-LHC and future colliders.

5.1 Stability analysis of λ_S

In this section we want to outline the stability condition on the running of λ_S for successful inflation. This in turn will lead to conditions on the Higgs portal couplings λ_{1S} , λ_{2S} , λ_{12S} and the right handed Yukawa couplings Y_N . We give to one-loop accuracy, the renormalization group evolution of $\lambda_S(\mu)$ (see Appendix D)

$$(4\pi)^2 \frac{d}{d \ln \mu} \lambda_S = 10\lambda_S^2 + 4\lambda_{1S}^2 + 4\lambda_{2S}^2 + 8\lambda_{12S}^2 - 2\text{Tr} \left(Y_N^\dagger Y_N Y_N^\dagger Y_N \right) + 2\lambda_S \text{Tr} \left(Y_N^\dagger Y_N \right). \quad (5.1)$$

As discussed in section 4.1, we require for successful inflation $\lambda_S(M_p) \lesssim 10^{-10}$ [2]. Such a small quartic coupling can in fact suffer from RG-running instability, i.e. large enhancements of λ_S at high energies, thus spoiling inflation. Therefore, we require $\lambda_S(m_s) \sim \lambda_S(M_p)$ for stability reasons. Imposing this requirement on eq. (5.1) leads to constraints on the squared Higgs portal couplings $\lambda_{1S,2S,12S}^2$ and on the trace of right handed neutrino Yukawas $\text{Tr} \left(Y_N^\dagger Y_N Y_N^\dagger Y_N \right)$, as we will argue now.

As a first observation, we can neglect the terms proportional to λ_S on the right hand side of eq. (5.1). This is per our request for negligible running of λ_S . Furthermore, the RG running effects of the portal couplings and the right handed neutrino Yukawas are taken to be negligible due to RG stability. With these reasonable assumptions, we can integrate eq. (5.1) and find

$$\frac{\lambda_S(\mu)}{\lambda_S(m_s)} \approx 1 + \frac{1}{4\pi^2 \lambda_S(m_s)} \left[\lambda_{1S}^2(m_s) + \lambda_{2S}^2(m_s) + 2\lambda_{12S}^2(m_s) - \frac{1}{2} \text{Tr} \left(Y_N^\dagger Y_N Y_N^\dagger Y_N \right)_{m_s} \right] \log \frac{\mu}{m_s}. \quad (5.2)$$

From eq. (5.2) we can see that the portal couplings enhance, while the right handed neutrino Yukawas diminish λ_S . This endangers vacuum stability (cf. Ref. [2]) and can be avoided in one of two ways. Either the portal coupling contribution is greater than the Yukawa contribution or both contributions are negligible compared to λ_S . By choosing the latter, we avoid tremendous fine tuning at the matching scale m_s which leads to the following constraints

$$\left. \begin{array}{l} |\lambda_{1S}(m_s)| \\ |\lambda_{2S}(m_s)| \\ |\lambda_{12S}(m_s)| \\ \sqrt{\text{Tr} \left(Y_N^\dagger Y_N Y_N^\dagger Y_N \right)_{m_s}} \end{array} \right\} \ll \sqrt{\lambda_S(m_s)} \approx 10^{-5}, \quad (5.3)$$

implying $\lambda_S(M_p) \approx \lambda_S(m_s) \approx 10^{-10}$ as expected. Note that the small value of λ_S is technically natural when the portal couplings are also small, as shown in eq.(5.3). The portal couplings are technically natural due to the enhanced Poincare symmetry as shown in sec. 3 and also pointed out in Ref. [23, 24].

5.2 RG-Analysis with BAU and thermal leptogenesis

In the previous section we derived an upper bound on $\text{Tr} \left(Y_N^\dagger Y_N Y_N^\dagger Y_N \right)$ at the scale m_s (see eq. (5.3)). This upper bound can be further specified for higher energy domains, e.g. $\mu \simeq 30M_p$, in order to investigate the minimum condition of λ_S [2]. Therefore, by considering $\mu \simeq 30M_p$ we obtain

$$Y_N \lesssim \left(\frac{8\pi^2 \lambda_S}{163 \log \left(\frac{30M_p}{m_s} \right)} \right)^{1/4}, \quad (5.4)$$

where $Y_{N,33} = Y_{N,22} = 3Y_{N,11}$ accommodates vanilla leptogenesis with hierarchical right-handed neutrinos. By considering the right-handed neutrino masses given by

$$M_{N,i} = \frac{Y_{N,i} v_S}{\sqrt{2}} \quad (5.5)$$

with $M_{N,3} = M_{N,2} = 3M_{N,1}$, we can convert the upper bound of eq. (5.4) to an upper bound on $M_{N,1}$:

$$M_{N,1} \lesssim \frac{\sqrt{2}}{v_S} \left(\frac{8\pi^2 \lambda_S}{163 \log \left(\frac{30M_p}{m_s} \right)} \right)^{1/4}. \quad (5.6)$$

The CP-violating and out-of-equilibrium decay of the lightest right-handed neutrino $N_1 \rightarrow l\Phi_1$ produces BAU via thermal leptogenesis [2, 23, 51]. This is quantified by the CP-asymmetry ϵ_1 which is given by [52–55]:

$$\epsilon_1 = \frac{\Gamma_D(N_1 \rightarrow l\Phi_1) - \Gamma_D(N_1 \rightarrow l^*\Phi_1^*)}{\Gamma_D(N_1 \rightarrow l\Phi_1) + \Gamma_D(N_1 \rightarrow l^*\Phi_1^*)} \simeq \frac{1}{8\pi} \frac{\sum_j \text{Im} \left[\left(Y_\nu Y_\nu^\dagger \right)_{1j}^2 \right]}{\left(Y_\nu Y_\nu^\dagger \right)_{11}} g(x_{1j}), \quad (5.7)$$

where $g_{1j}(x_{1j})$ is given as

$$g_{1j}(x_{1j}) = \sqrt{x_{1j}} \left(\frac{2 - x_{1j}}{x_{1j} - 1} + (1 + x_{1j}) \log \left(\frac{1 + x_{1j}}{x_{1j}} \right) \right) \quad \text{with} \quad x_{1j} = \frac{M_j^2}{M_1^2}. \quad (5.8)$$

For $x_{1j} > 1$ we can approximate the CP-asymmetry as follows [55]:

$$\epsilon_1 \simeq -\frac{3}{16\pi} \frac{\sum_j \text{Im} \left[\left(Y_\nu Y_\nu^\dagger \right)_{1j}^2 \right]}{\left(Y_\nu Y_\nu^\dagger \right)_{11}} \left(\frac{M_1}{M_j} \right) = -\frac{3M_1}{16\pi} \frac{\sum_j \text{Im} \left[\left(Y_\nu m_\nu^\dagger Y_\nu^\dagger \right)_{1j}^2 \right]}{\left(Y_\nu Y_\nu^\dagger \right)_{11}}, \quad (5.9)$$

where we used eq. (2.13) to substitute the light neutrino mass matrix m_ν . Based on the observed BAU we need to place an upper bound on ϵ_1 . Therefore, we further simplify ϵ_1 by using the Casas-Ibarra parametrization for the light neutrino Yukawa coupling Y_ν :

$$Y_\nu = \frac{\sqrt{2}}{v_1} D_{\sqrt{M}} R D_{\sqrt{m}} U_\nu^\dagger, \quad (5.10)$$

where $D_{\sqrt{A}} \equiv \text{diag}(\sqrt{a_1}, \sqrt{a_2}, \sqrt{a_3})$ and R is an orthogonal (complex) matrix with $R^\dagger R = \mathbb{1}$. In particular, we use the fact that we sum over two right-handed neutrinos and use the orthogonality condition $\sum_j R_{1j}^2 = 1$. We can therefore approximate the upper bound as:

$$|\epsilon_1| \lesssim \frac{3}{16\pi} \frac{M_1}{v_1^2} (m_3 - m_1). \quad (5.11)$$

For simplification we set $m_1 \simeq 0$ and therefore get:

$$|\epsilon_1| \lesssim \frac{3}{16\pi} \frac{M_1}{v_2^2} m_3. \quad (5.12)$$

This upper bound on ϵ_1 can be translated into a lower bound on the lightest right-handed neutrino mass $M_{N,1}$, i.e. Davidson-Ibarra bound [55]:

$$M_{N,1} \gtrsim \frac{5 \times 10^8 \text{ GeV}}{1 + t_\beta^2}, \quad (5.13)$$

which translates into a lower bound for $Y_{N,11}$

$$Y_{N,11} \gtrsim \frac{7.1 \times 10^8 \text{ GeV}}{v_S (1 + t_\beta^2)}. \quad (5.14)$$

By combining equations (5.14) and (5.4) we obtain the range for $Y_{N,11}$:

$$\frac{7.1 \times 10^8 \text{ GeV}}{v_S (1 + t_\beta^2)} \lesssim Y_{N,11} \lesssim \left(\frac{8\pi^2 \lambda_S}{163 \log \left(\frac{30 M_P}{m_s} \right)} \right)^{1/4}. \quad (5.15)$$

Once $Y_{N,11}$ is constrained by v_S , t_β and λ_S we are left with only nine degrees of freedom, namely $Y_{\nu,ij}$. In order to obtain the left-handed neutrino Yukawa couplings Y_ν , we need to calculate [56]

$$Y_\nu = \frac{\sqrt{1 + t_\beta^2}}{v} \mathcal{D}_{\sqrt{M}} O \mathcal{D}_{\sqrt{m_\nu}} U_\nu^\dagger, \quad (5.16)$$

where

$$\mathcal{D}_{\sqrt{M}} \equiv \text{diag} \left(\sqrt{M_{N,1}}, \sqrt{3M_{N,1}}, \sqrt{3M_{N,1}} \right), \quad (5.17)$$

$$\mathcal{D}_{\sqrt{m_\nu}} \equiv \text{diag} \left(\sqrt{m_{\nu,1}}, \sqrt{m_{\nu,2}}, \sqrt{m_{\nu,3}} \right) \quad (5.18)$$

denote the diagonalized right-handed Majorana and left-handed Dirac neutrino mass matrix respectively. U_ν is the PMNS-neutrino mixing matrix whose components are given by the best global fits of Ref. [57]. O is a 3×3 -orthogonal matrix which is in general complex and consists of three complex angles. However, we follow the same line of reasoning as in Ref. [2] by taking O to be of unity since we can neglect $\mathcal{O}(1)$ contributions for the RGE stability analysis. Furthermore, the left-handed neutrinos are constrained by neutrino oscillation experiments [57] and cosmological neutrino observations [42]. From the PLANCK 2018 [42] constraints we obtain the upper bound on the sum of the neutrino masses:

$$\sum_{i=1}^3 m_{\nu,i} < 0.12 \text{ eV} \quad (95\% \text{ C.L. Planck TT,TE,EE+lowE+lensing+BAO}). \quad (5.19)$$

The experimental best fit constraints of neutrino masses from atmospheric and solar mass splitting [57] for normal ordering (NO) are given by:

$$\Delta m_{21}^2 \left(10^{-5} \text{ eV}^2 \right) = 7.5_{-0.2}^{+0.22}, \quad \Delta m_{31}^2 \left(10^{-3} \text{ eV}^2 \right) = 2.55_{-0.03}^{+0.02} \quad (\text{best fit } \pm 1\sigma, \text{ NO}). \quad (5.20)$$

We consider a hierarchical mass ordering $m_{\nu,1} < m_{\nu,2} < m_{\nu,3}$ where we take, as mentioned above, $m_{\nu,1} \equiv m_1 \simeq 0$. Then, the left-handed neutrino Yukawa matrix is given by:

$$Y_{\nu,(i+1)j} \simeq \frac{1}{v} \sqrt{\frac{3}{\sqrt{2}} Y_{N,11} m_{\nu,(i+1)} \left(1 + t_\beta^2\right)} v_S U_{\nu,j(i+1)}^* \quad \text{with} \quad Y_{\nu,1j} \simeq 0, \quad (5.21)$$

where $m_{\nu,2}$ and $m_{\nu,3}$ are given by:

$$m_{\nu,2} \simeq \Delta m_{2,1} \simeq 8.66 \text{ meV} \quad , \quad m_{\nu,3} \simeq \sqrt{\Delta m_{2,1}^2 + \Delta m_{3,1}^2} \simeq 51.23 \text{ meV}. \quad (5.22)$$

Since $m_{\nu,3} \gg m_{\nu,2} \gg m_{\nu,1}$ and $U_{\nu,32,33}^* \gtrsim U_{\nu,ij}^*$, we only consider $Y_{\nu,32,33}$ for the remainder of this paper, i.e.

$$Y_{\nu,32,33} \simeq \frac{1}{v} \sqrt{\frac{3}{\sqrt{2}} Y_{N,11} m_{\nu,3} \left(1 + t_\beta^2\right)} v_S U_{\nu,32,33}^*. \quad (5.23)$$

The aforementioned nine degrees of freedom are thus constrained by experimental values and by the benchmark relevant parameter t_β . Hence, we can account for BAU by vanilla thermal leptogenesis with hierarchical normal ordering of the light neutrino masses.

There are a few caveats to consider regarding the size of the neutrino couplings in the RG-flow of λ_{1S} . Therefore, we consider the RGE of λ_{1S} :

$$\begin{aligned} \mathcal{D}\lambda_{1S} = & \lambda_{1S} \left(-\frac{3}{2}g_1^2 - \frac{9}{2}g_2^2 + 4\lambda_{1S} + 4\lambda_S + 6\lambda_1 \right) + \lambda_{2S} (4\lambda_3 + 2\lambda_4) + 8\lambda_{12S}^2 \\ & + \lambda_{1S} \left(6Y_b^2 + 2Y_\tau^2 + 2\text{Tr} \left(Y_\nu^\dagger Y_\nu \right) + \text{Tr} \left(Y_N^\dagger Y_N \right) \right) - 4\text{Tr} \left(Y_\nu^\dagger Y_\nu Y_N^\dagger Y_N \right). \end{aligned} \quad (5.24)$$

As we can see the running is dominated by the size of λ_{1S} , λ_{2S} and $\text{Tr} \left(Y_\nu^\dagger Y_\nu Y_N^\dagger Y_N \right)$ where the latter contributes negatively on the running. For PQTHI-scenarios we do not have to worry about the size of the neutrino Yukawa term since $\lambda_{1S,2S} \gg \text{Tr} \left(Y_\nu^\dagger Y_\nu Y_N^\dagger Y_N \right)$ which is thus negligible. However, for PQI the portal couplings can be of the same size as the neutrino Yukawa term, i.e. $\lambda_{1S,2S} \sim \text{Tr} \left(Y_\nu^\dagger Y_\nu Y_N^\dagger Y_N \right)$, which causes λ_{1S} to run negative at higher energies. In order to secure positive portal couplings at the inflationary scale for PQI, we impose a condition on the initial value of λ_{1S} to guarantee $\lambda_{1S}(M_P) > 0$:

$$\lambda_{1S} \gtrsim \text{Tr} \left(Y_\nu^\dagger Y_\nu Y_N^\dagger Y_N \right). \quad (5.25)$$

For the remainder of the paper, we will only consider the real entries of Y_ν , i.e. $\text{Re}(Y_{\nu,ij})$, since the RG-analysis, except for Y_ν itself, is independent of the imaginary part. The RG-running of Y_ν is severely suppressed by multiplicatives of its own value at the electroweak scale (see eq. (D.17)). Therefore, its value at the electroweak scale can be approximated to be the same at the inflationary scale. The same applies even more so for Y_N . We demonstrate this fact in figure 5 for $Y_{\nu,32,33}$ and $Y_{N,1}$. We can see that the values of the Yukawa couplings are approximately the same at the inflationary scale as they are at the electroweak scale. However, for completeness, we will include the running of the neutrino Yukawas into our RG-analysis but note that their value is almost scale-invariant, as we would expect from looking at the RGEs of eqns (D.17)-(D.18) of appendix D.

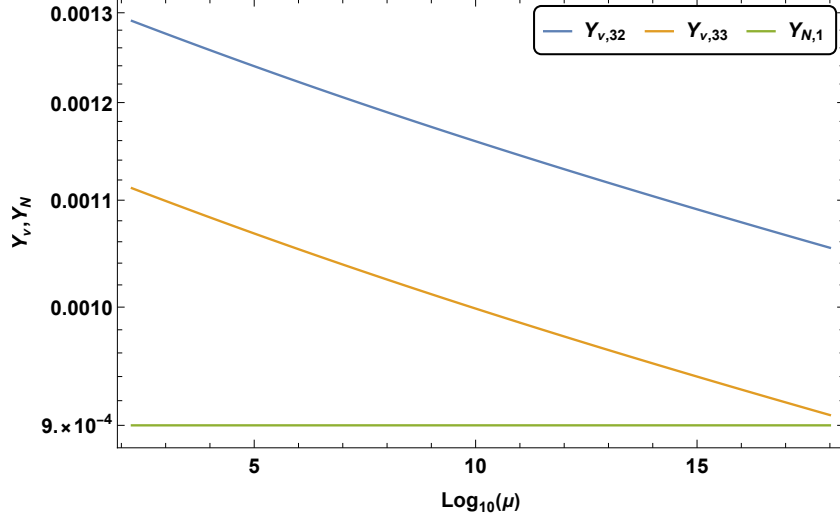


Figure 5: Shown are the the RG-running of the largest components of the Dirac neutrino couplings $Y_{\nu,32,33}$ and the main Majorana neutrino coupling $Y_{N,1}$ with $t_\beta = 5.5$, $\lambda_S = 10^{-10}$ and $v_S = 10^{10}$ GeV. The renormalization scale is set by the top pole mass $m_t = (172.5 \pm 0.7)$ GeV given by Ref. [49] to run from low- to high scale.

5.3 Interconnection of portal couplings

In this section we consider the effects of the one-loop RG running of the portal couplings and make the connection between inflation and Higgs phenomenology. We evolve the couplings from the electroweak scale all the way up to the Planck scale and discuss the intricacies of satisfying the constraints for successful inflation (see Table 3) while accommodating a 125 GeV Higgs with additional heavy Higgses at the electroweak/TeV scale. In particular, we will discuss the running of the portal couplings and its impact on the inflationary field direction with regard to inflationary conditions (see Table 3 for details). Therefore, we pay attention to the size of the portal coupling and consider its sign at the Planck scale. We introduce in Table 4 benchmark points representing inflation in the sh_{12} -, sh_2 - and s -direction which satisfy our considerations and convey the statement of our discussion.

As discussed in section 3 we determined that the squared masses of the heavy Higgses strongly depend on $\lambda_{12S}v_S^2$. In fact, a tiny value for λ_{12S} is preferred by high-scale validity analysis [58, 59] since $\lambda_{12S}v_S^2$ resembles a soft breaking parameter in a softly broken $U(1)$ -symmetric 2HDM⁹ [23, 60]. Therefore, we first consider the RG running of λ_{12S} . We can already see that the running of λ_{12S} is proportional to itself:

$$\mathcal{D}\lambda_{12S} = \lambda_{12S} \left(-\frac{3}{2}g_1^2 - \frac{9}{2}g_2^2 + 2\lambda_3 + 4\lambda_4 + 2\lambda_S + 4(\lambda_{1S} + \lambda_{2S}) + 3Y_t^2 + 3Y_b^2 + Y_\tau^2 \right). \quad (5.26)$$

By considering the value of λ_{12S} at the electroweak scale we determine the size of heavy Higgs masses since we fix the PQ-breaking scale at $v_S = 3 \times 10^{10}$ GeV. Hence, λ_{12S} is chosen to be tiny as argued in section 3 to acquire a phenomenologically viable model which can be tested at the HL-LHC or future colliders. This smallness is associated with an enhanced Poincaré symmetry which we have discussed in section F. The size of λ_{12S} will be preserved all the way up to the Planck scale, thus justifying the considerations of Section 4. By analyzing the RG evolution of λ_{1S} and λ_{2S} we can determine whether we satisfy PQI or PQTHI directions at the

⁹In section F we describe the effective low-energy matching of 2hdSMASH to a softly broken $U(1)$ -symmetric 2HDM.

Parameters	BP- sh_{12}	BP- sh_2	BP- s
λ_1	0.07	0.07	0.07
λ_2	0.263	0.287	0.258
λ_3	0.60	0.54	0.54
λ_4	-0.40	-0.14	-0.14
λ_S	6.5×10^{-10}	4.44×10^{-10}	10^{-10}
λ_{1S}	-6.59×10^{-6}	5.57×10^{-6}	4.8×10^{-14}
λ_{2S}	10^{-15}	-4.27×10^{-6}	10^{-15}
λ_{12S}	2.5×10^{-16}	2.5×10^{-16}	2.5×10^{-16}
$\tan \beta$	5.5	5.5	26
$Y_{N,1}$	9×10^{-4}	9×10^{-4}	4×10^{-5}
$Y_{\nu,3}$	5.18×10^{-3}	5.18×10^{-3}	1.09×10^{-3}
v_S	3×10^{10}	3×10^{10}	3×10^{10}
m_h (GeV)	125.2	125.2	125.1
m_H (GeV)	799.4	798.8	1711.5
m_s (GeV)	6.6×10^5	6.3×10^5	3×10^5
m_A (GeV)	799.5	799.5	1711.5
m_{H^\pm} (GeV)	807.0	802.2	1712.8

Table 4: Three benchmarks passing theoretical and experimental constraints representative for inflation in sh_{12} -, sh_2 - and s -direction. The top pole mass is given by Ref. [49] to be $m_t = (172.5 \pm 0.7)$ GeV.

Planck scale. The RGEs of λ_{1S} and λ_{2S} are given by:

$$\begin{aligned} \mathcal{D}\lambda_{1S} = & \lambda_{1S} \left(-\frac{3}{2}g_1^2 - \frac{9}{2}g_2^2 + 4\lambda_{1S} + 4\lambda_S + 6\lambda_1 \right) + \lambda_{2S} (4\lambda_3 + 2\lambda_4) + 8\lambda_{12S}^2 \\ & + \lambda_{1S} \left(6Y_b^2 + 2Y_\tau^2 + 2\text{Tr} \left(Y_\nu^\dagger Y_\nu \right) + \text{Tr} \left(Y_N^\dagger Y_N \right) \right) - 4\text{Tr} \left(y_\nu^\dagger Y_\nu Y_N^\dagger Y_N \right), \end{aligned} \quad (5.27)$$

$$\begin{aligned} \mathcal{D}\lambda_{2S} = & \lambda_{2S} \left(-\frac{3}{2}g_1^2 - \frac{9}{2}g_2^2 + 4\lambda_{2S} + 4\lambda_S + 6\lambda_2 \right) + \lambda_{1S} (4\lambda_3 + 2\lambda_4) + 8\lambda_{12S}^2 \\ & + \lambda_{2S} \left(6Y_t^2 + \text{Tr} \left(Y_N^\dagger Y_N \right) \right). \end{aligned} \quad (5.28)$$

Since λ_{12S} , Y_N and Y_ν are very small, we can safely neglect terms involving them. Thus, we can rewrite the RGEs of the portal couplings as follows:

$$\mathcal{D}\lambda_{1S} \simeq \lambda_{1S} \left(-\frac{3}{2}g_1^2 - \frac{9}{2}g_2^2 + 4\lambda_{1S} + 4\lambda_S + 6\lambda_1 + 6y_b^2 + 2y_\tau^2 \right) + \lambda_{2S} (4\lambda_3 + 2\lambda_4), \quad (5.29)$$

$$\mathcal{D}\lambda_{2S} \simeq \lambda_{2S} \left(-\frac{3}{2}g_1^2 - \frac{9}{2}g_2^2 + 4\lambda_{2S} + 4\lambda_S + 6\lambda_2 + 6y_t^2 \right) + \lambda_{1S} (4\lambda_3 + 2\lambda_4). \quad (5.30)$$

There are two terms to consider, namely the first term which is proportional to the evolving portal coupling itself and the second term which is proportional to the other portal coupling. We notice that the combination of both terms will determine the size of the portal coupling at the Planck scale. Unfortunately, we cannot solve these RGEs analytically but we can analyze their contributions and make a statement about the size and the behavior of their evolution so that we end up with the required conditions for PQI or PQTHI at the Planck scale. There are three separate scenarios concerning the size of the portal couplings, i.e.

$$|\lambda_{1S}| < |\lambda_{2S}| \quad , \quad |\lambda_{1S}| > |\lambda_{2S}| \quad , \quad |\lambda_{1S}| \sim |\lambda_{2S}|, \quad (5.31)$$

where only two of them will be our main focus. Therefore, we will consider without loss of generality benchmarks BP- sh_{12} and BP- sh_2 - BP- s of Table 4 for the cases $|\lambda_{1S}| > |\lambda_{2S}|$ and $|\lambda_{1S}| \sim |\lambda_{2S}|$ respectively. Starting with the latter will help clarify the various contributions to the RGEs of λ_{1S} and λ_{2S} .

$|\lambda_{1S}| \sim |\lambda_{2S}|$: Both portal couplings will influence the running of each other. Therefore it is necessary to analyze which contributions will have the dominant influence. Since the top Yukawa coupling is larger than the bottom- and the τ -Yukawa couplings, the influence of λ_{2S} will dominate the evolution of λ_{1S} . Hence, λ_{1S} will evolve towards the value of λ_{2S} when approaching the Planck scale. This can be circumvented by approximating the RGEs further and modifying the portal couplings accordingly. By comparison, we can neglect $Y_{b,\tau}$, $\lambda_{1,2,S}$ and $g_{1,2}$ since the portal couplings are equal in size and the top Yukawa term dominates the running of λ_{2S} . This is due to the fact that the top Yukawa dominates in the low-energy regime and becomes in comparison less dominant in the high energy regime. Thus, the running of λ_{2S} affects the running of λ_{1S} by the coupling term involving λ_3 and λ_4 . We therefore assume λ_3 and λ_4 not to grow significantly when approaching the Planck scale¹⁰. Hence, the RGEs of $\lambda_{1S,2S}$ for $|\lambda_{1S}| \sim |\lambda_{2S}|$ can be approximated to:

$$\mathcal{D}\lambda_{1S} \approx \lambda_{2S} (4\lambda_3 + 2\lambda_4), \quad (5.32)$$

$$\mathcal{D}\lambda_{2S} \approx 6\lambda_{2S}y_t^2. \quad (5.33)$$

The running of λ_{2S} will dominate unless we implement a correction to the initial value of λ_{1S} so that both portal couplings will preserve their respective sign and size at the Planck scale. Considering the chain rule, we can reformulate the two RGEs in order to obtain a differential equation:

$$\mathcal{D}\lambda_{1S} = \frac{\partial\lambda_{1S}}{\partial\lambda_{2S}}\mathcal{D}\lambda_{2S} \approx \lambda_{2S} (4\lambda_3 + 2\lambda_4) \quad (5.34)$$

$$\Rightarrow \frac{\partial\lambda_{1S}}{\partial\lambda_{2S}} \approx \frac{2\lambda_3 + \lambda_4}{3y_t^2}. \quad (5.35)$$

By integrating both sides, we obtain the necessary correction for λ_{1S} to counter the effect of the top Yukawa:

$$\delta\lambda_{1S} \approx \frac{\lambda_{2S} (2\lambda_3 + \lambda_4)}{3y_t^2}, \quad (5.36)$$

where $|\lambda_{1S}| \simeq |\lambda_{2S}|$. Hence, the initial value for λ_{1S} is given by:

$$|\lambda_{1S}^{\text{corr.}}(\mu_{EW})| = |\lambda_{1S} + \delta\lambda_{1S}|_{\mu_{EW}} \approx \left| \lambda_{2S} \times \left(1 + \frac{2\lambda_3 + \lambda_4}{3y_t^2} \right) \right|_{\mu_{EW}}, \quad (5.37)$$

where μ_{EW} is the electroweak scale and $\lambda_{1S}^{\text{corr.}}$ is the corrected value of λ_{1S} . This correction causes both RGEs to be of equal size and preserve their respective sign at the Planck scale. Therefore, this case describes inflation in the sh_1 or sh_2 direction where either portal coupling differs by sign change. For illustration we consider the case where $\lambda_{1S} > 0$ and $\lambda_{2S} < 0$ given by benchmark point BP- sh_2 . In figure 6 we can see the running of both portal couplings with and without a correction applied to $\lambda_{1S}(\mu)$. As described above, we can see that the correction preserves the sign of both portal couplings all the way up to the Planck scale. The same line of reasoning applies to sh_1 by switching signs of λ_{1S} and λ_{2S} . For the benchmark point BP- s

¹⁰We require λ_3 and λ_4 to run perturbative to high energies and thus prefer that exponential growth near the Planck scale is suppressed.

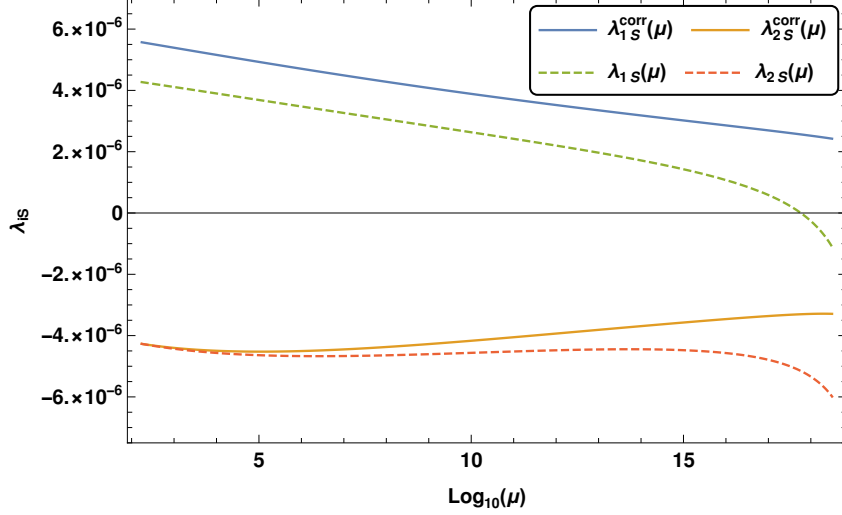


Figure 6: RG evolution of λ_{1S} and λ_{2S} of BP- sh_2 where $|\lambda_{1S}| \sim |\lambda_{2S}|$ with opposite signs. Here, the initial value of $\lambda_{1S}^{\text{corr}}$ is given by eq. (5.37) which affects the running of λ_{1S} positively compared to the running where no correction is applied.

of Table 4 both portal couplings are taken positive. However, the running of λ_{1S} and λ_{2S} is dominantly determined by the left- and right-handed Yukawa couplings. In section 5.2 we discussed the appropriate initial value λ_{1S} needs (see eq. (5.25)) in order for both portal couplings to remain positive at the Planck scale.

$|\lambda_{1S}| > |\lambda_{2S}|$: In general, this case describes either PQI or PQTHI- sh_{12} since both portal couplings will be either positive (PQI) or negative (PQTHI- sh_{12}) at the Planck scale, as we will argue now. For PQI, we consider tiny portal couplings which is represented in benchmark BP- s . Therefore, we will refer to PQTHI- sh_{12} for a more general discussion where portal couplings are assumed to be sizable compared to PQI. We consider BP- sh_{12} of table 4, where $\lambda_{1S} < 0$ and $\lambda_{2S} > 0$ but differ in size, i.e. $|\lambda_{1S}| > |\lambda_{2S}|$ at the electroweak scale. Thus, we can approximate the RGEs of λ_{1S} and λ_{2S} by

$$\mathcal{D}\lambda_{1S} \approx \lambda_{1S} \left(-\frac{3}{2}g_1^2 - \frac{9}{2}g_2^2 + 4\lambda_{1S} + 4\lambda_S + 6\lambda_1 + 6y_b^2 + 2y_\tau^2 \right), \quad (5.38)$$

$$\mathcal{D}\lambda_{2S} \approx \lambda_{1S} (4\lambda_3 + 2\lambda_4), \quad (5.39)$$

where only contributions of λ_{1S} are considered since λ_{2S} is sub-dominant in comparison. This approximation is illustrated in Figure 7 where λ_{2S} approaches the value of λ_{1S} and they become equal at the Planck scale.

5.4 Stability analysis

In this section we analyze vacuum stability, perturbative unitarity and high-scale validity of 2hdSMASH. Vacuum stability is mostly endangered by λ_2 running negative. For a Type-II 2HDM, the Higgs doublet Φ_2 couples to the top-quark which can force λ_2 into negative values. The same phenomenon has been observed in the SM, which is regarded as the top-quark instability. We show, that we can circumvent this problem by stabilizing the running of λ_2 with the mixing parameter λ_{34} . For that reason, we consider the necessary BfB condition of the 2HDM

$$\lambda_{34} \geq -\sqrt{\lambda_1 \lambda_2}, \quad (5.40)$$

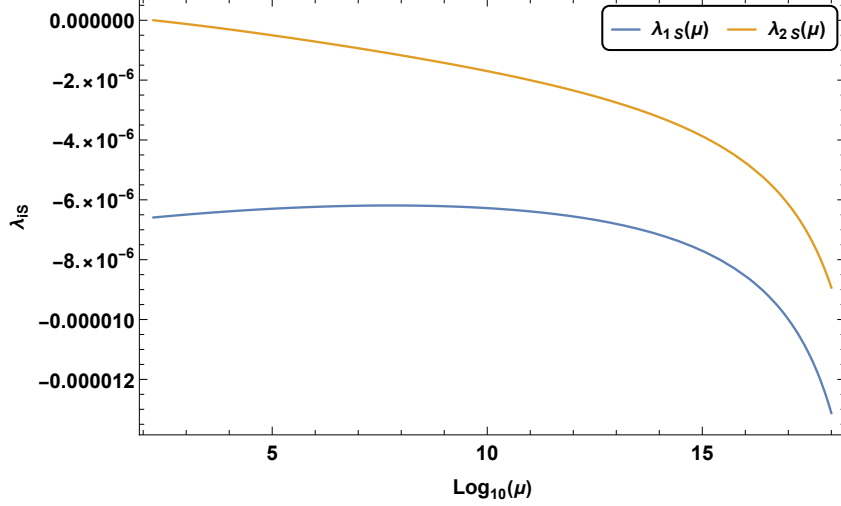


Figure 7: RG evolution of portal couplings λ_{1S} and λ_{2S} for sh_{12} -inflation using BP- sh_{12} from Table 4. The top pole mass $m_t = (172.5 \pm 0.7)$ GeV given by Ref. [49] is used to set the renormalization scale for the benchmarks to run from low- to high scale.

which we can translate into the following form

$$\frac{\lambda_{34}^2}{\lambda_1} \geq -\lambda_2. \quad (5.41)$$

We identify in eq. (5.41) the parameter δ given by

$$\delta \equiv \frac{\lambda_{34}^2}{\lambda_1}, \quad (5.42)$$

which we will use to stabilize the running effects of λ_2 as we will argue in the following.

The instability can be understood by considering the one-loop RGE of λ_2 :

$$\begin{aligned} \mathcal{D}\lambda_2 = & \frac{3}{4}g_1^4 + \frac{3}{2}g_1^2g_2^2 + \frac{9}{4}g_2^4 - \frac{9}{5}g_1^2\lambda_2 - 9g_2^2\lambda_2 + 12\lambda_2^2 + 2\lambda_{2s}^2 \\ & + 4\lambda_3^2 + 4\lambda_3\lambda_4 + 2\lambda_4^2 + 12\lambda_2Y_t^2 - 12Y_t^4, \end{aligned} \quad (5.43)$$

where the dominant negative top Yukawa contribution $\propto Y_t^4$ is competing with other dominant quartic coupling terms. It proves useful to consider λ_3 and λ_4 for stabilization since it contributes positively to its RG-running and λ_1 is absent. However, enhancing λ_1 would only contribute indirectly to the RG-running of λ_2 by its mediator couplings λ_3 and λ_4 . Hence, we fix λ_1 and vary λ_3 and λ_4 for stabilization. By considering the RGE of λ_1 , we recognize that the same λ_3 and λ_4 contributions affect its running

$$\begin{aligned} \mathcal{D}\lambda_1 = & \frac{3}{4}g_1^4 + \frac{3}{2}g_1^2g_2^2 + \frac{9}{4}g_2^4 - \lambda_1(3g_1^2 + 9g_2^2) + 12\lambda_1^2 + 4\lambda_3\lambda_4 + 4\lambda_3^2 + 2\lambda_4^2 + 2\lambda_{1S}^2 \\ & + 12\lambda_1Y_b^2 - 12Y_b^4 + 4\lambda_1Y_\tau^2 - 4Y_\tau^4 + 4\lambda_2\text{Tr}(Y_\nu^\dagger Y_\nu) - 4\text{Tr}(Y_\nu^\dagger Y_\nu Y_\nu^\dagger Y_\nu), \end{aligned} \quad (5.44)$$

where negative terms, such as the down-type Yukawa contribution is sub-dominant in comparison. Therefore, any enhancement of λ_3 and λ_4 will enhance λ_1 by going to higher energies and thus endangering perturbative unitarity. This can be avoided by applying the perturbative

unitarity bounds for λ_1 and λ_{34} , such that

$$|\delta| \equiv \left| \frac{\lambda_{34}^2(\mu)}{\lambda_1(\mu)} \right| < 8\pi \quad , \quad \forall \mu \quad (5.45)$$

is bounded from above. Furthermore, we have to ensure that we maintain a 125 GeV light Higgs. Its mass is approximately

$$m_h^2 \approx \frac{v_S^2}{(1+t_\beta^2)^2} \left[\lambda_1 + t_\beta^4 \lambda_2 + 2 t_\beta^2 \lambda_{34} \right] , \quad (5.46)$$

where portal terms are neglected for now. We can see that for $t_\beta > 1$, as considered in our case, the λ_2 term is t_β^2 times larger than the one with λ_{34} . Therefore, any enhancement in λ_{34} is met with a slight decrease in λ_2 since its decrease will counterbalance the increase of λ_{34} by a factor of t_β^2 . Thus, λ_{34} is capable to influence the RG-running of λ_2 without violating Higgs phenomenology.

There are two intertwining effects which stabilize the RG-running of λ_2 , namely

- 1) initial values given to λ_2 , λ_3 and λ_4 and
- 2) an RG-running effect caused by λ_3 and λ_4 .

Both effects, namely 1) and 2), contribute to the RG stabilization of λ_2 and are interconnected. Here, the emphasis is on the RG-running effects since they are responsible to uplift λ_2 from its negative top Yukawa running term at energy scales $\mu \gtrsim m_t$. In order to gain some analytical understanding, we consider the Coleman-Weinberg potential, cf. Ref. [61], which we will utilize to acquire $\lambda_2(\mu)$, i.e. the integrated version¹¹ of $\mathcal{D}\lambda_2$, to identify the dominant RG-running contributions. The full expression of the Coleman-Weinberg potential is given in appendix G, whose general analytical form is given by

$$V_{\text{CW}}(\phi_i) = \frac{1}{64\pi^2} \times \left(\sum_b g_b m_b^4(\phi_i) \left[\log \left(\frac{m_b^2(\phi_i)}{\Lambda^2} \right) - \frac{3}{2} \right] - \sum_f g_f m_f^4(\phi_i) \left[\log \left(\frac{m_f^2(\phi_i)}{\Lambda^2} \right) - \frac{5}{2} \right] \right) , \quad (5.47)$$

where $g_{f/b}$ are the degrees of freedom and $m_{f/b}$ are the masses of fermions/bosons. By performing a matching to an effective tree-level potential in the h_2 -direction

$$V_{\text{eff}} \simeq V_0 + V_{\text{CW}} \simeq \frac{\lambda_2^{\text{eff}} h_2^4}{8} \quad (5.48)$$

with

$$V_0 \simeq \frac{\lambda_2 h_2^4}{8} , \quad (5.49)$$

where $h_1 \simeq s \simeq 0$, we acquire an RG-improved potential for h_2 . As a result we obtain the effective coupling λ_2^{eff} by computing

$$\lambda_2^{\text{eff}} = \frac{8}{h_2^4} V_{\text{eff}}(h_2) , \quad (5.50)$$

¹¹This can be verified by using the *Callan-Symanzik* equation.

which is given by

$$\lambda_2^{\text{eff}} \simeq \lambda_2(m_t) + \frac{\lambda_{2S}^2 \left(\log \left(\frac{h_2^2 \lambda_{2S}^2}{2m_t^2} \right) - \frac{3}{2} \right) + \lambda_3^2 \left(\log \left(\frac{h_2^2 \lambda_3^2}{2m_t^2} \right) - \frac{3}{2} \right)}{16\pi^2} \quad (5.51)$$

$$+ \frac{(\lambda_3 + \lambda_4)^2 \left(\log \left(\frac{h_2^2 (\lambda_3 + \lambda_4)^2}{2m_t^2} \right) - \frac{3}{2} \right) + 6 \left(\lambda_2^2 \left(\log \left(\frac{27h_2^2 \lambda_2^2}{16m_t^2} \right) - \frac{3}{2} \right) - Y_t^4 \left(\log \left(\frac{h_2^2 Y_t^2}{2m_t^2} \right) - \frac{3}{2} \right) \right)}{16\pi^2},$$

where we neglected the sub-dominant gauge couplings $g_{1,2,3}$. Furthermore, we can neglect the portal coupling term $\propto \lambda_{2S}^2$ since its contribution is small in comparison¹². Thus, we find

$$\lambda_2^{\text{eff}} \approx \lambda_2(m_t) + \frac{\lambda_3^2 \left(\log \left(\frac{h_2^2 \lambda_3^2}{2m_t^2} \right) - \frac{3}{2} \right) + (\lambda_3 + \lambda_4)^2 \left(\log \left(\frac{h_2^2 (\lambda_3 + \lambda_4)^2}{2m_t^2} \right) - \frac{3}{2} \right)}{16\pi^2} \quad (5.52)$$

$$+ \frac{6 \left(\lambda_2^2 \left(\log \left(\frac{27h_2^2 \lambda_2^2}{16m_t^2} \right) - \frac{3}{2} \right) - Y_t^4 \left(\log \left(\frac{h_2^2 Y_t^2}{2m_t^2} \right) - \frac{3}{2} \right) \right)}{16\pi^2}$$

with running scale $\mu \equiv h_2$. We can identify four stabilizing contributions, namely $\lambda_2(m_t)$, λ_2^2 , λ_{34}^2 and λ_3^2 . The former two, i.e. $\lambda_2(m_t)$ and λ_2^2 , are capable of stabilizing its running when large initial conditions are applied. Moreover, we can see that contributions proportional to λ_{34}^2 and λ_3^2 , enter quadratically as well and provide a further source of stabilization. In the case where λ_4 is negative, as we consider in our benchmarks, the most important parameter for RG-running stability becomes λ_3 which enters quadratically in two terms of eq. (5.52). This phenomenon is illustrated in figure 8 where $\lambda_2(\mu)$ is depicted for benchmark points BP- sh'_2 and BP- sh''_2 of table 5. Naively, we would expect that benchmark BP- sh'_2 has a sub-dominant effect on the running of λ_2 compared to BP- sh''_2 . Despite the fact, that the initial value of λ_2 is smaller in comparison, the dominance of λ_3 causes $\lambda_2(\mu)$ to run higher. This leaves BP- sh'_2 with the biggest impact. Moreover, we can associate the tree-level stability condition of eq. (5.41) to an RG-running stability condition

$$\delta(\mu) + \lambda_2(\mu) \geq 0 \quad , \quad \forall \mu, \quad (5.53)$$

where negative $\lambda_2(\mu)$ can be counterbalanced by $\delta(\mu)$. This effect can be seen in figure 9 by considering benchmarks BP- sh_2 and BP- sh'_2 of table 5. The tree-level effect is given by BP- sh_2 and depicted in figure 9 (left) with $\delta^{\text{BP-}sh_2} > \lambda_2^{\text{BP-}sh_2}$. By comparison, we can see in figure 9 (right) the RG-running effect of benchmark BP- sh'_2 which is mainly caused by the term $\sim \lambda_3^2$ of eq. (5.52). In our analysis we neglected terms $\propto \lambda_{2S}^2$ in the RG-running of λ_2 . This is due to the fact, that λ_{2S} is constrained by another stability condition, namely

$$\tilde{\lambda}_S \equiv \lambda_S - \frac{\lambda_{2S}^2}{\lambda_2} \geq 0. \quad (5.54)$$

This stability condition would be violated if we chose $\lambda_{2S}^2 \sim \lambda_2$, since $\lambda_S \sim 10^{-10}$. Thus, the portal coupling is constrained to be $\lambda_{2S} \lesssim \sqrt{\lambda_S}$ (see sec. 5.1). We show in figure 10 the RG-evolution of $\tilde{\lambda}_S$ and its scale-invariance. We note, that λ_3 and λ_{34}

¹²We list in table 5 three benchmarks, which represent the most extreme case where portal couplings are sizable, i.e. benchmarks for PQTHI- sh_2 . The contribution of the shown portal couplings is sub-dominant to eq. (5.51).

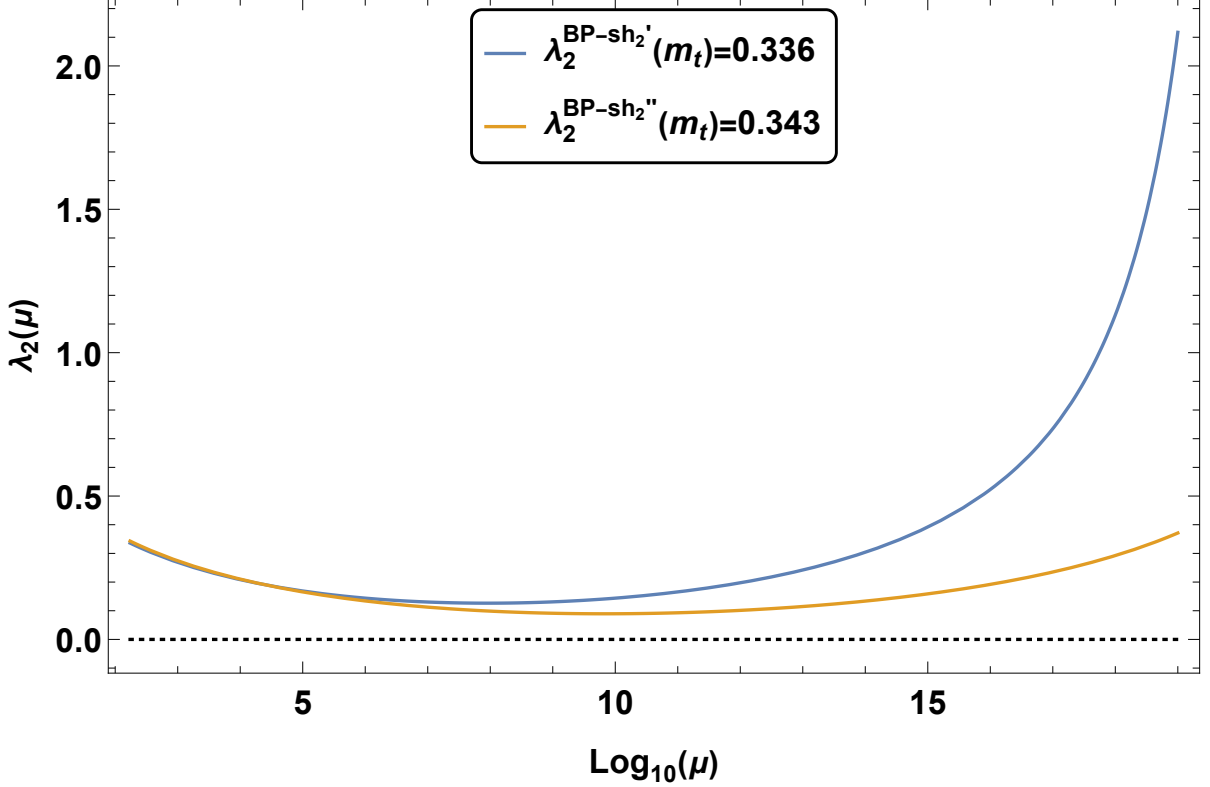


Figure 8: Shown are $\lambda_2(\mu)$ from benchmark BP- sh'_2 and BP- sh''_2 given in table 5. The top pole mass $m_t = (172.5 \pm 0.7)$ GeV given by Ref. [49] is used to set the renormalization scale for the benchmarks to run from low- to high scale.

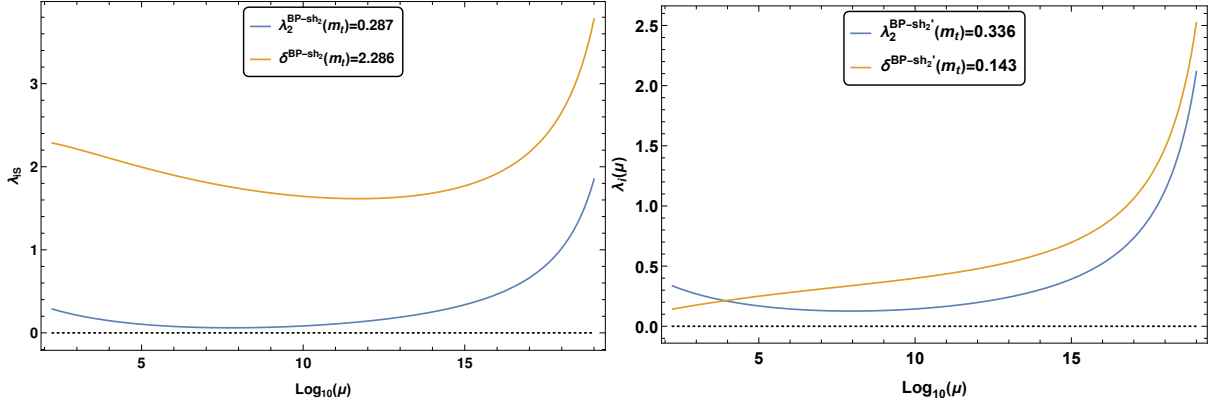


Figure 9: Shown are the RG-running of λ_2 and δ given by benchmark BP- sh_2 (left) and the RG-running of λ_2 and δ given by benchmark BP- sh'_2 of table 5. The renormalization scale is set at the top pole mass $m_t = (172.5 \pm 0.7)$ GeV, cf. Ref. [49], to run from low- to high scale.

are mainly responsible for stabilizing the RG-running of λ_2 . By erasing λ_1 , λ_3 , λ_4 , λ_{1S} and λ_{12S} from our model, we would recover the SMASH model. In particular, in the absence of λ_3 and λ_4 , the RG-running of λ_2 in 2hdSMASH becomes the RGE of λ_H in SMASH. By comparison, 2hdSMASH provides further parameters for stabilization, i.e. λ_3 and λ_4 , which is depicted in figure 11. We conclude, the mixing parameters λ_3 and λ_4 assist stabilizing the RG-running of λ_2 . Furthermore, the two intertwining effects, i.e. tree-level initial conditions and RG-effects, provide an analytic understanding how

Parameters	BP- sh_2	BP- sh'_2	BP- sh''_2
λ_1	0.07	0.07	0.07
λ_2	0.287	0.336	0.343
λ_3	0.54	0.54	0.44
λ_4	-0.14	-0.44	-0.44
λ_S	4.44×10^{-10}	4.44×10^{-10}	4.44×10^{-10}
λ_{1S}	5.57×10^{-6}	5.57×10^{-6}	5.57×10^{-6}
λ_{2S}	-4.27×10^{-6}	-4.27×10^{-6}	-4.27×10^{-6}
λ_{12S}	2.5×10^{-16}	2.5×10^{-16}	2.5×10^{-16}
$\tan \beta$	5.5	5.5	5.5
$Y_{N,1}$	9×10^{-4}	9×10^{-4}	9×10^{-4}
$Y_{\nu,3}$	5.18×10^{-3}	5.18×10^{-3}	5.18×10^{-3}
v_S	3×10^{10}	3×10^{10}	3×10^{10}
m_h (GeV)	125.2	125.1	125.2
m_H (GeV)	798.7	799.5	799.7
m_s (GeV)	6.3×10^5	6.3×10^5	6.3×10^5
m_A (GeV)	799.5	799.5	799.5
m_{H^\pm} (GeV)	802.1	807.7	807.7

Table 5: List of three benchmarks representing the most extreme case of portal coupling configuration which pass theoretical and experimental constraints and differ by λ_2 , λ_3 and λ_4 .

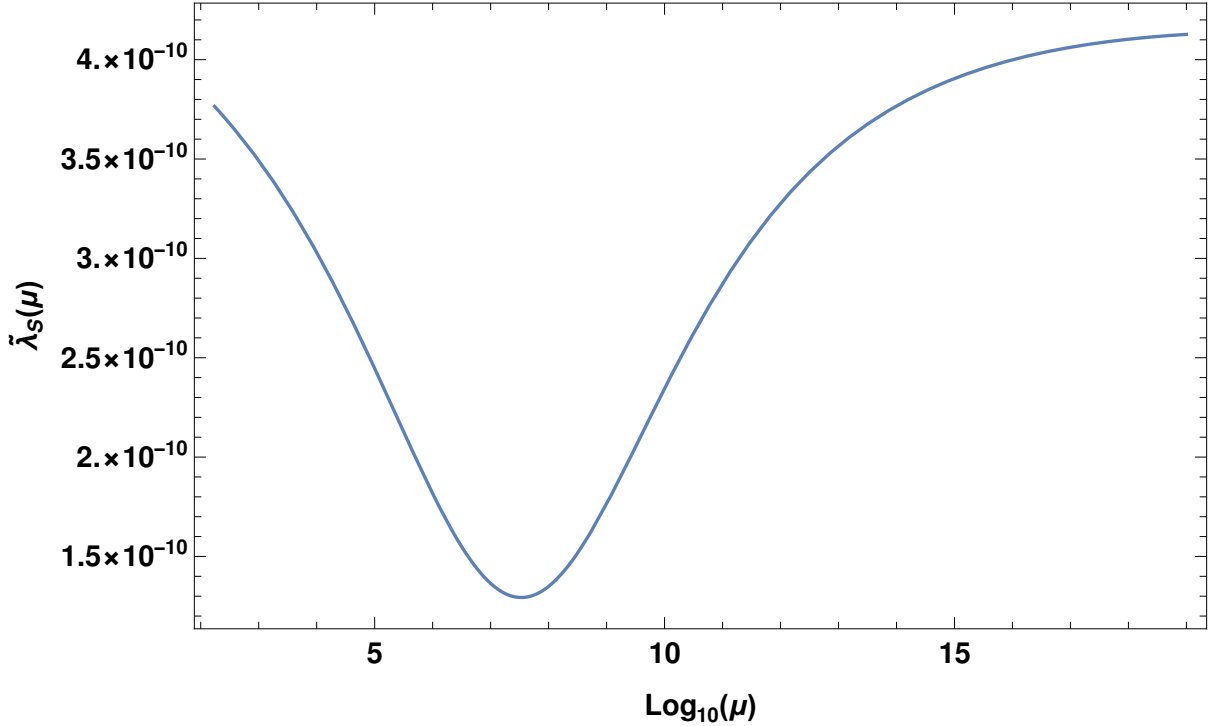


Figure 10: RG-evolution of $\tilde{\lambda}_S(\mu) \equiv \lambda_S(\mu) - \frac{\lambda_{2S}^2(\mu)}{\lambda_2(\mu)}$ from benchmark BP- sh_2 . The renormalization scale is set at the top pole mass $m_t = (172.5 \pm 0.7)$ GeV, cf. Ref. [49], to run from low- to high scale.

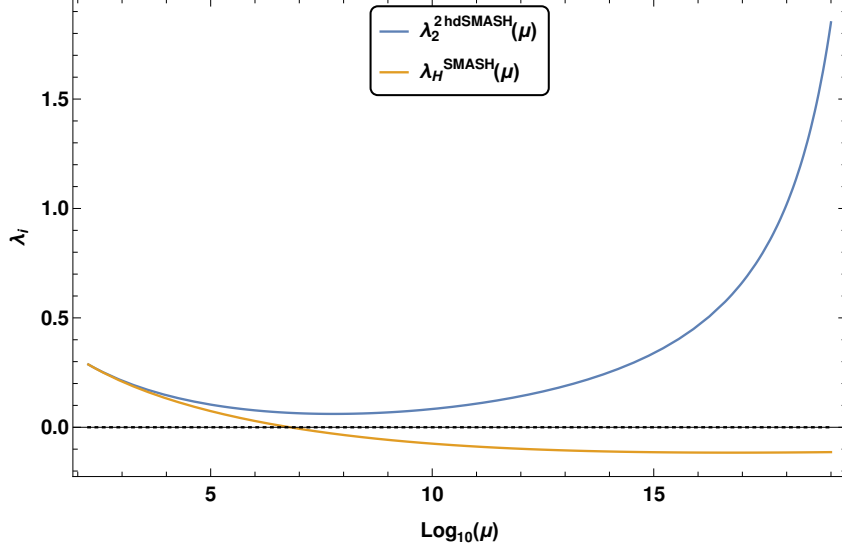


Figure 11: Depicted are the RG evolutions of $\lambda_2(\mu)$ for 2hdSMASH (blue solid curve) and SMASH (orange solid curve) for PQTHI using BP- sh_2 of Table 4. The renormalization scale is set at the top pole mass $m_t = (172.5 \pm 0.7)$ GeV, cf. Ref. [49], to run from low- to high scale.

$\lambda_2(\mu)$ behaves. The analysis of this section is representative of the analysis done for all benchmarks acquired in section 5.5. We chose benchmarks of type PQTHI- sh_2 in table 5 as an extreme case where portal couplings become sizable and thus provide a more general discussion. We were able to see that portal couplings are constrained and have a sub-dominant effect. This can be seen on tree-level by the following relation

$$\lambda_2 + \frac{1}{2} \left(\delta - \frac{\lambda_{2S}^2}{\lambda_S} \right) \geq 0, \quad (5.55)$$

where δ is typically larger. Moreover, we demand that perturbative unitarity constraints (2.16)-(2.21) must be obeyed along the RG evolution, thus ensuring high-scale validity by avoiding Landau-Poles, cf. Ref. [60]. In section 5.5, we give benchmark points which satisfy all theoretical constraints at tree- and one-loop level. The analysis of this section can be easily adopted to scenarios where we consider PQI and other PQTHI directions.

5.5 Benchmark points

The discussion of inflation in section 4.1 and its connection to electroweak physics by means of RG-analysis in sections 5.1-5.4, culminates to the discussion of benchmark points which satisfy theoretical and experimental constraints. We present benchmarks which are consistent with BfB- and perturbative unitarity conditions from electroweak-all the way up to the Planck scale, thus providing high-scale validity and vacuum stability. Furthermore, the benchmarks are tested against experimental constraints from B-physics and collider experiments on the Higgs sector, thus ensuring 2hdSMASH to be phenomenologically viable.

For this part of the analysis, 2hdSMASH was implemented in SARAH-v4.14.4 [62], SPheno-v4.0.4 [63], HiggsSignals-v2 [64] and HiggsBounds-v5 [65].

With SARAH-v4.14.4, the necessary equations were provided to use in SPheno-v4.0.4,

such as the RGEs given in appendix D, the scalar- and fermionic masses and its decays. For a given benchmark, this was computed with **SPheno-v4.0.4** and checked with **HiggsSignals-v2** to account for a low-energy signal-strength measurement of the 125 GeV SM-like Higgs scalar at the LHC. Furthermore, the same **SPheno** output was cross-checked with **HiggsBounds-v5** against constraints from heavy Higgs searches at LEP, Tevatron and LHC. With the benchmarks **BP1-BP5** listed in table 6 we cover all in-

Parameters	BP1	BP2	BP3	BP4	BP5
λ_1	0.07	0.07	0.07	0.07	0.07
λ_2	0.287	0.263	0.257	0.258	0.257
λ_3	0.54	0.60	0.24	0.54	0.24
λ_4	-0.14	-0.4	0.27	-0.14	-0.28
λ_S	4.44×10^{-10}	6.5×10^{-10}	1.0×10^{-10}	1.0×10^{-10}	1.0×10^{-10}
λ_{1S}	5.57×10^{-6}	-6.59×10^{-6}	4.8×10^{-14}	4.8×10^{-14}	3.6×10^{-13}
λ_{2S}	-4.27×10^{-6}	1.0×10^{-15}	1.0×10^{-15}	1.0×10^{-15}	1.0×10^{-15}
λ_{12S}	2.5×10^{-16}	2.5×10^{-16}	2.5×10^{-16}	2.5×10^{-16}	2.5×10^{-16}
$\tan \beta$	5.5	5.5	26	26	18
$Y_{N,1}$	9×10^{-4}	9×10^{-4}	4×10^{-5}	4×10^{-5}	10^{-4}
$Y_{\nu,3}$	5.175×10^{-3}	5.175×10^{-3}	1.09×10^{-3}	1.09×10^{-3}	1.2×10^{-3}
v_S	3.0×10^{10}	3.0×10^{10}	3.0×10^{10}	3.0×10^{10}	3.0×10^{10}
m_h (GeV)	125.2	125.3	125.0	124.9	125.4
m_H (GeV)	798.7	799.4	1711.5	1711.5	1425.2
m_s (GeV)	6.3×10^5	6.7×10^5	3.0×10^5	3.0×10^5	3.0×10^5
m_A (GeV)	799.5	799.5	1711.5	1711.5	1425.2
m_{H^\pm} (GeV)	802.1	807.0	1709.1	1712.8	1422.2

Table 6: List of benchmarks passing the theoretical constraints and experimental constraints as discussed in the text with a pole top mass of $m_t = (172.5 \pm 0.7)$ GeV according to Ref. [49].

teresting parameter configurations which also allow for PQI and PQTHI. The 2HDM couplings λ_1 - λ_4 are of $\mathcal{O}(1)$ such that the SM-like Higgs mass $m_h = (125.10 \pm 0.14)$ GeV [49] is obtained. Furthermore, we consider $\tan \beta \gtrsim 5.5$ to accommodate the constraint on the axion decay constant f_a as discussed in appendix B. There is a stringent constraint from $B \rightarrow X_s \gamma$ [66] on the charged Higgs sector of the Type-II 2HDM which provides a lower bound on the charged Higgs masses

$$m_{H^\pm} > 650 \text{ GeV} . \quad (5.56)$$

This lower bound was recently corrected to be higher in Type-II 2HDM models by computation of $(B \rightarrow X_s \gamma)$ at NNLO QCD level [67]

$$m_{H^\pm} > 800 \text{ GeV} . \quad (5.57)$$

For choosing $\lambda_{12S} \simeq \mathcal{O}(\frac{v}{v_S})^2$, as discussed in section 3 (cf. Ref. [24]), the heavy Higgs sector becomes nearly degenerate with $m_H \approx m_A \approx m_{H^\pm}$. The constraints from electroweak precision tests, namely S, T, U variables, are satisfied for the nearly degenerate mass spectrum of the neutral heavy Higgs sector. We note that the charged Higgs mass

has a small mass splitting compared to the other heavy Higgses which is conceived by considering the change in value for λ_4 of table 6. The portal couplings λ_{1S} and λ_{2S} do not have a sizable effect on the scalar masses. However, they are considered in the RG-analysis and connect inflation with particle phenomenology, as discussed in section 5.3. The portal couplings are chosen such that successful inflation is guaranteed and constraints from neutrino physics for thermal leptogenesis and BAU are considered for RG-evolution. The neutrino Yukawa couplings given in table 6 satisfy the constraints from neutrino oscillation experiments and BAU as discussed in sec. 5.2. Moreover, the portal couplings are naturally small which protects the SM-like Higgs mass from high-scale radiative corrections. The benchmarks given in table 6 are in the TeV range which is established by $\lambda_{12S} \simeq \mathcal{O}(\frac{v}{v_S})^2$. Due to this relation, $\lambda_{12S}v_S^2$ is of order $\mathcal{O}(v^2)$ and resembles a soft breaking parameter of the effective 2HDM low-energy theory. This provides an additional parameter to control the mass spectrum without endangering Higgs phenomenology and its RG evolution all the way up to the Planck scale, cf. Ref. [59].

Therefore, the benchmarks provided in table 6 facilitate a mass spectrum at the TeV scale which are allowed by theoretical and experimental constraints. The smallness of the portal couplings imply a considerable suppression of Higgs to axion decays. Hence, 2hdSMASH is indistinguishable from other extended Higgs sectors without axion at upcoming collider experiments based on Higgs decays. However, signals from axion dark matter searches may serve as detection probe of 2hdSMASH.

6 Allowed Parameter Space

In this section, we discuss the constraints from the Higgs sector on the allowed parameter space and scan over the parameter space. We choose **BP2** and vary v_S and λ_{12S} for $\tan\beta = 5.5$ and 10 to illustrate the different aspects of the mass spectra over the allowed range of v_S (eq. 2.6) and $\lambda_{12S} \simeq 10^{-16}$ - 10^{-15} . We ensure the points are allowed by **HiggsBounds-v5** [65] and **HiggsSignals-v2** [64] and satisfy collider bounds on heavy Higgs masses from Tevatron, LEP and LHC as well as signal strength measurements for the 125 GeV SM-like Higgs as can be seen in Figs. 12-15 for both $\tan\beta = 5.5$ and 10.

As discussed in sec. 3, the Higgs masses, at the tree-level, are determined by $\tan\beta$, v_S and λ_{12S} . Low values of λ_{12S} ($\sim \mathcal{O}(\frac{v}{v_S})^2$) are favoured from inflationary context as discussed in sec. 4 as well as provide testable benchmark scenarios [24] for future colliders. Figure 12 (left) shows the variation of λ_{12S} against m_H , the mass of the heavy CP-even Higgs with v_S on the coloured palette for $\tan\beta = 5.5$. We observe for a fixed v_S , m_H decreases as λ_{12S} decreases, while, for a fixed λ_{12S} , m_H increases as v_S increases. Fig 12 (right) shows the $\lambda_{12S} - m_H$ plane for a higher $\tan\beta = 10$. For high $\tan\beta$ the mass scale of the heavy Higgses allowed from Higgs constraints increases with an increase in $\tan\beta$. In Fig. 13 and 14, we observe that the charged Higgs, the pseudoscalar and the heavy CP-even Higgs are mass degenerate and accessible at upcoming colliders while being allowed from current experimental constraints for two values of $\tan\beta = 5.5$ and 10. Fig. 15 shows the variation of the allowed mass ranges for h, H, A and ρ with varying v_S and λ_{12S} for fixed $\tan\beta = 5.5$ and 10. While m_ρ is typically at the PQ scale, lighter scalars and pseudoscalar are still achievable for low values of λ_{12S} over the entire range of v_S and a large fraction of the parameter space is within the scope of detection at the upcoming HL-LHC [68]. However, for such low values of the portal

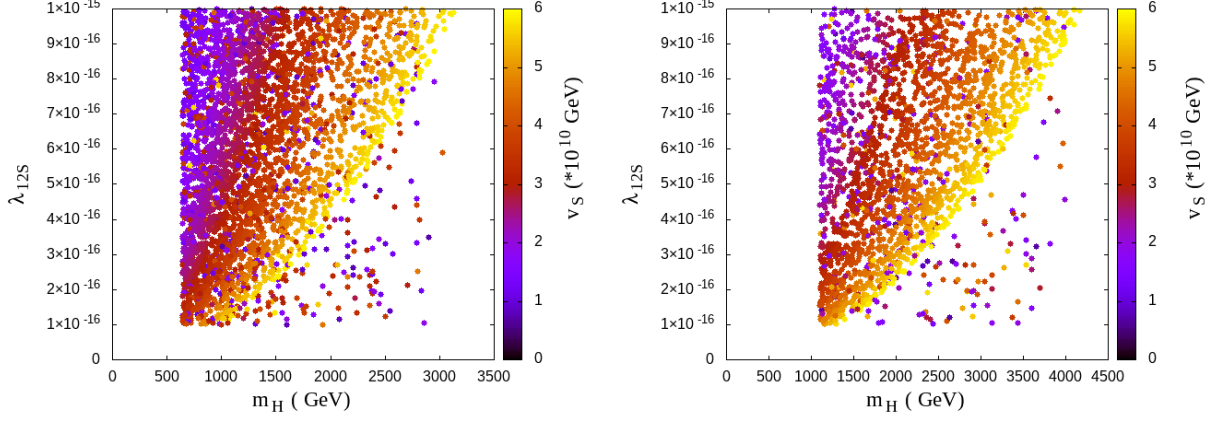


Figure 12: Variation of λ_{12S} against m_H with v_s on the coloured palette for $\tan \beta = 5.5$ (left) and 10 (right).

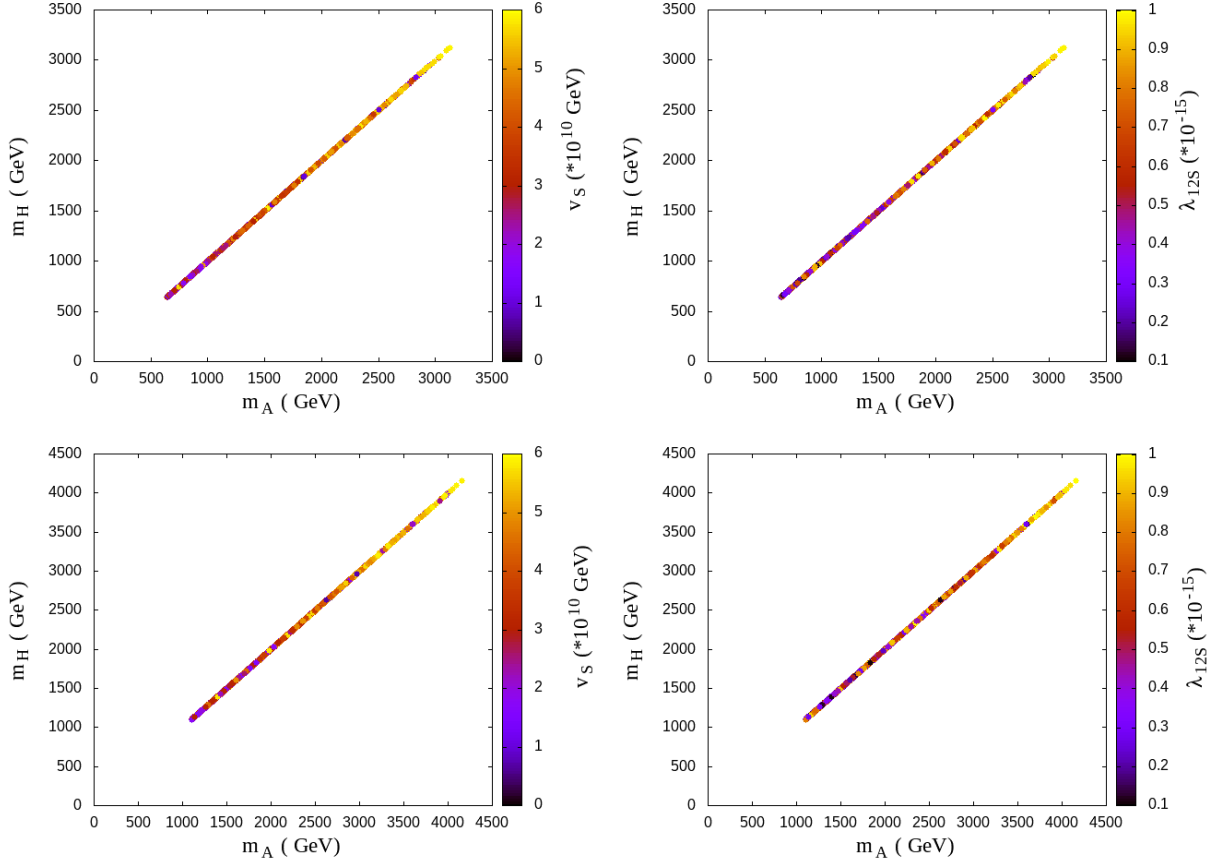


Figure 13: The mass planes of the light CP-even and CP-odd Higgs against v_S (left) and λ_{12S} (right) for $\tan \beta = 5.5$ (top) and 10 (bottom).

couplings, the Higgs couple primarily to the SM particles and the model is an effective U(1) symmetric 2HDM at low energy scales as discussed in appendix F. One must look forward to the upcoming axion experiments in order to constrain the mass of the axion and consequently, v_S . The mass spectrum would then be dictated by $\tan \beta$ and λ_{12S} and hence considerably difficult to distinguish between 2HDM and 2hdSMASH at low energy experiments, probing the Higgs sector. Therefore, experimental observations at

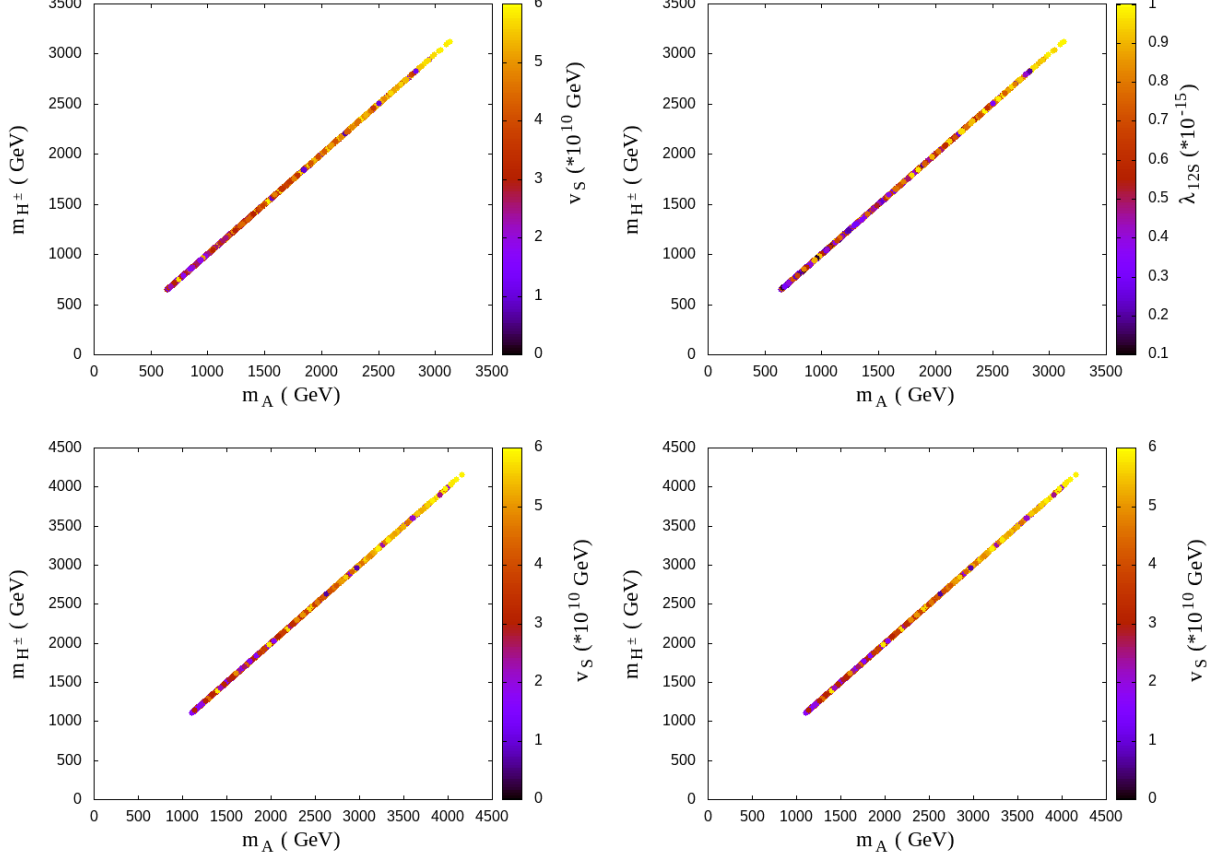


Figure 14: The mass planes of the charged Higgs and CP-odd Higgs against v_S (left) and λ_{12S} (right) for $\tan \beta = 5.5$ (top) and 10 (bottom).

PLANCK and BICEP/KECK could provide conclusive evidence of 2hdSMASH while precision measurements of the Higgs sector at upcoming lepton colliders in correlation with studies of axion dark matter could provide complimentary evidence to observe or constrain the model in the upcoming decade.

7 Summary and Conclusions

We have investigated the 2hdSMASH model consisting of two SU(2) Higgs doublets, a SM complex scalar singlet and three SM right-handed neutrinos addressing dark matter, inflation and neutrino masses. In this paper, we focus on the interconnection of inflation and low energy phenomenology and present representative benchmarks consistent with theoretical and experimental constraints.

We have realized effective single inflation with stable attractor solutions thereby neglecting isocurvature perturbation which we have analyzed in section 4.1. The orthogonal directions are verified by analysis to be heavy [17]. Therefore 2hdSMASH accommodates four effective single field directions, namely the direction of the PQ-scalar s termed PQ-Inflation (PQI) and three effective single field mixed directions sh_1 , sh_2 and sh_{12} termed PQ-Two-Higgs-Inflation (PQTHI). These field directions are acquired by establishing a hierarchy of non-minimal couplings to gravity $\xi_S \gg \xi_{1,2} \simeq 0$, thereby avoiding unpredictable inflation in 2HDM-directions. Both, PQI and PQTHI- sh_{ij} require $\xi_S \lesssim 1$ to ensure

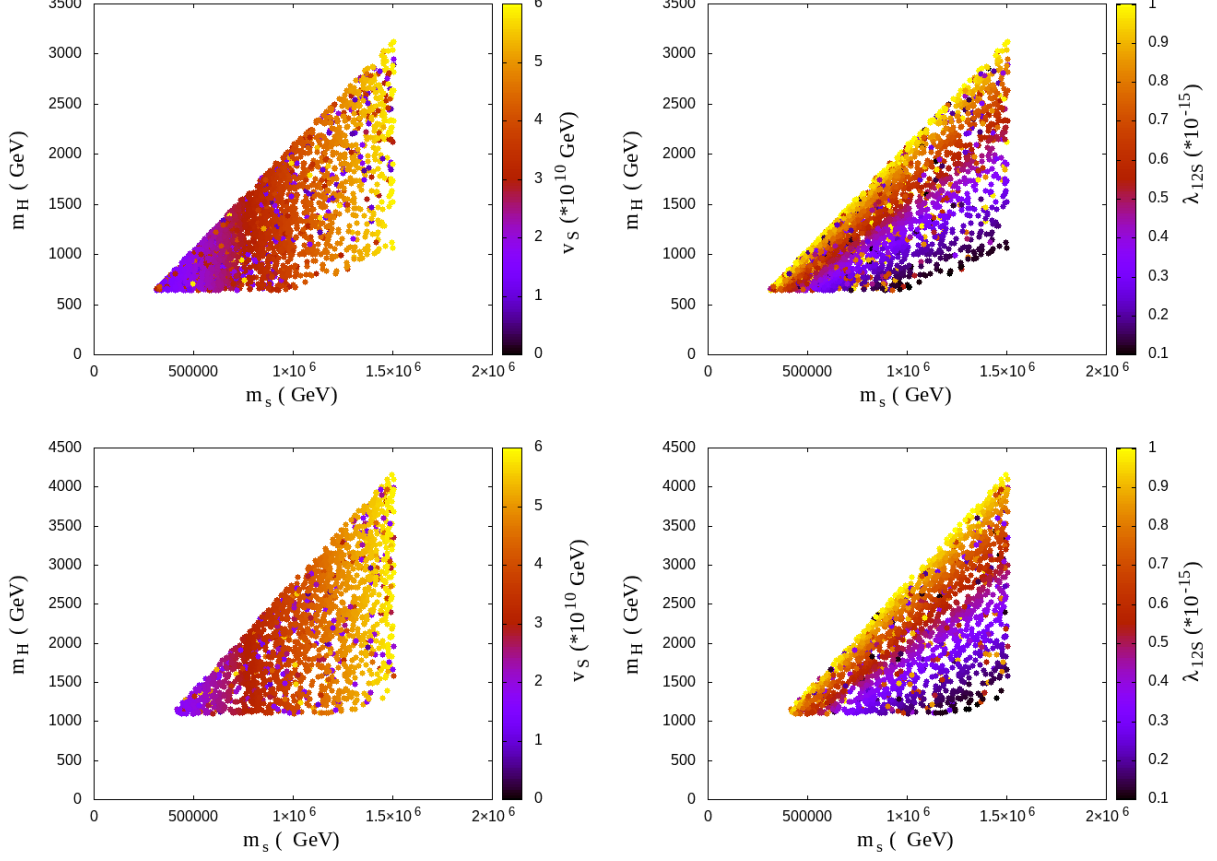


Figure 15: Different mass planes of the heavy CP-even scalar against v_s (left) and λ_{12s} (right) for $\tan \beta = 5.5$ (top) and 10 (bottom).

predictive inflation without breaking unitarity. This sets stringent constraints on the effective PQ-scalar self coupling $\tilde{\lambda}_S$ (4.41), namely $\tilde{\lambda}_S \sim 10^{-10} \xi_S^2$, which are required by the PLANCK 2018 [38, 42] constraint on the scalar perturbation amplitude $A_S \sim 10^{-10}$, i.e. $\tilde{\lambda}_S \sim 10^{-10}$. Accounting for post-inflationary expansion of the universe and considering the PLANCK 2018 [38, 42] and BICEP/KECK XIII [43] measurements on the spectral tilt n_s and the tensor-to-scalar-ratio r , we obtain the following constraints on $\tilde{\lambda}_S$, ξ_S and the e-fold number N_* , i.e.

$$9 \times 10^{-10} \gtrsim \tilde{\lambda}_S \gtrsim 2.2 \times 10^{-12} \quad , \quad 1.35 \times 10^{-2} \lesssim \xi_S \lesssim 1 \quad , \quad 59.3 \lesssim N_* \lesssim 60.7.$$

For $\xi_S \sim 1$ we obtain the following range for n_s and r :

$$0.966 \lesssim n_s \lesssim 0.967 \quad \text{and} \quad 0.0037 \gtrsim r \gtrsim 0.0036$$

satisfying the PLANCK 2018 [38, 42] and BICEP/KECK XIII [43] measurements as can be seen in figure 4. The two variants of inflation realizing these predictions, namely PQI and PQTHI, can be distinguished via the portal couplings. While all portal couplings are required to fulfill $|\lambda_{1S,2S,12S}| \ll \sqrt{\tilde{\lambda}_S}$ to ensure stability of λ_S all the way up to the Planck scale, there are two distinguishable scenarios of portal coupling regimes, namely

$$\lambda_{12S} \ll \lambda_S \lesssim \lambda_{1S,2S} \ll \lambda_{1,2,34} \quad \text{with} \quad \lambda_{iS}^2/\lambda_S \ll \lambda_{1,2,34} \quad (\text{I})$$

$$\lambda_{12S} \lesssim \lambda_{1S} \sim \lambda_{2S} \ll \lambda_{1,2,34,S} \quad , \quad (\text{II})$$

describing PQTHI and PQI respectively. These two scenarios are associated with an enhanced Poincaré symmetry $\mathcal{G}_P^{\text{PQ}} \times \mathcal{G}_P^{2\text{HDM}}$ where the 2HDM-sector effectively decouples from the PQ-scalar sector as it was shown in Ref. [23]. This accommodates a scale-invariant theory where radiative corrections are negligible due to the smallness of the portal couplings. In particular, a tiny value for λ_{12S} ensures high-scale validity since $\lambda_{12S}v_S^2$ resembles a low energy soft breaking parameter of a softly broken $U(1)$ -symmetric 2HDM. Moreover, the portal couplings are required to preserve their sign at the Planck scale following the inflationary conditions

$$\begin{aligned} \lambda_{1S,2S} &> 0, \\ (\lambda_{iS} > 0 \wedge \lambda_{jS} < 0) \vee (\lambda_{1S,2S} < 0), \end{aligned}$$

for PQI and PQTHI- $sh_{i,j,ij}$ respectively.

These constraints were considered in an extensive analysis on the one-loop RG-running of λ_{1S} and λ_{2S} , thereby accounting for low energy effects from thermal leptogenesis, BAU, Higgs phenomenology as well as vacuum stability and perturbative unitarity. For PQI, we obtained constraints from thermal leptogenesis and BAU in the one-loop RG-analysis on the portal couplings

$$\lambda_{1S} \gtrsim \text{Tr} \left(Y_\nu^\dagger Y_\nu Y_N^\dagger Y_N \right).$$

ensuring λ_{1S} to remain positive all the way up to the Planck scale. For PQTHI-scenarios, we considered two cases, namely PQTHI- sh_i represented by $|\lambda_{1S}|_{\mu_{\text{ew}}} \simeq |\lambda_{2S}|_{\mu_{\text{ew}}}$ and PQTHI- sh_{12} represented by $|\lambda_{1S}|_{\mu_{\text{ew}}} \leq |\lambda_{2S}|_{\mu_{\text{ew}}}$. Considering PQTHI- sh_i , we obtained a correction to the initial value of λ_{1S} which counterbalances the negative top Yukawa contribution of λ_{2S} ,

$$|\lambda_{1S}^{\text{corr.}}(\mu_{EW})| = |\lambda_{1S} + \delta\lambda_{1S}|_{\mu_{EW}} \approx \left| \lambda_{2S} \times \left(1 + \frac{2\lambda_3 + \lambda_4}{3y_t^2} \right) \right|_{\mu_{EW}}, \quad (7.1)$$

where $\lambda_{1S}^{\text{corr.}}$ is the corrected initial value of λ_{1S} . In the case of PQTHI- sh_{12} , we found the responsible couplings, i.e. λ_3 and λ_4 , which force λ_{2S} to run towards λ_{1S} . Furthermore, we obtained an analytic understanding of RG-running in the 2HDM, where the couplings λ_3 and λ_4 provide RG-running stability. This is ensured by the relation

$$\delta(\mu) + \lambda_2(\mu) \equiv \frac{\lambda_{34}^2(\mu)}{\lambda_1(\mu)} + \lambda_2(\mu) \geq 0 \quad , \quad \forall \mu \quad (7.2)$$

which prevents $\lambda_2(\mu)$ to run negative. We identified two intertwining effects which stabilize $\lambda_2(\mu)$ by 1) the initial value and 2) by RG-effects caused by λ_3^2 and λ_{34}^2 . Moreover, we included perturbative unitarity conditions in our RG-analysis which causes the couplings to be bounded from above. Amongst others, we considered the most prominent perturbative unitarity conditions on the couplings which we used for stabilization, i.e.

$$|\lambda_{1,3}(\mu)| < 8\pi \quad , \quad |\lambda_3(\mu) \pm \lambda_4(\mu)| < 8\pi \quad , \quad |\delta(\mu)| < 8\pi, \quad (7.3)$$

in order to avoid Landau poles. From this elaborate RG-stability analysis we acquired viable benchmark points which account for all theoretical and experimental constraints, i.e. vacuum stability, perturbative unitarity, inflationary cosmology, thermal leptogenesis, BAU and Higgs phenomenology. The latter was confirmed by testing the benchmarks

with `HiggsSignals-v2` and `HiggsBounds-v5` which are in accordance with current LEP, Tevatron and LHC data.

In summary, the salient points of our work are,

- Realising inflation in the singlet scalar directions set a stringent constraint on the effective self-coupling $\tilde{\lambda}_S \sim 10^{-10}$. This sets stringent constraints on the portal couplings λ_{1S} and λ_{2S} . On the other hand, BfB conditions also set an upper bound on λ_{12S} depending on λ_{1S} and λ_{2S} .
- We observed that the favoured range of portal couplings from inflation, especially λ_{12S} along with v_S and $\tan \beta$ have a strong bearing on the mass of the heavy Higgs spectra. For axionic dark matter, the present constraints on f_a , and thermal relic abundance restricts the singlet vev v_S to be $\mathcal{O}(10^9-10^{10})$ GeV. The large hierarchy between v and v_S leads to a naturally *compressed* heavy Higgs spectrum, at the tree-level. Ref. [24] previously discussed that $\mathcal{O}(\text{TeV})$ scale Higgs spectra are obtainable for portal couplings of the order $\frac{v^2}{v_S^2}$. Additionally, we observe that this region remains favoured from the inflationary point of view which also favour such low portal couplings, thereby predicting $\mathcal{O}(\text{TeV})$ scale BSM Higgses accessible at HL-LHC and future colliders.
- We obtained representative benchmarks satisfying both theoretical conditions (BfB, high scale validity, perturbative unitarity) and experimental constraints from the Higgs sector consistent with inflationary conditions at the high scale and within the projected reach of the HL-LHC.
- Lastly, we note that although a light TeV scale Higgs sector may be possible, it would be difficult to distinguish this model from 2HDM at LHC and its future upgrades. Such searches coupled with axion dark matter searches could be good complementary channels with observations at axion detection experiments, while observations by PLANCK would be more conclusive in discovering or excluding this model.

We have omitted the discussion on preheating and reheating which is crucial to understand whether each inflationary scenario is able to reheat the universe efficiently enough to provide the correct thermal history of our universe. Subsequently, this will affect the number of e-folds needed to sufficiently inflate the universe and its complete thermal predictions regarding PQ-symmetry restoration, leptogenesis and BAU. The predictions of this paper, do however provide an answer to whether inflation in one or the other direction is preferred while accommodating phenomenological constraints. We leave the remaining investigation of the thermal history in 2hdSMASH for a future study.

During the final stages of our study, we came across Ref. [25] which addresses a similar problem as in this paper. However, our work is different from theirs in several respects including the model which has been studied. While both studies deal with the νDFSZ model, Ref. [25] works with a trilinear $U(1)$ breaking term, discussing the inflationary directions in a top specific νDFSZ model termed as $\text{VISH}\nu$ which serves as a complementary model for our study. In our work, we deal with a quadratic $U(1)$ breaking term and determine the inflationary conditions subject to all theoretical conditions including unitarity, boundedness-from-below and high-scale validity to arrive at phenomenologically relevant benchmarks for future collider searches.

Acknowledgements

The authors acknowledge support by the Deutsche Forschungsgemeinschaft (DFG, German Research Foundation) under Germany's Excellence Strategy EXC 2121 "Quantum Universe" - 390833306. This work has been partially funded by the Deutsche Forschungsgemeinschaft (DFG, German Research Foundation) - 491245950. JD acknowledges support from the HEP Dodge Family Endowment Fellowship at the Homer L.Dodge Department of Physics & Astronomy at the University of Oklahoma. The authors thank A.H. Sopov and C. Tamarit for helpful discussions.

Appendix

A Derivation of CP-even/odd Scalar Masses

We derive the charged, neutral CP-odd and CP-even scalar masses by diagonalizing the corresponding squared mass matrices respectively. We will see that computing the charged and CP-odd scalar masses is simpler than computing the CP-even scalar masses. In fact, we will have to use an expansion in order of v/v_S for the latter, while the computation of the former is exact. In the following we will start with the derivation of the charged and CP-odd scalar masses, i.e. H^\pm and A , before we move on to the neutral CP-even scalar masses.

For the charged CP-even and the neutral CP-odd masses, we expand the Higgs doublets Φ_i and the PQ-scalar singlet S about their vacuum:

$$\Phi_1 = (h_1^+, \frac{1}{\sqrt{2}}(v_1 + h_1 + ia_1))^T, \quad (\text{A.1})$$

$$\Phi_2 = (h_2^+, \frac{1}{\sqrt{2}}(v_2 + h_2 + ia_2))^T, \quad (\text{A.2})$$

$$S = \frac{1}{\sqrt{2}}(v_S + s + ia_S). \quad (\text{A.3})$$

in order to derive the squared mass matrices:

$$\mathcal{M}_{H^\pm}^2 = \begin{pmatrix} \frac{v_2(v_S^2\lambda_{12S} - \lambda_4 v_1 v_2)}{2v_1} & \frac{1}{2}(\lambda_4 v_1 v_2 - v_S^2\lambda_{12S}) \\ \frac{1}{2}(\lambda_4 v_1 v_2 - v_S^2\lambda_{12S}) & \frac{v_1(v_S^2\lambda_{12S} - \lambda_4 v_1 v_2)}{2v_2} \end{pmatrix}, \quad (\text{A.4})$$

$$\mathcal{M}_A^2 = \begin{pmatrix} \frac{v_2 v_S^2 \lambda_{12S}}{2v_1} & -\frac{v_S^2 \lambda_{12S}}{2} & -v_2 v_S \lambda_{12S} \\ -\frac{v_S^2 \lambda_{12S}}{2} & \frac{v_1 v_S^2 \lambda_{12S}}{2v_2} & v_1 v_S \lambda_{12S} \\ -v_2 v_S \lambda_{12S} & v_1 v_S \lambda_{12S} & 2v_1 v_2 \lambda_{12S} \end{pmatrix}, \quad (\text{A.5})$$

which can be diagonalized by considering the characteristic polynomial in an eigenvalue equation:

$$\det(\mathcal{M}_i^2 - \mathbb{1}\lambda) = 0. \quad (\text{A.6})$$

The obtained eigenvalues correspond to the charged CP-even and neutral CP-odd masses. In the case of the charged CP-even eigenvalues, we acquire a charged Goldstone boson which is "eaten" by the W^\pm -bosons and a charged Higgs with a squared mass given by:

$$m_{H^\pm}^2 = \frac{1}{2}v_S^2 \left(\frac{(t_\beta^2 + 1) \lambda_{12S}}{t_\beta} - \frac{\lambda_4 v^2}{v_S^2} \right). \quad (\text{A.7})$$

For the CP-odd eigenvalues, we get two pseudo-Nambu-Goldstone bosons and one pseudoscalar Higgs. One of the two pseudo-Nambu-Goldstone bosons is "eaten" by the Z -Boson while the other one corresponds to the axion acquiring a mass from the mixing with the neutral pion. The squared pseudoscalar Higgs mass is given by:

$$m_A^2 = \frac{2\lambda_{12S}v_S^2}{1+t_\beta^2} \left(\frac{v^2}{v_S^2} t_\beta + \frac{(1+t_\beta^2)^2}{4t_\beta} \right). \quad (\text{A.8})$$

We proceed with the CP-even scalar masses and derive the squared-mass matrix in the right basis by making an ansatz for the unitary rotation matrix R . The procedure is the following:

- 1.) Calculate the squared-mass matrix in the correct basis, i.e. the basis-vectors need to be specified with respect to the physical field basis given by (h, β, s) :

$$\mathcal{M}_{0+}^{\prime 2} = \begin{pmatrix} \left. \frac{\partial^2 V}{\partial h \partial h} \right|_{v, v_S} & \left. \frac{1}{h} \frac{\partial^2 V}{\partial h \partial \beta} \right|_{v, v_S} & \left. \frac{\partial^2 V}{\partial h \partial s} \right|_{v, v_S} \\ \left. \frac{1}{h} \frac{\partial^2 V}{\partial \beta \partial h} \right|_{v, v_S} & \left. \frac{1}{h^2} \frac{\partial^2 V}{\partial \beta \partial \beta} \right|_{v, v_S} & \left. \frac{1}{h} \frac{\partial^2 V}{\partial \beta \partial s} \right|_{v, v_S} \\ \left. \frac{\partial^2 V}{\partial s \partial h} \right|_{v, v_S} & \left. \frac{1}{h} \frac{\partial^2 V}{\partial s \partial \beta} \right|_{v, v_S} & \left. \frac{\partial^2 V}{\partial s \partial s} \right|_{v, v_S} \end{pmatrix}. \quad (\text{A.9})$$

- 2.) Make use of the fact that $v/v_S \ll 1$ by factoring out v_S from $\mathcal{M}_{0+}^{\prime 2}$:

$$\mathcal{M}_{0+}^{\prime 2} = v_S^2 \begin{pmatrix} \left(\frac{v}{v_S} \right)^2 \frac{(\lambda_2 t_\beta^4 + 2\lambda_{34} t_\beta^2 + \lambda_1)}{(t_\beta^2 + 1)^2} & \left(\frac{v}{v_S} \right)^2 \frac{t_\beta (\lambda_2 - \lambda_{34}) t_\beta^2 - \lambda_1 + \lambda_{34}}{(t_\beta^2 + 1)^2} & \left(\frac{v}{v_S} \right) \frac{(\lambda_{2S} t_\beta^2 - 2\lambda_{12S} t_\beta + \lambda_{1S})}{t_\beta^2 + 1} \\ \left(\frac{v}{v_S} \right)^2 \frac{t_\beta (\lambda_2 - \lambda_{34}) t_\beta^2 - \lambda_1 + \lambda_{34}}{(t_\beta^2 + 1)^2} & \left(\frac{v}{v_S} \right)^2 \frac{t_\beta (\lambda_1 + \lambda_2 - 2\lambda_{34})}{(t_\beta^2 + 1)^2} + \frac{(t_\beta^2 + 1) \lambda_{12S}}{2t_\beta} & \left(\frac{v}{v_S} \right) \frac{((t_\beta^2 - 1) \lambda_{12S} + t_\beta (\lambda_{2S} - \lambda_{1S}))}{t_\beta^2 + 1} \\ \left(\frac{v}{v_S} \right) \frac{(\lambda_{2S} t_\beta^2 - 2\lambda_{12S} t_\beta + \lambda_{1S})}{t_\beta^2 + 1} & \left(\frac{v}{v_S} \right) \frac{((t_\beta^2 - 1) \lambda_{12S} + t_\beta (\lambda_{2S} - \lambda_{1S}))}{t_\beta^2 + 1} & \lambda_S \end{pmatrix}. \quad (\text{A.10})$$

- 3.) Choose the unitary matrix, cf. Ref. [69]¹³

$$R = \exp \left\{ A \left(\frac{v}{v_S} \right) + B \left(\frac{v}{v_S} \right)^2 \right\}, \quad (\text{A.11})$$

where $A, B \in \mathbb{R}^{3 \times 3}$ with $A^T = -A$ and $B^T = -B$, to diagonalize the squared-mass matrix $\mathcal{M}_{0+}^{\prime 2}$.

¹³This ansatz was introduced in Ref. [69] in order to diagonalize the neutral CP even squared mass matrix of the DFSZ model with a cubic term $\propto c \Phi_2^\dagger \Phi_1 S + h.c.$ instead of a quartic term.

4.) Match $A \left(\frac{v}{v_S} \right) + B \left(\frac{v}{v_S} \right)^2$ in powers of v/v_S with $\mathcal{M}_{0+}^{\prime 2}$:

$$A \left(\frac{v}{v_S} \right) + B \left(\frac{v}{v_S} \right)^2 = \begin{pmatrix} 0 & B_{12} \left(\frac{v}{v_S} \right)^2 & A_{13} \left(\frac{v}{v_S} \right) \\ -B_{12} \left(\frac{v}{v_S} \right)^2 & 0 & A_{23} \left(\frac{v}{v_S} \right) \\ -A_{13} \left(\frac{v}{v_S} \right) & -A_{23} \left(\frac{v}{v_S} \right) & 0 \end{pmatrix} \quad (\text{A.12})$$

with $A_{12} = B_{13} = B_{23} = 0$.

5.) Diagonalize the squared-mass matrix by calculating:

$$\mathcal{D} = R^T \mathcal{M}_{0+}^{\prime 2} R \quad (\text{A.13})$$

and expanding \mathcal{D} up to second order in v/v_S , cf. Refs. [24, 69]

$$\mathcal{D} = \sum_{n=0}^{\infty} \frac{\partial^n}{\partial x^n} \left(R^T \mathcal{M}_{0+}^2 R \right) \Big|_{x=0} \frac{x^n}{n!} \Big|_{x=\left(\frac{v}{v_S}\right)} \simeq \tilde{\mathcal{D}} + \mathcal{O} \left(\left(\frac{v}{v_S} \right)^3 \right) \quad (\text{A.14})$$

$$\Rightarrow \tilde{\mathcal{D}} = \begin{pmatrix} m_h^2/v_S^2 & 0 & 0 \\ 0 & m_H^2/v_S^2 & 0 \\ 0 & 0 & m_s^2/v_S^2 \end{pmatrix} = \begin{pmatrix} \tilde{\mathcal{D}}_{11} & \tilde{\mathcal{D}}_{12} & \tilde{\mathcal{D}}_{13} \\ \tilde{\mathcal{D}}_{12} & \tilde{\mathcal{D}}_{22} & \tilde{\mathcal{D}}_{23} \\ \tilde{\mathcal{D}}_{13} & \tilde{\mathcal{D}}_{23} & \tilde{\mathcal{D}}_{33} \end{pmatrix}. \quad (\text{A.15})$$

6.) Utilize the fact that we have three equations $\left(\tilde{\mathcal{D}}_{12,13,23} \stackrel{!}{=} 0 \right)$ for three parameters $(B_{12}, A_{13,23})$ and solve these equations for these parameters:

$$\tilde{\mathcal{D}}_{12,13,23} \stackrel{!}{=} 0 \implies B_{12}, A_{13,23}. \quad (\text{A.16})$$

7.) Use the results of B_{12} , $A_{13,23}$ to obtain $\tilde{\mathcal{D}}_{11,22,33}$ in order to calculate the masses:

$$\frac{m_h^2}{v_S^2} = \frac{\left(\frac{v}{v_S}\right)^2}{(1+t_\beta^2)^2} \left[\lambda_1 + t_\beta^4 \lambda_2 + 2t_\beta^2 \lambda_{34} - \frac{(\lambda_{1S} + t_\beta^2 \lambda_{2S} - 2t_\beta \lambda_{12S})^2}{\lambda_S} \right] + \mathcal{O}\left(\left(\frac{v}{v_S}\right)^4\right), \quad (\text{A.17})$$

$$\frac{m_H^2}{v_S^2} = \frac{(1+t_\beta^2) \lambda_{12S}}{2t_\beta} + \frac{t_\beta}{(1+t_\beta^2)^2} \left[\frac{2((\lambda_{1S} - \lambda_{2S})t_\beta + \lambda_{12S}(1-t_\beta^2))^2}{\lambda_{12S}(1+t_\beta^2) - 2t_\beta \lambda_S} + (\lambda_1 + \lambda_2 - 2\lambda_{34})t_\beta \right] \left(\frac{v}{v_S}\right)^2 + \mathcal{O}\left(\left(\frac{v}{v_S}\right)^4\right), \quad (\text{A.18})$$

$$\frac{m_s^2}{v_S^2} = \lambda_S + \frac{t_\beta}{(1+t_\beta^2)^2} \left[\frac{(\lambda_{1S} + \lambda_{2S}t_\beta^2 - 2t_\beta \lambda_{12S})^2}{\lambda_S} - \frac{2t_\beta^2((\lambda_{1S} - \lambda_{2S})t_\beta + \lambda_{12S}(1-t_\beta^2))^2}{\lambda_{12S}(1+t_\beta^2) - 2t_\beta \lambda_S} \right] \left(\frac{v}{v_S}\right)^2 + \mathcal{O}\left(\left(\frac{v}{v_S}\right)^4\right). \quad (\text{A.19})$$

These analytically derived masses are valid for **BP1-BP4** of section 3.

8.) The limit of small portal couplings ($\lambda_{1S,2S,12S} \ll 1$) represents the decoupling of the 2HDM from the PQ-scalar singlet. We choose the following ansatz for the unitary matrix R :

$$R = \exp \left\{ M \left(\frac{v}{v_s} \right)^2 \right\}, \quad (\text{A.20})$$

which makes the components $(\mathcal{M}_{0+}^{\prime 2})_{12,13,23}$ marginally small since they are weighted up to second order in v/v_s . Thus, we obtain

$$m_h^2 \approx \frac{v^2}{(1+t_\beta^2)^2} (\lambda_1 + \lambda_2 t_\beta^4 + 2\lambda_{34} t_\beta^2), \quad (\text{A.21})$$

$$m_H^2 \approx \frac{v_S^2 \lambda_{12S} (1+t_\beta^2)}{2t_\beta^2} + \frac{t_\beta^2 (\lambda_1 + \lambda_2 - 2\lambda_{34}) v^2}{(1+t_\beta^2)^2}, \quad (\text{A.22})$$

$$m_s^2 \approx \lambda_S v_S^2, \quad (\text{A.23})$$

which are represented by **BP4** of section 3.

B Constraints on the Axion Decay Constant

There are astrophysical and cosmological constraints on the axion decay constant f_a . In fact, the measured duration of the neutrino signal of the supernova SN 1987A provides an upper bound on the emission rate of axions [70] that can be translated into a lower bound on the decay constant. Most recent improved determinations of the axion emission rate result in [71, 72]

$$f_a \gtrsim \begin{cases} 5.2 \times 10^8 \text{ GeV}, & \text{for } \tan \beta \lesssim 0.5, \\ 9.8 \times 10^8 \text{ GeV}, & \text{for } \tan \beta \gtrsim 5, \end{cases} \quad (\text{B.1})$$

where $\tan \beta \equiv v_2/v_1$.

Axion dark matter considerations bring further restrictions. We will argue that preheating in 2hdSMASH is quite similar to preheating in SMASH [1, 2]. In particular, the PQ symmetry is restored in the preheating phase and later broken during the radiation dominated era of the hot big bang phase. Correspondingly, axion dark matter is produced not only by the misalignment mechanism [6–8], but also by the decay of topological defects [73, 74]: strings – vortex-like defects, which are formed at the PQ phase transition – and domain walls – surface-like defects by which the strings are attached when the temperature of the Universe becomes comparable to critical temperature of the QCD crossover. The structure of the domain walls is determined by the domain wall number N . For $N > 1$, as in 2hdSMASH, domain walls are stable, as long as the $U(1)_{\text{PQ}}$ is an exact global symmetry. In this case, they would overclose the Universe, in conflict with standard cosmology [75, 76]. However, there are very good arguments that the PQ symmetry – like any global symmetry – is not protected from explicit symmetry breaking effects by PLANCK-scale-suppressed operators appearing in the low-energy effective Lagrangian [77–80]. However, these operators modify also the axion potential, eventually shifting its minimum away from zero, thereby destroying the solution of the strong CP problem, namely, the axion quality problem. Crucially, this drawback is absent in models where the Peccei-Quinn symmetry is not ad hoc but instead an automatic or accidental symmetry of an exact discrete $Z_{\mathcal{N}}$ symmetry [81]. In fact, for $\mathcal{N} \geq 9$, the discrete symmetry can protect the axion against semiclassical gravity effects [82–88], while it can at the same time provide for the small explicit symmetry breaking term needed to make the $N > 1$ models cosmologically viable. Assuming such a $Z_{\mathcal{N}}$ symmetry at action in 2hdSMASH, the required value of f_a to explain all the cold dark matter in the universe by axions is [88, 89]¹⁴

$$4.4 \times 10^7 \text{ GeV} \lesssim f_a \lesssim 9.9 \times 10^9 \text{ GeV}, \text{ for } \mathcal{N} = 9, \quad (\text{B.2})$$

$$1.3 \times 10^9 \text{ GeV} \lesssim f_a \lesssim 9.9 \times 10^9 \text{ GeV}, \text{ for } \mathcal{N} = 10. \quad (\text{B.3})$$

Clearly, part of the parameter range required for $\mathcal{N} = 9$ is already excluded by the SN 1987A constraint. We conclude, that the preferred PQ scale range of 2hdSMASH is

$$3.1 \times 10^9 \text{ GeV} \lesssim v_S \lesssim 5.9 \times 10^{10} \text{ GeV}, \text{ for } \tan \beta \lesssim 0.5, \quad (\text{B.4})$$

$$5.9 \times 10^9 \text{ GeV} \lesssim v_S \lesssim 5.9 \times 10^{10} \text{ GeV}, \text{ for } \tan \beta \gtrsim 5. \quad (\text{B.5})$$

¹⁴Recently, there has been an investigation [90] that argued that for domain wall number $N = 6$ in DFSZ models $f_a \lesssim 5.4 \times 10^8 \text{ GeV}$.

C Theoretical Constraints

We give the derivation of the two theoretical constraints, namely the Bounded from Below conditions, and the perturbative unitarity conditions for the 2hdSMASH model.

C.1 Bounded from below conditions

We derive the BfB conditions in 2hdSMASH by imposing copositivity (conditionally positive conditions) where the biquadratic form of the quartic scalar potential is positive on non-negative vectors. This is realized by applying Sylvester's criterion. We quote the copositivity condition from Refs. [91, 92] and Sylvester's criterion from Ref. [91] in the following:

Copositivity:

“A symmetric matrix A is copositive if the quadratic form $x^T A x \geq 0$ for all vectors $x \geq 0$ in the non-negative orthant \mathbb{R}_+^n . (The notation $x \geq 0$ means that $x_i \geq 0$ for each $i = 0, \dots, n$.) A symmetric matrix A is strictly copositive if the quadratic form $x^T A x > 0$ for all vectors $x > 0$ in the non-negative orthant \mathbb{R}_+^n .”, cf. Refs. [91, 92].

Sylvester's criterion:

“...for a symmetric matrix A to be positive semidefinite, the principal minors of A have to be non-negative. (The principal minors are determinants of the principal submatrices. The principal submatrices of A are obtained by deleting rows and columns of A in a symmetric way, i.e. if the i_1, \dots, i_k rows are deleted, then the i_1, \dots, i_k columns are deleted as well. The largest principal submatrix of A is A itself.) Thus if the matrix A is positive, all of its submatrices, in particular the diagonal elements a_{ii} have to be non-negative.”, cf. Ref. [91].

Note that Sylvester's criterion is a necessary requirement for a matrix A to be copositive and by extension $V_4 > 0$. In order to utilize copositivity and thus Sylvester's criterion, we write the quartic part of the scalar potential V_4 :

$$V_4 = \frac{1}{8} (\lambda_1 h_1^4 + \lambda_2 h_2^4 + \lambda_S s^4) \quad (C.1)$$

$$+ \frac{1}{4} (h_1^2 h_2^2 (\lambda_3 + \zeta_4 \lambda_4) + \lambda_{1S} h_1^2 s^2 + \lambda_{2S} h_2^2 s^2 - 2\lambda_{12S} \zeta_{12S} h_1 h_2 s^2) > 0,$$

where

$$\Phi_1^\dagger \Phi_2 = \zeta_4 h_1 h_2 \quad , \quad \zeta_4 = \frac{|\Phi_1^\dagger \Phi_2|^2}{|\Phi_1|^2 |\Phi_2|^2}, \quad (C.2)$$

$$\Phi_1^\dagger \Phi_2 S^2 = \zeta_{12S} h_1 h_2 s^2 \quad , \quad \zeta_{12S} = \frac{\text{Re}(\Phi_1^\dagger \Phi_2 S^2)}{|S|^2 |\Phi_1| |\Phi_2|} \quad (C.3)$$

with $\zeta_4 \in [0, 1]$ and $\zeta_{12S} \in [-1, 1]$. As a first step, we consider the biquadratic form by imposing $\lambda_{12S} = 0$:

$$V'_4 \equiv V_4|_{\lambda_{12S}=0} = \begin{pmatrix} h_1^2 & h_2^2 & s^2 \end{pmatrix} \begin{pmatrix} \lambda_1 & \lambda_3 + \zeta_4 \lambda_4 & \lambda_{1S} \\ \lambda_3 + \zeta_4 \lambda_4 & \lambda_2 & \lambda_{2S} \\ \lambda_{1S} & \lambda_{2S} & \lambda_S \end{pmatrix} \begin{pmatrix} h_1^2 \\ h_2^2 \\ s^2 \end{pmatrix} > 0 \quad (C.4)$$

to obtain the necessary BFB conditions by applying Sylvester's criterion:

$$\begin{aligned} \lambda_1 &> 0 \quad , \quad \lambda_2 > 0 \quad , \quad \lambda_3 + \min\{0, \lambda_4\} > -\sqrt{\lambda_1 \lambda_2} \, , \\ \lambda_S &> 0 \quad , \quad \sqrt{\lambda_1 \lambda_S} > \lambda_{1S} > -\sqrt{\lambda_1 \lambda_S} \quad , \quad \sqrt{\lambda_2 \lambda_S} > \lambda_{2S} > -\sqrt{\lambda_2 \lambda_S} \, , \\ \sqrt{\lambda_1 \lambda_2 \lambda_S} + \lambda_{2S} \sqrt{\lambda_1} + \lambda_{1S} \sqrt{\lambda_2} + (\lambda_3 + \min\{0, \lambda_4\}) \sqrt{\lambda_S} \\ + \sqrt{2 \left((\lambda_3 + \min\{0, \lambda_4\}) + \sqrt{\lambda_1 \lambda_2} \right) \left(\lambda_{1S} + \sqrt{\lambda_1 \lambda_S} \right) \left(\lambda_{2S} + \sqrt{\lambda_2 \lambda_S} \right)} &> 0 \, , \end{aligned}$$

where the last condition is given by the combination of the following two conditions¹⁵ [91, 92]:

$$\det A > 0 \, , \tag{C.5}$$

$$\sqrt{a_{11} a_{22} a_{33}} + a_{12} \sqrt{a_{33}} + a_{13} \sqrt{a_{22}} + a_{23} \sqrt{a_{11}} > 0 \tag{C.6}$$

with a_{ij} as the components of $A \in \mathbb{R}^{3 \times 3}$ where

$$A = \begin{pmatrix} \lambda_1 & \lambda_3 + \zeta_4 \lambda_4 & \lambda_{1S} \\ \lambda_3 + \zeta_4 \lambda_4 & \lambda_2 & \lambda_{2S} \\ \lambda_{1S} & \lambda_{2S} & \lambda_S \end{pmatrix} .$$

By considering the s -dependent portal terms of the quartic scalar potential with $\zeta_{12S} = \pm 1$ we get:

$$\begin{aligned} V_4^{\text{Portal}} &= \lambda_{1S} h_1^2 s^2 + \lambda_{2S} h_2^2 s^2 - 2 (\pm \lambda_{12S} h_1 h_2 s^2) \\ &= (h_1 s \quad h_2 s) \begin{pmatrix} \lambda_{1S} & \mp \lambda_{12S} \\ \mp \lambda_{12S} & \lambda_{2S} \end{pmatrix} \begin{pmatrix} h_1 s \\ h_2 s \end{pmatrix} \end{aligned} \tag{C.7}$$

to obtain the sufficient BFB conditions:

$$\lambda_{1S} > 0 \quad , \quad \lambda_{2S} > 0 \quad , \quad \lambda_{1S} \lambda_{2S} - |\lambda_{12S}|^2 > 0 . \tag{C.8}$$

It's important to note that the sufficient BfB conditions can be overly strict and therefore exclude parameter points which are BfB but do not pass these conditions. Sufficient BfB conditions ensure that $V_4 > 0$ but they are not necessary. For that reason we chose to break these sufficient BfB conditions and checked numerically whether individual parameter points are BfB. We have used the **Mathematica** package BFB by Ref. [30].

C.2 Perturbative unitarity bounds

The full tree-level perturbative unitarity constraints are calculated by requiring that the unique eigenvalues of the $2 \rightarrow 2$ scalar scattering matrix (scalar S-matrix) $\mathcal{M}_{2 \rightarrow 2}$ are below the upper bound of 8π (suggested in Refs. [93] and [94]). The following calculations are done by using the perturbative unitarity **Mathematica** package included in the directory of **ScannerS** which is described in Ref. [95]. Therefore we follow the calculations on perturbative unitarity of Ref. [95].

¹⁵Either of the two conditions of eqns. (C.5)-(C.6) has to hold for $V_4' > 0$

First, we need to derive the $2 \rightarrow 2$ scalar S-matrix which is given by:

$$\mathcal{M}_{AB \rightarrow CD} = \langle AB | \mathcal{M} | CD \rangle = \frac{1}{\sqrt{(1 + \delta_{AB})(1 + \delta_{CD})}} \frac{\partial^4 V_4}{\partial A \partial B \partial C \partial D}, \quad (\text{C.9})$$

where the δ_{ij} - functions are necessary symmetry factors. Here, we have used the quartic scalar potential V_4 in the gauge eigenbasis $(h_{1,2}, s, h_{1,2}^\pm, a_{1,2,S})$ which is given by the following field definition:

$$\Phi_1 = \begin{pmatrix} h_1^+ \\ \frac{1}{\sqrt{2}} \cdot (h_1 + v_1 + i \cdot a_1) \end{pmatrix}, \quad (\text{C.10})$$

$$\Phi_2 = \begin{pmatrix} h_2^+ \\ \frac{1}{\sqrt{2}} \cdot (h_2 + v_2 + i \cdot a_2) \end{pmatrix}, \quad (\text{C.11})$$

$$S = \frac{1}{\sqrt{2}} \cdot (s + v_S + i \cdot a_S). \quad (\text{C.12})$$

The resulting $2 \rightarrow 2$ scalar S-matrix $\mathcal{M}_{2 \rightarrow 2}$ is block diagonal and its eigenvalues $\mathcal{M}_{2 \rightarrow 2}^i$ for $i = \{1, \dots, n\}$ are bounded by 8π :

$$|\mathcal{M}_{2 \rightarrow 2}^i| < 8\pi. \quad (\text{C.13})$$

It's important to note that the eigenvalues are basis independent since unitary transformations are basis independent (see Ref.[95, 96] for details). Part of the eigenvalues reproduce the same eigenvalues for a soft $U(1)$ -symmetric 2HDM in the absence of the PQ-scalar s :

$$e_{1,2,3} = \lambda_{1,2,3}, \quad (\text{C.14})$$

$$e_4 = \lambda_3 - \lambda_4, \quad (\text{C.15})$$

$$e_5 = \lambda_3 + \lambda_4, \quad (\text{C.16})$$

$$e_\pm = \frac{1}{2} \left(\lambda_1 + \lambda_2 \pm \sqrt{(\lambda_1 - \lambda_2)^2 + 4\lambda_4^2} \right). \quad (\text{C.17})$$

By including the PQ-scalar s we get the following additional eigenvalues:

$$s_{1,2} = \lambda_{1S,2S}, \quad (\text{C.18})$$

$$s_{3\pm} = \frac{1}{2} \left(\lambda_{1S} + \lambda_{2S} \pm \sqrt{16\lambda_{12S}^2 + (\lambda_{1S} - \lambda_{2S})^2} \right), \quad (\text{C.19})$$

$$s_{4\pm} = \frac{1}{2} \left(\lambda_3 + 2\lambda_4 + \lambda_S \pm \sqrt{16\lambda_{12S}^2 + (\lambda_3 + 2\lambda_4 - \lambda_S)^2} \right), \quad (\text{C.20})$$

$$\frac{1}{2} k_{1,2,3}, \quad (\text{C.21})$$

where the eigenvalues $\frac{1}{2}|k_{1,2,3}|$ are the real roots of the following cubic potential:

$$\frac{1}{2} (48\lambda_1\lambda_{2S}^2 + 48\lambda_{1S}^2\lambda_2 - 144\lambda_1\lambda_2\lambda_S - 64\lambda_{1S}\lambda_{2S}\lambda_3 - 32\lambda_{1S}\lambda_{2S}\lambda_4 + 64\lambda_3^2\lambda_S) \quad (\text{C.22})$$

$$\begin{aligned}
& + \frac{1}{2} (64\lambda_3\lambda_4\lambda_S + 16\lambda_4^2\lambda_S + x (36\lambda_1\lambda_2 + 24\lambda_1\lambda_S - 8\lambda_{1S}^2 + 24\lambda_2\lambda_S - 8\lambda_{2S}^2)) \\
& - \frac{x}{2} (\lambda_3^2 - 16\lambda_3\lambda_4 - 4\lambda_4^2) + \frac{1}{2} (x^2(-6\lambda_1 - 6\lambda_2 - 4\lambda_S) + x^3) .
\end{aligned}$$

Taking the absolute value of all eigenvalues, we obtain the full tree-level perturbative unitarity conditions for 2hdSMASH:

$$|\lambda_{1,2,3,1S,2S}| < 8\pi, \quad (\text{C.23})$$

$$|\lambda_3 \pm \lambda_4| < 8\pi, \quad (\text{C.24})$$

$$\left| \frac{1}{2} \left(\lambda_1 + \lambda_2 \pm \sqrt{(\lambda_1 - \lambda_2)^2 + 4\lambda_4^2} \right) \right| < 8\pi, \quad (\text{C.25})$$

$$\left| \frac{1}{2} \left(\lambda_{1S} + \lambda_{2S} \pm \sqrt{16\lambda_{12S}^2 + (\lambda_{1S} - \lambda_{2S})^2} \right) \right| < 8\pi, \quad (\text{C.26})$$

$$\left| \frac{1}{2} \left(\lambda_3 + 2\lambda_4 + \lambda_S \pm \sqrt{16\lambda_{12S}^2 + (\lambda_3 + 2\lambda_4 - \lambda_S)^2} \right) \right| < 8\pi, \quad (\text{C.27})$$

$$\frac{1}{2} |k_{1,2,3}| < 8\pi. \quad (\text{C.28})$$

D Renormalisation Group Equations

Following is the full list of one-loop RGEs in the 2hdSMASH model¹⁶:

$$\mathcal{D}M_{11}^2 = M_{11}^2 \left(6\lambda_1 - \frac{3}{2}g_1^2 - \frac{9}{2}g_2^2 + 6Y_t^2 \right) + M_{22}^2 (4\lambda_3 + 2\lambda_4) + M_{SS}^2 2\lambda_{1S}, \quad (\text{D.1})$$

$$\mathcal{D}M_{22}^2 = M_{22}^2 \left(6\lambda_2 - \frac{3}{2}g_1^2 - \frac{9}{2}g_2^2 + 6Y_b^2 + 2Y_\tau^2 + 2\text{Tr} \left(Y_\nu^\dagger Y_\nu \right) \right) + M_{11}^2 (4\lambda_3 + 2\lambda_4) + M_{SS}^2 2\lambda_{2S}, \quad (\text{D.2})$$

$$\mathcal{D}M_{SS}^2 = M_{SS}^2 \left(4\lambda_S + \text{Tr} \left(Y_N^\dagger Y_N \right) \right) + M_{11}^2 4\lambda_{1S} + M_{22}^2 4\lambda_{2S}, \quad (\text{D.3})$$

$$\mathcal{D}\langle S \rangle^2 = -\text{Tr} \left(Y_N^\dagger Y_N \right) \langle S \rangle^2 \quad [\text{i.e. the wave function renormalisation}], \quad (\text{D.4})$$

$$\mathcal{D}g_{\{1,2,3\}} = \{7, -3, -7\} g_{\{1,2,3\}}^3, \quad (\text{D.5})$$

$$\begin{aligned}
\mathcal{D}\lambda_1 = & \frac{3}{4}g_1^4 + \frac{3}{2}g_1^2g_2^2 + \frac{9}{4}g_2^4 - \lambda_1 (3g_1^2 + 9g_2^2) + 12\lambda_1^2 + 4\lambda_3\lambda_4 + 4\lambda_3^2 + 2\lambda_4^2 + 2\lambda_{1S}^2 \\
& + 12\lambda_1Y_b^2 - 12Y_b^4 + 4\lambda_1Y_\tau^2 - 4Y_\tau^4 + 4\lambda_2\text{Tr} \left(Y_\nu^\dagger Y_\nu \right) - 4\text{Tr} \left(Y_\nu^\dagger Y_\nu Y_\nu^\dagger Y_\nu \right),
\end{aligned} \quad (\text{D.6})$$

$$\begin{aligned}
\mathcal{D}\lambda_2 = & \frac{3}{4}g_1^4 + \frac{3}{2}g_1^2g_2^2 + \frac{9}{4}g_2^4 - \lambda_2 (3g_1^2 + 9g_2^2) + 12\lambda_2^2 + 4\lambda_3\lambda_4 + 4\lambda_3^2 + 2\lambda_4^2 + 2\lambda_{2S}^2 \\
& + 12\lambda_2Y_t^2 - 12Y_t^4,
\end{aligned} \quad (\text{D.7})$$

$$\begin{aligned}
\mathcal{D}\lambda_3 = & \frac{3}{4}g_1^4 - \frac{3}{2}g_1^2g_2^2 + \frac{9}{4}g_2^4 - \lambda_3 (3g_1^2 + 9g_2^2) + (6\lambda_3 + 2\lambda_4) (\lambda_1 + \lambda_2) + 4\lambda_3^2 + 2\lambda_4^2 + 2\lambda_{1S}\lambda_{2S} \\
& + \lambda_3 \left(6Y_t^2 + 6Y_b^2 + 2Y_\tau^2 + 2\text{Tr} \left(Y_\nu^\dagger Y_\nu \right) \right) - 12Y_t^2Y_b^2,
\end{aligned} \quad (\text{D.8})$$

$$\mathcal{D}\lambda_4 = 3g_1^2g_2^2 - \lambda_4 (3g_1^2 + 9g_2^2) + 2\lambda_4 (\lambda_1 + \lambda_2) + 8\lambda_4\lambda_3 + 4\lambda_4^2 + 4\lambda_{12S}^2$$

¹⁶Ref. [23] has also given the one-loop RGEs of 2hdSMASH, but neglected terms quadratic in λ_{12S} systematically. We have restored them here using SARAH and PYR@TE.

$$+ \lambda_4 \left(6Y_t^2 + 6Y_b^2 + 2Y_\tau^2 + 2\text{Tr} \left(Y_\nu^\dagger Y_\nu \right) \right) + 12Y_t^2 Y_b^2, \quad (\text{D.9})$$

$$\mathcal{D}\lambda_S = 10\lambda_S^2 + 2\lambda_S \text{Tr} \left(Y_N^\dagger Y_N \right) + 4\lambda_{1S}^2 + 4\lambda_{2S}^2 + 8\lambda_{12S}^2 - 2\text{Tr} \left(Y_N^\dagger Y_N Y_N^\dagger Y_N \right), \quad (\text{D.10})$$

$$\begin{aligned} \mathcal{D}\lambda_{1S} = & \lambda_{1S} \left(-\frac{3}{2}g_1^2 - \frac{9}{2}g_2^2 + 4\lambda_{1S} + 4\lambda_S + 6\lambda_2 \right) + \lambda_{2S} (4\lambda_3 + 2\lambda_4) + 8\lambda_{12S}^2 \\ & + \lambda_{1S} \left(6Y_b^2 + 2Y_\tau^2 + 2\text{Tr} \left(Y_\nu^\dagger Y_\nu \right) + \text{Tr} \left(Y_N^\dagger Y_N \right) \right) - 4\text{Tr} \left(Y_\nu^\dagger Y_\nu Y_N^\dagger Y_N \right), \end{aligned} \quad (\text{D.11})$$

$$\begin{aligned} \mathcal{D}\lambda_{2S} = & \lambda_{2S} \left(-\frac{3}{2}g_1^2 - \frac{9}{2}g_2^2 + 4\lambda_{2S} + 4\lambda_S + 6\lambda_2 \right) + \lambda_{1S} (4\lambda_3 + 2\lambda_4) + 8\lambda_{12S}^2 \\ & + \lambda_{2S} \left(6Y_t^2 + \text{Tr} \left(Y_N^\dagger Y_N \right) \right), \end{aligned} \quad (\text{D.12})$$

$$\begin{aligned} \mathcal{D}\lambda_{12S} = & \lambda_{12S} \left(-\frac{3}{2}g_1^2 - \frac{9}{2}g_2^2 + 2\lambda_3 + 4\lambda_4 + 2\lambda_S + 4\lambda_{1S} + 4\lambda_{2S} + 3Y_t^2 + 3Y_b^2 + Y_\tau^2 \right) \\ & + \lambda_{12S} \left(\text{Tr} \left(Y_\nu^\dagger Y_\nu \right) + \text{Tr} \left(Y_N^\dagger Y_N \right) \right), \end{aligned} \quad (\text{D.13})$$

$$\mathcal{D}Y_t = Y_t \left(-\frac{17}{12}g_1^2 - \frac{9}{4}g_2^2 - 8g_3^2 + \frac{9}{2}Y_t^2 + \frac{1}{2}Y_b^2 \right), \quad (\text{D.14})$$

$$\mathcal{D}Y_b = Y_b \left(-\frac{5}{12}g_1^2 - \frac{9}{4}g_2^2 - 8g_3^2 + \frac{9}{2}Y_b^2 + \frac{1}{2}Y_t^2 + Y_\tau^2 \right), \quad (\text{D.15})$$

$$\mathcal{D}Y_\tau = Y_\tau \left(-\frac{15}{4}g_1^2 - \frac{9}{4}g_2^2 + \frac{5}{2}Y_\tau^2 + 3Y_b^2 \right), \quad (\text{D.16})$$

$$\begin{aligned} \mathcal{D}Y_\nu = & Y_\nu \left(-\frac{3}{4}g_1^2 - \frac{9}{4}g_2^2 + 3Y_b^2 + \text{Tr} \left(Y_\nu^\dagger Y_\nu \right) \right) + Y_\nu Y_\tau^2 - \frac{3}{2}\text{Diag} (0, 0, Y_\tau^2) Y_\nu \\ & + \frac{3}{2}Y_\nu Y_\nu^\dagger Y_\nu + \frac{1}{2}Y_\nu Y_N^\dagger Y_N, \end{aligned} \quad (\text{D.17})$$

$$\mathcal{D}Y_N = \frac{1}{2}\text{Tr} \left(Y_N^\dagger Y_N \right) Y_N + Y_N Y_N^\dagger Y_N + Y_N Y_\nu^\dagger Y_\nu + Y_\nu^T Y_\nu^* Y_N, \quad (\text{D.18})$$

where $\mathcal{D} \equiv (4\pi)^2 \frac{d}{d \ln \mu_R}$.

E 2HDM inflation in 2hdSMASH

In this section we will introduce THI by deriving its field directions, its inflationary conditions and its slow-roll potential. Inflation in the 2HDM model has already been discussed in numerous Refs. [39, 97–99]. In order to decouple the 2HDM-field directions from the PQ-direction we implement a hierarchy of non-minimal couplings, i.e. $\xi_{1,2} \gg \xi_S$. The effective scalar potential is thus given by

$$\begin{aligned} \tilde{V}_{\text{quartic}}(\vartheta, \gamma) \simeq & \\ M_p^4 \frac{t_\gamma^4 (\lambda_1 + \lambda_2 t_\vartheta^4 + 2\lambda_{34} t_\vartheta^2) + 2t_\gamma^2 (t_\vartheta^2 + 1) (\lambda_{1S} + \lambda_{2S} t_\vartheta^2) + \lambda_S (t_\vartheta^2 + 1)^2}{8t_\gamma^4 (\xi_1 + \xi_2 t_\vartheta^2)^2}. \end{aligned} \quad (\text{E.1})$$

The Jacobian from eq. (4.17) for the 2HDM-field directions is determined by γ_{THI} :

$$J(\vartheta, \gamma_{\text{THI}}) = \left(\frac{\partial \tilde{V}_{\text{quartic}}(\vartheta, \gamma)}{\partial \vartheta} \quad \frac{\partial \tilde{V}_{\text{quartic}}(\vartheta, \gamma)}{\partial \gamma} \right)^T \bigg|_{\gamma=\gamma_{\text{THI}}} \quad (\text{E.2})$$

$$= \begin{pmatrix} 0 & \frac{t_\vartheta (t_\vartheta^2 + 1) (-\lambda_1 \xi_2 + \lambda_{34} \xi_1 + t_\vartheta^2 (\lambda_2 \xi_1 - \lambda_{34} \xi_2))}{2 (\xi_1 + \xi_2 t_\vartheta^2)^3} \end{pmatrix}^T,$$

for which we acquire via $J_2(\vartheta, \gamma_{\text{THI}}) = 0$ the extrema ϑ_{THI} :

$$\vartheta_{\text{THI}} = \begin{cases} \vartheta_{h_1} = 0 \\ \vartheta_{h_2} = \frac{\pi}{2} \\ \vartheta_{h_{12}} = \arctan \left(\sqrt{\frac{\lambda_{34} \xi_1 - \lambda_1 \xi_2}{\lambda_{34} \xi_2 - \lambda_2 \xi_1}} \right) \end{cases}. \quad (\text{E.3})$$

The corresponding inflationary vacuum energies are thus given by [97]

$$\tilde{V}_0^{\text{THI}} = \begin{cases} \tilde{V}_0^{h_1} \simeq \frac{\lambda_1}{8\xi_1^2} \\ \tilde{V}_0^{h_2} \simeq \frac{\lambda_2}{8\xi_2^2} \\ \tilde{V}_0^{h_{12}} \simeq \frac{\lambda_1 \lambda_2 - \lambda_{34}^2}{8(\lambda_1 \xi_2^2 + \lambda_2 \xi_1^2 - 2\lambda_{34} \xi_1 \xi_2)} \end{cases} \quad (\text{E.4})$$

with quartic couplings λ_i

$$2\text{HDM-}h_1 : \lambda_1 \quad , \quad 2\text{HDM-}h_2 : \lambda_2 \quad , \quad 2\text{HDM-}h_{12} : \lambda_{12} \equiv \lambda_1 \lambda_2 - \lambda_{34}^2. \quad (\text{E.5})$$

The critical points $\{\gamma_{\text{THI}}, \vartheta_{\text{THI}}\}$ of eq. (E.3) correspond to the three field space directions, i.e. h_1 , h_2 and h_{12} . The hessian matrix in two dimensional space is required

$$H(\vartheta_{\text{THI}}, \gamma_{\text{THI}}) = \begin{pmatrix} \frac{\partial^2 \tilde{V}_{\text{quartic}}(\vartheta, \gamma)}{\partial \gamma^2} & \frac{\partial^2 \tilde{V}_{\text{quartic}}(\vartheta, \gamma)}{\partial \gamma \partial \vartheta} \\ \frac{\partial^2 \tilde{V}_{\text{quartic}}(\vartheta, \gamma)}{\partial \gamma \partial \vartheta} & \frac{\partial^2 \tilde{V}_{\text{quartic}}(\vartheta, \gamma)}{\partial \vartheta^2} \end{pmatrix} \bigg|_{\substack{\gamma=\gamma_{\text{THI}} \\ \vartheta=\vartheta_{\text{THI}}}} \quad (\text{E.6})$$

in order to obtain the sufficient minimum conditions

$$\begin{aligned} \det H(\vartheta_{\text{THI}}, \gamma_{\text{THI}}) &\geq 0, \\ H_{1,1}(\vartheta_{\text{THI}}, \gamma_{\text{THI}}) &\geq 0 \quad \text{or} \quad H_{2,2}(\vartheta_{\text{THI}}, \gamma_{\text{THI}}) \geq 0. \end{aligned} \quad (\text{E.7})$$

These are calculated to be:

2HDM- (h_1) :

$$\begin{aligned} \kappa_1 &\equiv \lambda_{34} \xi_1 - \lambda_1 \xi_2 > 0, \\ \kappa_{1s} &\equiv \lambda_{1s} > 0. \end{aligned}$$

2HDM- (h_2) :

$$\begin{aligned} \kappa_2 &\equiv \lambda_{34} \xi_2 - \lambda_2 \xi_1 > 0, \\ \kappa_{2s} &\equiv \lambda_{2s} > 0. \end{aligned}$$

2HDM- (h_{12}) :

$$\begin{aligned} -\kappa_1 \kappa_2 (\kappa_1 \xi_2 + \kappa_2 \xi_1) &> 0, \\ \kappa_1 \kappa_2 (\kappa_1 + \kappa_2) (\kappa_1 \xi_2 + \kappa_2 \xi_1) (\kappa_1 \lambda_{2s} + \kappa_2 \lambda_{1s}) &> 0. \end{aligned}$$

We note that these conditions simplify drastically for tiny portal couplings and reproduce the known results for pure 2HDM inflation [97] where $\kappa_{1s} = \kappa_{2s} \simeq 0$. As discussed in section 4 this is regarded as the limit from case (I) to case (II). For the remainder, we keep the discussion on the minimum conditions for 2HDM-inflation as general as possible and consider case (I) in order to quantify the results in comparison to PQI and PQTHI.

These minimum conditions, however, just describe a part of the inflationary conditions. Since inflation proceeds along a valley (minimum) of a given field space direction it requires that orthogonal field space directions are ridges (maxima). Therefore, the minimum conditions need to be supplemented by the maximum conditions of the other field space directions in order to fully describe the inflationary conditions. This applies, in particular to the 2HDM- h_1 and 2HDM- h_2 direction. For the 2HDM- h_{12} direction this is already an automatic feature since this field direction is described by a mixture of both field directions and thus requires each individual field direction to be a ridge. However, the minimum conditions for the 2HDM- h_{12} direction needs more refining. Effectively, the first one of the two conditions states

$$\kappa_1 \leq 0 \quad , \quad \kappa_2 \leq 0. \quad (\text{E.8})$$

Therefore, the second condition for $\xi_{1,2} > 0$ reads

$$\kappa_1 \lambda_{2s} + \kappa_2 \lambda_{1s} > 0, \quad (\text{E.9})$$

which is only true for

$$\kappa_{1s} \equiv \lambda_{1s} < 0 \quad , \quad \kappa_{2s} \equiv \lambda_{2s} < 0. \quad (\text{E.10})$$

Moreover, there are kinetic mixing terms for the 2HDM- h_{12} direction. These are quantified by

$$K = \frac{6\xi_1\xi_2}{\Omega^2} \frac{h_1 h_2}{M_p^2}, \quad (\text{E.11})$$

where we avoid in the field space metric by assuming a hierarchy for the non-minimal couplings, i.e. $\xi_i \gg \xi_j$. The inflaton field ϕ proceeds along the mixed direction composed by h_1 and h_2 but is parametrically close to either h_1 or h_2 . Both options are equivalent since either self-coupling, i.e. λ_1 and λ_2 , is of $\mathcal{O}(1)$ and allows for the same predictions. We therefore choose without loss of generality to make the 2HDM- h_{12} -direction parametrically close to the h_2 direction¹⁷. Hence, we assume a hierarchy for the non-minimal couplings, i.e. $\xi_2 \gg \xi_1$. Given this hierarchy, the inflationary conditions for the 2HDM- h_{12} direction simplify

$$\kappa_{1s,2s,2} \simeq \lambda_{1s,2s,34} \leq 0 \quad \wedge \quad \kappa_1 \simeq \lambda_1 \geq 0. \quad (\text{E.12})$$

The field space metric of (4.13) reduces for all 2HDM-directions to a two dimensional field space and becomes quite simple under the above assumptions for the 2HDM- h_{12} direction

$$\mathcal{G}_{ij}^{h_{12}} \simeq \frac{b}{\Omega_{12}^2} \begin{pmatrix} 1 & 0 \\ 0 & \frac{\Omega_{12}^2 + 6\xi_2^2 \frac{\phi^2}{M_p^2}}{\Omega_{12}^2} \end{pmatrix}, \quad (\text{E.13})$$

¹⁷The same discussion applies to the 2HDM- h_{12} direction being parametrically close to h_1 .

where b is the mixing parameter given by

$$b \equiv 1 + \left| \frac{\lambda_{34}}{\lambda_1} \right|, \quad (\text{E.14})$$

which is determined via $\cos^2 \vartheta_{h_{12}} = 1 - b^{-1}$. The frame function Ω_{12}^2 for the mixed direction becomes

$$\Omega_{12}^2 = b + \xi_2 \frac{\phi^2}{M_p^2}, \quad (\text{E.15})$$

which reduces to the frame function for the 2HDM- h_2 direction when $\lambda_{34} \rightarrow 0$. This would be the limit where the 2HDM becomes an effective SM. However, we demand $\lambda_{34} \neq 0$ since it will be useful for RG-analysis (see section 5). In order to justify our approach for describing 2HDM- h_{12} -inflation in an effective single field regime, we need to compute the instantaneous masses of h_1 and h_2

$$m_{h_i}^2 \Big|_{\substack{\vartheta=\vartheta_{h_{12}} \\ \gamma=\gamma_{\text{THI}}}} \simeq \mathcal{G}^{h_i h_i} \partial_{h_i}^2 \tilde{V}_{\text{quartic}} \Big|_{\substack{\vartheta=\vartheta_{h_{12}} \\ \gamma=\gamma_{\text{THI}}}} \simeq \begin{cases} -\frac{\lambda_{34}}{\xi_2} & (h_1) \\ \frac{\lambda_{34}^2}{6\lambda_1 \xi_2^2} & (h_2) \end{cases}. \quad (\text{E.16})$$

To estimate whether the orthogonal directions are heavy, i.e. stabilized, or light, i.e. dynamical, we relate those masses to the Hubble rate $\mathcal{H}^2 \approx \tilde{V}/3M_p^2$

$$\frac{m_{h_i}^2}{\mathcal{H}^2} \simeq \begin{cases} -\frac{24\lambda_1 \lambda_{34} \xi_2}{\lambda_1 \lambda_2 - \lambda_{34}^2} \gtrsim 1 & (h_1) \\ \frac{4\lambda_{34}^2}{\lambda_1 \lambda_2 - \lambda_{34}^2} \lesssim 1 & (h_2) \end{cases}, \quad (\text{E.17})$$

which shows that h_1 is stabilized for $\xi_2 \gg 1$ and h_2 is dynamical for sufficiently small λ_{34} , i.e. $\lambda_1 \lambda_2 \geq 5\lambda_{34}^2$.

There are three inflationary trajectories where effective single field inflation proceeds with the inflaton ϕ which can be seen in figure 16. Since ϕ is a non-canonical field we introduce a canonical normalization in the h_1 - and h_2 -field directions via

$$\Omega^2 \frac{d\chi_i}{d\phi} = \sqrt{\Omega^2 + 6\xi_i^2 \frac{\phi^2}{M_p^2}} \quad \text{for } i = 1, 2. \quad (\text{E.18})$$

The canonically normalized 2HDM- h_{12} -field direction is determined by a mixture of h_1 and h_2 which is controlled by the mixing parameter b and is given by

$$\Omega_{12}^2 \frac{d\chi_{12}}{d\phi} = \sqrt{b \left(\Omega_{12}^2 + 6\xi_2^2 \frac{\phi^2}{M_p^2} \right)}. \quad (\text{E.19})$$

This allows us to determine the effective single-field slow-roll potential with canonically normalized inflaton field χ_j , for $j = 1, 2, 12$:

$$\tilde{V}_j^{\text{THI}}(\phi) = \frac{\lambda_j^{\text{THI}} \phi^4(\chi_j)}{8 \left(1 + \xi_j \frac{\phi^2(\chi_j)}{M_p^2} \right)^2}. \quad (\text{E.20})$$

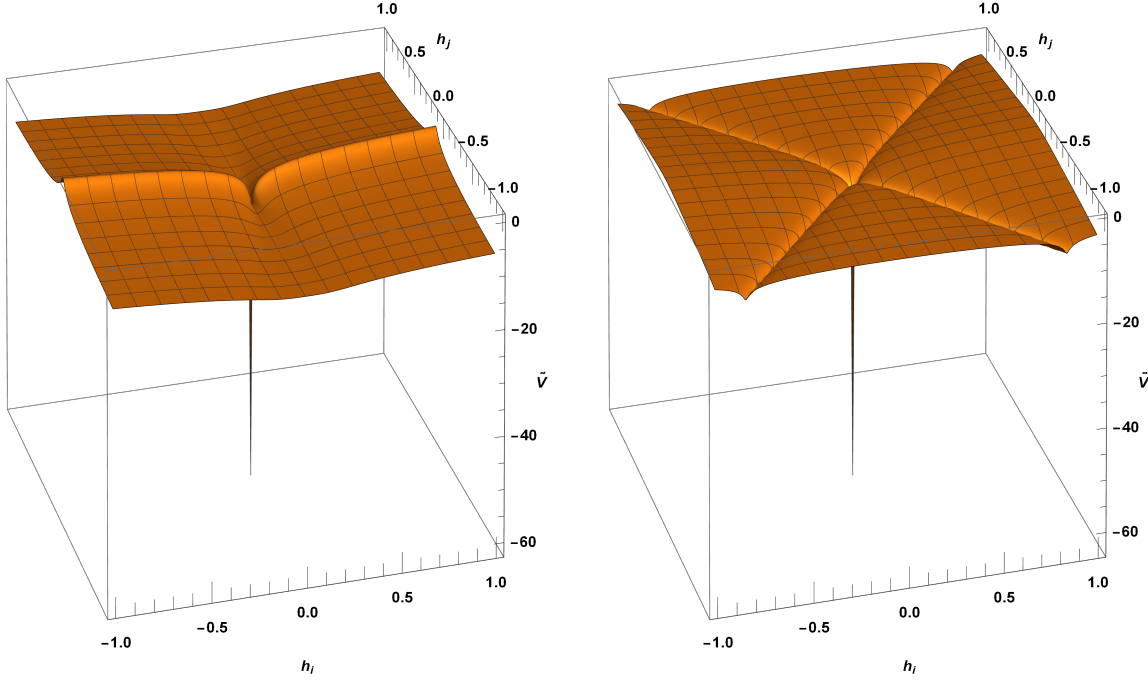


Figure 16: Decadic log Einstein frame scalar potential depicting the 2HDM-field directions in 2hdSMASH shown in units of M_p as a function of the two Higgs fields h_1 and h_2 for pure single field directions (left) and mixed single field direction (right).

The conditions on the coupling parameters for inflation in each 2HDM field direction along with the corresponding effective single field slow-roll potential are summarized in Table 7

Inflation occurs when the Hubble radius decreases at which point the potential energy

inflation along	Potential (E.1) minimized at	Inflationary conditions	Einstein frame slow roll potential
h_1	$\gamma_0 = \frac{\pi}{2}$ $\vartheta_0 = 0$	$\kappa_1 \geq 0$, $\kappa_{1s} \geq 0$ $\kappa_2 \leq 0$, $\kappa_{2s} \leq 0$	$\frac{\lambda_1}{8} \phi^4 \left(1 + \xi_1 \frac{\phi^2}{M_P^2}\right)^{-2}$
h_2	$\gamma_0 = \frac{\pi}{2}$ $\vartheta_0 = \frac{\pi}{2}$	$\kappa_2 \geq 0$, $\kappa_{2s} \geq 0$ $\kappa_1 \leq 0$, $\kappa_{1s} \leq 0$	$\frac{\lambda_2}{8} \phi^4 \left(1 + \xi_2 \frac{\phi^2}{M_P^2}\right)^{-2}$
h_{12}	$\gamma_0 = \frac{\pi}{2}$ $\vartheta_0 = \arctan\left(\sqrt{\frac{\kappa_1}{\kappa_2}}\right)$	$\kappa_1 \leq 0$, $\kappa_2 \leq 0$ $\kappa_{1s} \leq 0$, $\kappa_{2s} \leq 0$	$\frac{\lambda_{12}}{8} \phi^4 \left(1 + \xi_2 \frac{\phi^2}{M_P^2}\right)^{-2}$

Table 7: Conditions & characteristics for h_1 -, h_2 - and h_{12} -inflation in 2hdSMASH.

density dominates the universe. This process is quantified by the slow-roll parameters demanding that the inflaton rolls down the potential well slowly. In slow-roll approximation,

these parameters are expressed as

$$\epsilon_V = \frac{M_p^2}{2} \left(\frac{\tilde{V}'(\chi)}{\tilde{V}(\chi)} \right)^2, \quad \eta_V = M_p^2 \frac{\tilde{V}''(\chi)}{\tilde{V}(\chi)} \quad (\text{E.21})$$

where primes denote derivatives w.r.t. χ and are used to calculate the inflationary observables created during slow-roll inflation. Due to this prolonged stage of slow-roll inflation, the inflaton produces quantum fluctuations along the field trajectory. These quantum fluctuations are transferred to scalar metric perturbations in form of density waves $P_s(k)$ and tensor metric perturbations in form of gravitational waves $P_t(k)$. We give $P_s(k)$ and $P_t(k)$ as (see Ref.[17])

$$P_s(k) = A_s \left(\frac{k}{k_*} \right)^{n_s-1+\dots}, \quad P_t(k) = A_t \left(\frac{k}{k_*} \right)^{n_t+\dots} \quad (\text{E.22})$$

with n_s as the spectral scalar index and n_t as the tensor spectral index, quantifying the deviation from scale-invariance of the power spectra. The scalar- and tensor metric perturbations are reduced to the scalar perturbation amplitude A_s and to the tensor perturbation amplitude A_t for $k = k_*$ when the modes exit the horizon at the pivot scale k_* . Moreover, the gravitational amplitude A_t is normalized by A_s to acquire the tensor-to-scalar ratio r which relates gravitational waves to CMB measurements. Additionally, the spectral tensor index n_t is related to the tensor-scalar ratio r for single field inflation via

$$n_t = -\frac{r}{8}, \quad (\text{E.23})$$

which leaves us with the relevant inflationary observables A_s , n_s and r in slow-roll approximation for single field inflation:

$$A_s = \frac{1}{24\pi^2 M_{Pl}^4 \epsilon_V} \tilde{V}, \quad n_s = 1 - 6\epsilon_V + 2\eta_V, \quad r = 16\epsilon_V. \quad (\text{E.24})$$

As discussed in Refs. [39, 97–99], we consider large non-minimal couplings in order to satisfy the scalar density perturbations of the CMB given by PLANCK [38, 42]. We will show that this is required for the 2HDM-field directions by calculating the expression for A_s and constraining the non-minimal couplings $\xi_{1,2}$ with CMB measurements by PLANCK [38, 42]. Moreover, we will calculate n_s and r_s in the large non-minimal coupling limit and relate their expressions to the number of e-folds and make the well-know predictions for Higgs inflation [14].

In the large field limit, i.e. $\xi_{1,2} \gg 1$, we can approximate $\phi(\chi)$ and its inverse $\chi(\phi)$ by solving equations (E.18) and (E.19)

$$\phi_i(\chi_i) \simeq \frac{M_p}{\sqrt{\xi_i}} \sqrt{\exp \left(\sqrt{\frac{2}{3}} \frac{\chi_i}{M_p} \right) - b}, \quad (\text{E.25})$$

$$\chi(\phi_i) \simeq \sqrt{\frac{3}{2}} M_p \log \left(b M_p^2 + \xi_i \frac{\phi_i^2}{M_p^2} \right), \quad (\text{E.26})$$

from which we acquire with $\phi(\chi)$ the following slow-roll potential

$$\tilde{V}(\chi_i) \simeq \frac{\lambda}{8\xi^2} M_p^4 \left(1 - b \exp \left(-\sqrt{\frac{2}{3}} \frac{\chi}{M_p} \right) \right)^2 \quad (\text{E.27})$$

with mixing parameter b which quantifies whether inflation proceeds in a mixed direction ($b \neq 1$) or in a non-mixed direction ($b = 1$). By taking the first and second partial derivatives of \tilde{V} allows us to compute the slow-roll parameters and thus the inflationary observables A_s , n_s and r in the large ξ limit [2]

$$A_s \simeq \frac{\lambda_i}{128\pi^2 \xi_i^2 b} \frac{(1 - b x_i)^4}{x_i^2}, \quad n_s \simeq 1 - \frac{8b}{3} \frac{b + x_i}{(b - x_i)^2}, \quad \simeq \frac{64 b^2}{3(x_i - b)^2} \quad (\text{E.28})$$

with $x_i \equiv \exp \left(\sqrt{2/3} \chi_i / M_p \right)$. This reduces for $b = 1$ to

$$A_s \simeq \frac{3\lambda \sinh^4 \left(\frac{\chi}{\sqrt{6} M_p} \right)}{2\xi^2}, \quad r \simeq \frac{64 b^2}{3(x_i - b)^2}, \quad (\text{E.29})$$

$$n_s \simeq \frac{4}{3} \left(\coth \left(\frac{\chi}{\sqrt{6} M_p} \right) - \text{csch}^2 \left(\frac{\chi}{\sqrt{6} M_p} \right) - 1 \right) - \frac{1}{3}. \quad (\text{E.30})$$

These quantities can be constrained by CMB measurements. Current constraints on r , A_s and n_s are given by PLANCK 2018 data [42],[38] which were recently updated by Ref. [43]:

$$r_{0.002} < 0.0387985 \quad (95\% \text{C.L., TT,TE,EE+lowE+lensing+BK18+BAO}), \quad (\text{E.31})$$

$$A_s = (2.105 \pm 0.030) \times 10^{-9} \quad (68\% \text{C.L., TT,TE,EE+lowE+lensing+BAO}), \quad (\text{E.32})$$

$$n_s = 0.9665 \pm 0.0038 \quad (68\% \text{C.L., TT,TE,EE+lowE+lensing+BAO}). \quad (\text{E.33})$$

The scalar perturbation amplitude A_s can be used to relate the non-minimal coupling ξ_i to the self-coupling λ_i . From eq. (E.28) we can approximate $A_s \propto \lambda_i / \xi_i^2$ for which we obtain an approximate relation

$$A_s \propto \frac{\lambda_i}{\xi_i^2} \propto 10^{-9} \quad (\text{E.34})$$

$$\Rightarrow \xi_i \propto \sqrt{\lambda_i} 10^{-5}. \quad (\text{E.35})$$

We show this λ - ξ relation in figure 17 (left), which we acquired numerically. This relation is furthermore constrained by n_s and r : the non-minimal coupling ξ is constrained by r as shown in figure 17 (right) and r is constrained by n_s with PLANCK 2018 [42],[38] and BICEP 2021 [43] data. The blue and red curves correspond to a bluer and redder spectrum of n_s , respectively. The 2HDM quartic couplings are of order $\lambda \sim \mathcal{O}(1)$ at the Planck scale. This is required by RG running and Higgs phenomenology to accommodate a 125 GeV Higgs mass at low energies. Later, we will see that the size of 2HDM quartic couplings cannot be changed by considering different field space directions since the RGEs are strongly coupled. From figure 17 (left) and from eq. (E.35) we can see that the non-minimal coupling is of the order $\xi \sim 10^4$.

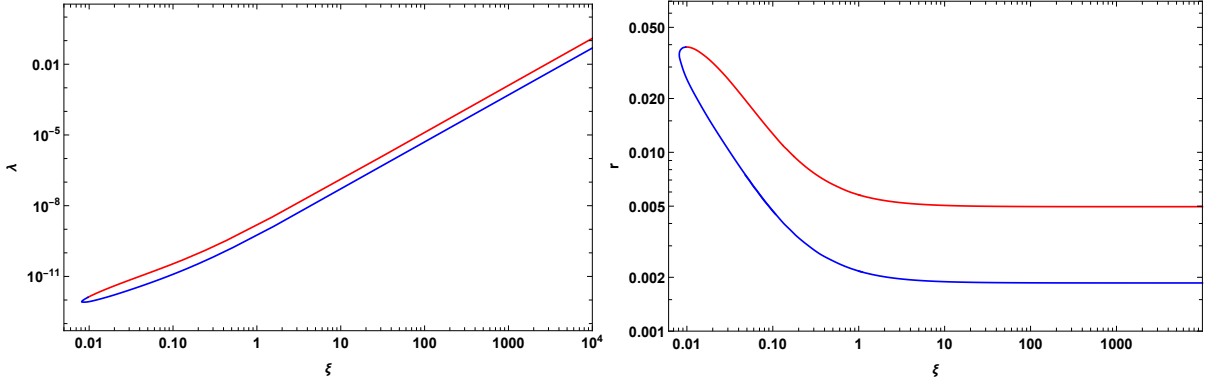


Figure 17: Shown are the 95% C.L. contours of λ vs. ξ (left) and r vs. ξ (right). The red and blue curves indicate the redder and bluer spectrum of n_s .

In order to determine the inflationary observables A_s , n_s and r in the large ξ limit from equation (E.28) properly, we require χ_I and χ_E at horizon crossing and at the end of inflation, respectively. Therefore, we need to compute $\chi(N)$ to determine the number of e-folds required for successful inflation. The number of e-folds during inflation between some initial time t_I and the time at the end of inflation is given by

$$N = \int_{t_I}^{t_{\text{end}}} \mathcal{H}(t) dt \simeq \int_{\chi_I}^{\chi_{\text{end}}} \frac{d\chi}{\sqrt{2\epsilon}} \quad (\text{E.36})$$

and is approximated to

$$N \simeq \frac{1 + 6\xi_i}{8M_p^2} (\phi_I^2 - \phi_E^2) - \frac{3b}{4} \log \left(\frac{b M_p^2 + \xi_i \phi_I^2}{b M_p^2 + \xi_i \phi_E^2} \right). \quad (\text{E.37})$$

However, the exact number of e-folds can be obtained by solving the Klein-Gordon equation for the canonically normalized field χ . The Klein-Gordon equation for χ with regard to N can be derived to be

$$\frac{d^2\chi}{dN^2} + 3\frac{d\chi}{dN} - \frac{1}{2M_p^2} \left(\frac{d\chi}{dN} \right)^3 + \sqrt{2\epsilon} \left(3M_p - \frac{1}{2M_p} \left(\frac{d\chi}{dN} \right)^2 \right) = 0, \quad (\text{E.38})$$

which is evaluated until the condition where $\epsilon = 1$ marks the end of inflation. This differential equation, however, can only be computed numerically and requires appropriate initial conditions. These initial conditions can be estimated by determining $\chi(\Delta N)$

$$\chi(\Delta N) \simeq \sqrt{\frac{3}{2}} M_p \log \left(\frac{b^2(1 + 6\xi) + 8\Delta N \xi}{b(1 + 6\xi)} \right) \approx 5M_p, \quad (\text{E.39})$$

$$\chi'(\Delta N) \simeq M_p \frac{4\sqrt{6}M_p}{\Delta N (b^2(1 + 6\xi) + 8\Delta N \xi)} \approx 0.02M_p. \quad (\text{E.40})$$

Furthermore, we utilize the e-fold dependencies of A_s , n_s and r . This gives us a better understanding of the parameter scale. In the large ξ limit, these quantities are given by

$$n_s(\Delta N) \simeq 1 - \frac{2}{\Delta N}, \quad r \simeq \frac{12b}{\Delta N^2}, \quad A_s(\Delta N) \simeq \frac{\lambda \Delta N^2}{144\pi^2 b \xi^2}, \quad (\text{E.41})$$

where in the non-mixed direction they are given by

$$n_s(\Delta N) \simeq 1 - \frac{2}{\Delta N} \quad , \quad r \simeq \frac{12}{\Delta N^2} \quad , \quad A_s(\Delta N) \simeq \frac{\Delta N^2}{144\pi^2} \frac{\lambda}{\xi^2} . \quad (\text{E.42})$$

These inflationary predictions resemble the results of Starobinsky-type inflation [100–103] and Higgs inflation [14]. As in Higgs inflation and Starobinsky’s R^2 -inflation, the spectral index n_s and the tensor-to-scalar ratio r are solely dependent on ΔN and independent of ξ . In figure 18 we plot the r vs. n_s predictions for 2HDM inflation in the large ξ limit. The general n_s and r predictions are shown as black solid lines which go from low to large ξ where the red dots at $\xi = \infty$ mark our r vs. n_s predictions. Each solid black line corresponds to a given number of e-fold which is in the range of $N \in [50, 70]$. Furthermore, we show the isocontours of constant ξ as gray dashed lines. In fact, the n_s

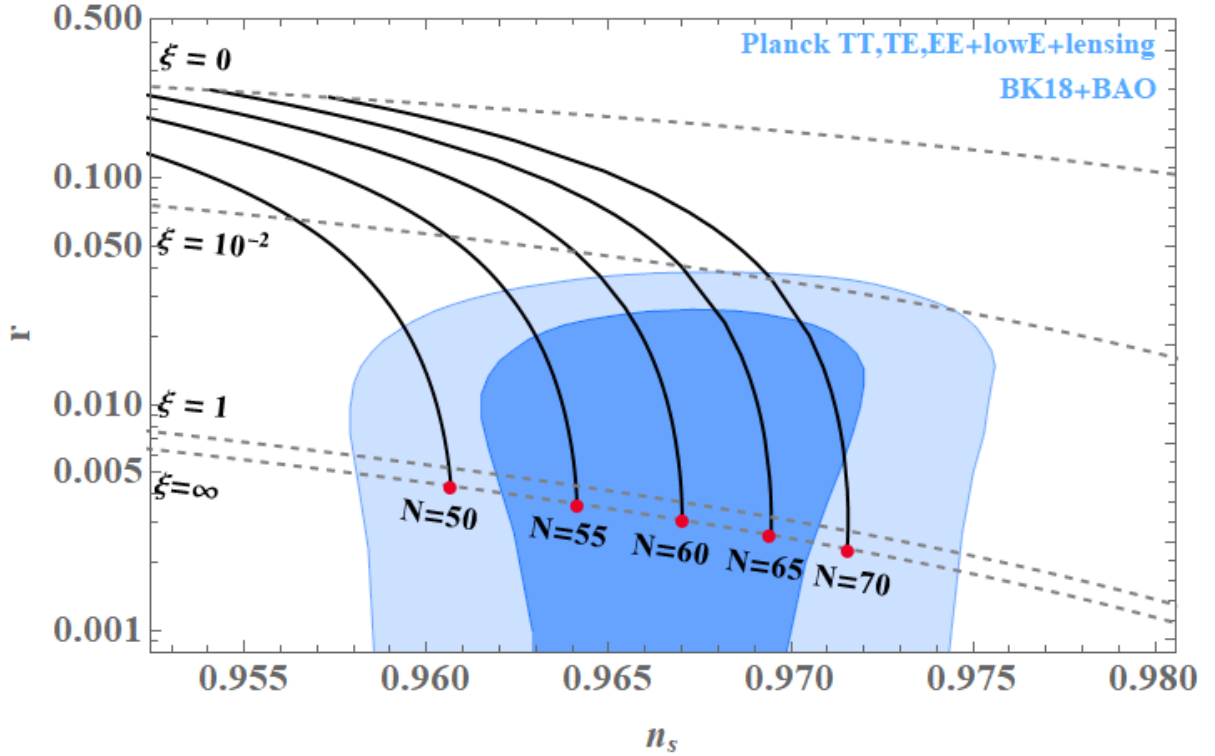


Figure 18: Shown are the 95% and 68% C.L. contours of r vs. n_s (blue) and the inflationary predictions by 2hdSMASH for 2HDM-inflation (solid black). The dashed curves correspond to the isocontours of constant ξ . The main inflationary prediction for the 2HDM are given by $\xi = \infty$ and $N \in [50, 70]$ (red dot).

and r predictions are true for any chaotic inflationary model with a single field attractor. The predictions are constrained by the 95% and 68% C.L. contours of PLANCK 2018 data [38, 42] and the BICEP update [43]. Furthermore, we note the remarkable r vs. n_s prediction for $N = 60$, which we will also encounter for PQI and PQTHI.

As mentioned before, we require for THI non-minimal couplings of the order of $\xi \sim 10^4$. Various authors have discussed the negative impact of such a large non-minimal coupling on perturbative unitarity (e.g. Refs. [104, 105]). The claim is that the unitarity scale is below the inflationary scale, i.e. $\Lambda_U = M_P/\xi_{1,2} \lesssim M_P/\sqrt{\xi_{1,2}} = \Lambda_{\text{Inf}}$ for $\xi_{1,2} \gg 1$, which puts predictiveness under scrutiny. Recently, this issue was addressed by Ref. [106] in which they claim that the unitarity scale during inflation is actually higher than

previously calculated and thus resolving this issue. However, the results of Ref. [106] are beyond the scope of this work and we leave it to future explorations to investigate whether this applies to Higgs inflation in our model. For our considerations, large non-minimal couplings are unnatural since there isn't an explanation on how these large couplings were generated. The approach by the authors of Refs. [2, 40, 41] alleviate the above concerns on predictive power by non-minimal couplings of the size $\xi_i \lesssim 1$ which implies $\lambda \lesssim 10^{-10}$. We adopt these considerations of Refs. [2, 40, 41] which is according to our philosophy more natural. Non-minimal couplings with the size of $\xi_i \lesssim 1$ can be radiatively generated in the very early universe. Therefore, we require the inflaton's quartic self-coupling to be of order $\lambda \lesssim 10^{-10}$. However, the RGEs for λ_1 and λ_2 are dominated by couplings which are of $\mathcal{O}(1)$ as can be seen by eqs. (E.43)-(E.44)

$$\begin{aligned} \mathcal{D}\lambda_1 = & \frac{3}{4}g_1^4 + \frac{3}{2}g_1^2g_2^2 + \frac{9}{4}g_2^4 - \lambda_1(3g_1^2 + 9g_2^2) + 12\lambda_1^2 \\ & + 4\lambda_3\lambda_4 + 4\lambda_3^2 + 2\lambda_4^2 + 2\lambda_{1S}^2 + 12\lambda_1Y_b^2 - 12Y_b^4 \\ & + 4\lambda_1Y_\tau^2 - 4Y_\tau^4 + 4\lambda_2\text{Tr}\left(Y_\nu^\dagger Y_\nu\right) - 4\text{Tr}\left(Y_\nu^\dagger Y_\nu Y_\nu^\dagger Y_\nu\right), \end{aligned} \quad (\text{E.43})$$

$$\begin{aligned} \mathcal{D}\lambda_2 = & \frac{3}{4}g_1^4 + \frac{3}{2}g_1^2g_2^2 + \frac{9}{4}g_2^4 - \lambda_2(3g_1^2 + 9g_2^2) + 12\lambda_2^2 \\ & + 4\lambda_3\lambda_4 + 4\lambda_3^2 + 2\lambda_4^2 + 2\lambda_{2S}^2 + 12\lambda_2Y_t^2 - 12Y_t^4. \end{aligned} \quad (\text{E.44})$$

On the other hand, any scenario with $\lambda_{1,2,34} \sim 10^{-10}$ would endanger Higgs phenomenology since these small self-couplings could not reproduce a 125 GeV Higgs. Therefore, we can safely neglect inflationary realizations where only 2HDM-fields are involved. This is the main reason to solely focus on PQI and PQTHI.

F 2hdSMASH at the Matching Scale

In this section we show that the full high energy theory of 2hdSMASH reduces to a softly broken $U(1)$ -symmetric ν 2HDM low-energy theory where the extra $U(1)_L$ -symmetry can be associated with lepton number caused by a technically natural limit for $Y_N, Y_\nu, \lambda_{12S} \rightarrow 0$, cf. [23]. We consider the limit $\lambda_{1S,2S,12S}, Y_{N,\nu} \rightarrow 0$ corresponding to the enhanced Poincaré symmetry $\mathcal{G}_P^\nu \times \mathcal{G}_P^{2\text{HDM}} \times \mathcal{G}_P^S$ which protects the electroweak scale from large radiative corrections, cf. [23, 32]. We will motivate these consideration by matching 2hdSMASH at the matching scale m_s to its low-energy theory where we show that tiny portal couplings will prove to protect the electroweak scale. Therefore, we consider the equation of motion of s at zero momentum at m_s :

$$\frac{\partial V}{\partial s} = 0 \quad \Rightarrow \quad s^2 = -\frac{h_1^2\lambda_{1S}}{\lambda_S} + \frac{2h_1h_2\lambda_{12S}}{\lambda_S} - \frac{h_2^2\lambda_{2S}}{\lambda_S} - \frac{2M_{SS}^2}{\lambda_S}. \quad (\text{F.1})$$

By considering now the scalar potential with s at zero momentum, i.e. integrating s out, we obtain the threshold corrected scalar potential:

$$\begin{aligned} V = & \frac{h_1^2}{2} \left(M_{11}^2 - \frac{\lambda_{1S}M_{SS}^2}{\lambda_S} \right) + \frac{h_2^2}{2} \left(M_{22}^2 - \frac{\lambda_{2S}M_{SS}^2}{\lambda_S} \right) + \frac{\lambda_{12S}M_{SS}^2}{2\lambda_S} h_1h_2 \left(\frac{h_1^2\lambda_{1S} + h_2^2\lambda_{2S}}{M_{SS}^2} + 2 \right) \\ & + \frac{h_1^4}{8} \left(\lambda_1 - \frac{\lambda_{1S}^2}{\lambda_S} \right) + \frac{h_2^4}{8} \left(\lambda_2 - \frac{\lambda_{2S}^2}{\lambda_S} \right) + \frac{h_1^2h_2^2}{4} \left(\lambda_{34} - \frac{\lambda_{1S}\lambda_{2S} + 2\lambda_{12S}^2}{\lambda_S} \right) - \frac{M_{SS}^2}{2\lambda_S}. \end{aligned} \quad (\text{F.2})$$

The third quadratic term of eq. (F.2) constitutes a non-linear term given by the coupling λ_{12S} . By taking into account that $h_1^2\lambda_{1S} + h_2^2\lambda_{2S} \ll M_{SS}^2 \sim m_s^2$ we can approximate the terms as follows:

$$\frac{\lambda_{12S}M_{SS}^2}{2\lambda_S}h_1h_2\left(\frac{h_1^2\lambda_{1S} + h_2^2\lambda_{2S}}{M_{SS}^2} + 2\right) \approx \frac{\lambda_{12S}M_{SS}^2}{\lambda_S}h_1h_2. \quad (\text{F.3})$$

Therefore, the scalar potential can be approximated to:

$$\begin{aligned} V \simeq & \frac{h_1^2}{2}\left(M_{11}^2 - \frac{\lambda_{1S}M_{SS}^2}{\lambda_S}\right) + \frac{h_2^2}{2}\left(M_{22}^2 - \frac{\lambda_{2S}M_{SS}^2}{\lambda_S}\right) + \frac{\lambda_{12S}M_{SS}^2}{\lambda_S}h_1h_2 \\ & + \frac{h_1^4}{8}\left(\lambda_1 - \frac{\lambda_{1S}^2}{\lambda_S}\right) + \frac{h_2^4}{8}\left(\lambda_2 - \frac{\lambda_{2S}^2}{\lambda_S}\right) + \frac{h_1^2h_2^2}{4}\left(\lambda_{34} - \frac{\lambda_{1S}\lambda_{2S} + 2\lambda_{12S}^2}{\lambda_S}\right) - \frac{M_{SS}^4}{2\lambda_S}. \end{aligned} \quad (\text{F.4})$$

The corresponding threshold corrections for the matching of 2hdSMASH to its effective low energy theory can be read off:

$$\overline{M}_{11,22}^2 = \left(M_{11,22}^2 - \frac{\lambda_{1S,2S}M_{SS}^2}{\lambda_S}\right), \quad (\text{F.5})$$

$$\overline{M}_{12}^2 = 2\lambda_{12S}M_{SS}^2, \quad (\text{F.6})$$

$$\overline{\lambda}_{1,2} = \left(\lambda_{1,2} - \frac{\lambda_{1S,2S}^2}{\lambda_S}\right), \quad (\text{F.7})$$

$$\overline{\lambda}_{34} = \left(\lambda_{34} - \frac{\lambda_{1S}\lambda_{2S} + 2\epsilon^2}{\lambda_S}\right), \quad (\text{F.8})$$

which represents a softly broken $U(1)$ -symmetric 2HDM. The tadpole equation for M_{SS}^2 is calculated by:

$$\frac{\partial V}{\partial s} \stackrel{!}{=} 0 \Rightarrow M_{SS}^2 = \frac{1}{2}(-\lambda_{1S}v_1^2 + 2v_1v_2\lambda_{12S} - \lambda_{2S}v_2^2 - \lambda_Sv_S^2). \quad (\text{F.9})$$

The VEVs $v_{1,2,S}$ follow a hierarchy, namely $v_S^2 \gg v_{1,2}^2$. Hence, the tadpole equation M_{SS}^2 can be approximated as follows:

$$M_{SS}^2 = \frac{v_S^2}{2}\left(-\lambda_{1S}\frac{v_1^2}{v_S^2} + 2\frac{v_1v_2}{v_S^2}\lambda_{12S} - \lambda_{2S}\frac{v_2^2}{v_S^2} - \lambda_S\right) \stackrel{v_S^2 \gg v_{1,2}^2}{\approx} -\frac{\lambda_Sv_S^2}{2}. \quad (\text{F.10})$$

Finally, the threshold corrected scalar potential of the effective low-energy theory is acquired and reads:

$$\begin{aligned} V \simeq & \frac{h_1^2}{2}\left(M_{11}^2 + \frac{\lambda_{1S}v_S^2}{2}\right) + \frac{h_2^2}{2}\left(M_{22}^2 + \frac{\lambda_{2S}v_S^2}{2}\right) - \frac{h_1h_2\lambda_{12S}v_S^2}{2} \\ & + \frac{h_1^4}{8}\left(\lambda_1 - \frac{\lambda_{1S}^2}{\lambda_S}\right) + \frac{h_2^4}{8}\left(\lambda_2 - \frac{\lambda_{2S}^2}{\lambda_S}\right) + \frac{h_1^2h_2^2}{4}\left(\lambda_{34} - \frac{\lambda_{1S}\lambda_{2S} + 2\lambda_{12S}^2}{\lambda_S}\right), \end{aligned} \quad (\text{F.11})$$

where the effective mass term $m_s^2v_S^2 \propto \lambda_Sv_S^4$ was omitted. The following coupling associations for the effective low-energy theory are thus given by:

$$m_{11,22}^2 = \left(M_{11,22}^2 + \frac{\lambda_{1S,2S}v_S^2}{2}\right),$$

$$\begin{aligned}
m_{12}^2 &= \lambda_{12S} v_S^2, \\
\bar{\lambda}_{1,2} &= \left(\lambda_{1,2} - \frac{\lambda_{1S,2S}^2}{\lambda_S} \right), \\
\bar{\lambda}_{34} &= \left(\lambda_{34} - \frac{\lambda_{1S}\lambda_{2S} + 2\lambda_{12S}^2}{\lambda_S} \right), \\
M_{SS}^2 &\simeq -\frac{\lambda_S v_S^2}{2},
\end{aligned} \tag{F.12}$$

where M_{SS}^2 is related to the aforementioned matching-scale via $m_s \simeq \sqrt{-2M_{SS}^2}$. The threshold corrections are negligible, i.e. $\lambda_{iS}^2/\lambda_S \ll 1$. Therefore, the effective low energy theory of a softly broken $U(1)$ -symmetric 2HDM has approximately the following scalar potential $V^{\nu 2\text{HDM}}$:

$$\begin{aligned}
V^{\nu 2\text{HDM}} &\simeq m_{11}^2 |\Phi_1|^2 + m_{22}^2 |\Phi_2|^2 - m_{12}^2 (\Phi_1^\dagger \Phi_2 + \Phi_2^\dagger \Phi_1) \\
&\quad + \frac{\lambda_1}{2} |\Phi_1|^4 + \frac{\lambda_2}{2} |\Phi_2|^4 + \lambda_3 |\Phi_1|^2 |\Phi_2|^2 + \lambda_4 (\Phi_1^\dagger \Phi_2) (\Phi_2^\dagger \Phi_1).
\end{aligned} \tag{F.13}$$

G Coleman-Weinberg Potential

The Coleman-Weinberg potential is an RG-improved potential which is given by, cf. Ref. [61],

$$\begin{aligned}
V_{\text{CW}}(\phi_i) &= \frac{1}{64\pi^2} \\
&\times \left(\sum_b g_b m_b^4(\phi_i) \left[\log \left(\frac{m_b^2(\phi_i)}{\Lambda^2} \right) - \frac{3}{2} \right] - \sum_f g_f m_f^4(\phi_i) \left[\log \left(\frac{m_f^2(\phi_i)}{\Lambda^2} \right) - \frac{5}{2} \right] \right)
\end{aligned} \tag{G.1}$$

where $g_{f/b}$ are the degrees and $m_{f/b}$ are the masses of fermions/bosons. The sum is performed over all scalars $S = \{h_1, h_2, s, h_1^+, h_2^+, a_1, a_2, a_S\}$, Fermions¹⁸ $F = \{t, N_i\}$ and transverse (longitudinal) vectors $V_{T,L} = \{Z_{T,L}, W_{T,L}^\pm\}$ with the following degrees of freedom:

$$\begin{aligned}
g_{Z_T} &= 2 \quad , \quad g_{Z_L} = 1 \quad , \quad g_{W_T^\pm} = 4 \quad , \quad g_{W_L^\pm} = 2 \quad , \quad g_t = 12 \quad , \quad g_{h_1} = g_{h_2} = g_s = 1 \\
g_{h_1^+} &= g_{h_2^+} = 2 \quad , \quad g_{a_1} = g_{a_2} = g_{a_S} = 1 \quad , \quad g_N = 6.
\end{aligned} \tag{G.2}$$

The masses of S , F and V are given by:

$$\begin{aligned}
m_Z^2 &= \frac{1}{4} (h_1^2 + h_2^2) (g_1^2 + g_2^2) \quad , \quad m_{W^\pm}^2 = \frac{1}{4} (h_1^2 + h_2^2) g_1^2 \quad , \quad m_t^2 = \frac{Y_t}{2} h_2^2, \\
m_{h_{1,2}}^2 &= \frac{3h_{1,2}^2 \lambda_{1,2} + h_{2,1}^2 \lambda_{34} + s^2 \lambda_{1S,2S}}{2} \quad , \quad m_s^2 = \frac{h_1^2 \lambda_{1S} - 2h_1 h_2 \lambda_{12S} + h_2^2 \lambda_{2S} + 3s^2 \lambda_S}{2}, \\
m_{a_{1,2}}^2 &= \frac{1}{2} (h_{1,2}^2 \lambda_{1,2} + h_{2,1}^2 (\lambda_3 + \lambda_4) + h_3^2 \lambda_{1S}) \quad , \quad m_{h_{1,2}^+}^2 = \frac{1}{2} (h_{1,2}^2 \lambda_{1,2} + h_{2,1}^2 \lambda_3 + h_3^2 \lambda_{1S}) \quad , \\
m_{a_s}^2 &= \frac{1}{2} (h_1^2 \lambda_{1S} + 2h_1 h_2 \lambda_{12S} + h_2^2 \lambda_{2S} + s^2 \lambda_S) \quad .
\end{aligned} \tag{G.3}$$

¹⁸We only consider the top quark and Majorana neutrino contributions since their masses are the largest amongst the fermions. However, we note that one has to include all fermions in order to give a complete description, which is beyond the scope of what we are considering.

References

- [1] Guillermo Ballesteros, Javier Redondo, Andreas Ringwald, and Carlos Tamarit. Unifying inflation with the axion, dark matter, baryogenesis and the seesaw mechanism. *Phys. Rev. Lett.*, 118(7):071802, 2017. [3](#), [21](#), [49](#)
- [2] Guillermo Ballesteros, Javier Redondo, Andreas Ringwald, and Carlos Tamarit. Standard Model—axion—seesaw—Higgs portal inflation. Five problems of particle physics and cosmology solved in one stroke. *JCAP*, 08:001, 2017. [3](#), [13](#), [20](#), [21](#), [22](#), [24](#), [25](#), [26](#), [49](#), [60](#), [63](#)
- [3] Jihn E. Kim. Weak Interaction Singlet and Strong CP Invariance. *Phys. Rev. Lett.*, 43:103, 1979. [3](#)
- [4] Mikhail A. Shifman, A. I. Vainshtein, and Valentin I. Zakharov. Can Confinement Ensure Natural CP Invariance of Strong Interactions? *Nucl. Phys. B*, 166:493–506, 1980. [3](#)
- [5] R. D. Peccei and Helen R. Quinn. CP Conservation in the Presence of Instantons. *Phys. Rev. Lett.*, 38:1440–1443, 1977. [3](#)
- [6] John Preskill, Mark B. Wise, and Frank Wilczek. Cosmology of the Invisible Axion. *Phys. Lett. B*, 120:127–132, 1983. [3](#), [49](#)
- [7] L. F. Abbott and P. Sikivie. A Cosmological Bound on the Invisible Axion. *Phys. Lett. B*, 120:133–136, 1983.
- [8] Michael Dine and Willy Fischler. The Not So Harmless Axion. *Phys. Lett. B*, 120:137–141, 1983. [3](#), [49](#)
- [9] Peter Minkowski. $\mu \rightarrow e\gamma$ at a Rate of One Out of 10^9 Muon Decays? *Phys. Lett. B*, 67:421–428, 1977. [3](#), [6](#)
- [10] Murray Gell-Mann, Pierre Ramond, and Richard Slansky. Complex Spinors and Unified Theories. *Conf. Proc. C*, 790927:315–321, 1979.
- [11] Tsutomu Yanagida. Horizontal gauge symmetry and masses of neutrinos. *Conf. Proc. C*, 7902131:95–99, 1979.
- [12] Rabindra N. Mohapatra and Goran Senjanovic. Neutrino Mass and Spontaneous Parity Nonconservation. *Phys. Rev. Lett.*, 44:912, 1980. [3](#), [6](#)
- [13] M. Fukugita and T. Yanagida. Baryogenesis Without Grand Unification. *Phys. Lett. B*, 174:45–47, 1986. [3](#)
- [14] Fedor L. Bezrukov and Mikhail Shaposhnikov. The Standard Model Higgs boson as the inflaton. *Phys. Lett. B*, 659:703–706, 2008. [3](#), [10](#), [59](#), [62](#)
- [15] Oleg Lebedev and Hyun Min Lee. Higgs Portal Inflation. *Eur. Phys. J. C*, 71:1821, 2011. [3](#)
- [16] Guillermo Ballesteros, Javier Redondo, Andreas Ringwald, and Carlos Tamarit. Several Problems in Particle Physics and Cosmology Solved in One SMASH. *Front. Astron. Space Sci.*, 6:55, 2019. [3](#)

- [17] Michael Maxim Matlis. *Inflation and Phenomenology in an Extended Two-Higgs-Doublet-Model*. PhD thesis, Hamburg U., Hamburg, 2022. [3](#), [4](#), [41](#), [59](#)
- [18] Sayantan Choudhury and Supratik Pal. Fourth level MSSM inflation from new flat directions. *JCAP*, 04:018, 2012. [3](#)
- [19] Wolfgang Gregor Hollik, Cheng Li, Gudrid Moortgat-Pick, and Steven Paasch. Phenomenology of a Supersymmetric Model Inspired by Inflation. *Eur. Phys. J. C*, 81(2):141, 2021. [3](#)
- [20] A. R. Zhitnitsky. On Possible Suppression of the Axion Hadron Interactions. (In Russian). *Sov. J. Nucl. Phys.*, 31:260, 1980. [3](#)
- [21] Michael Dine, Willy Fischler, and Mark Srednicki. A Simple Solution to the Strong CP Problem with a Harmless Axion. *Phys. Lett. B*, 104:199–202, 1981. [3](#)
- [22] R. R. Volkas, A. J. Davies, and Girish C. Joshi. NATURALNESS OF THE INVISIBLE AXION MODEL. *Phys. Lett. B*, 215:133–138, 1988. [3](#), [5](#), [9](#), [23](#)
- [23] Jackson D. Clarke and Raymond R. Volkas. Technically natural nonsupersymmetric model of neutrino masses, baryogenesis, the strong CP problem, and dark matter. *Phys. Rev. D*, 93(3):035001, 2016. [3](#), [4](#), [5](#), [9](#), [12](#), [13](#), [23](#), [24](#), [25](#), [28](#), [43](#), [53](#), [63](#)
- [24] Domenec Espriu, Federico Mescia, and Albert Renau. Axion-Higgs interplay in the two Higgs-doublet model. *Phys. Rev. D*, 92(9):095013, 2015. [3](#), [5](#), [8](#), [9](#), [24](#), [38](#), [39](#), [44](#), [47](#)
- [25] Alexei H. Sopov and Raymond R. Volkas. VISH ν : a unified solution to five SM shortcomings with a protected electroweak scale. 6 2022. [3](#), [13](#), [44](#)
- [26] Z. G. Berezhiani and M. Yu. Khlopov. Cosmology of Spontaneously Broken Gauge Family Symmetry. *Z. Phys. C*, 49:73–78, 1991. [5](#)
- [27] Steven Weinberg. A New Light Boson? *Phys. Rev. Lett.*, 40:223–226, 1978. [5](#)
- [28] Frank Wilczek. Problem of Strong P and T Invariance in the Presence of Instantons. *Phys. Rev. Lett.*, 40:279–282, 1978. [5](#)
- [29] R. L. Workman et al. Review of Particle Physics. *PTEP*, 2022:083C01, 2022. [6](#)
- [30] Igor P. Ivanov, Marcel Köpke, and Margarete Mühlleitner. Algorithmic Boundedness-From-Below Conditions for Generic Scalar Potentials. *Eur. Phys. J. C*, 78(5):413, 2018. [7](#), [51](#)
- [31] Chien-Yi Chen and S. Dawson. Exploring Two Higgs Doublet Models Through Higgs Production. *Phys. Rev. D*, 87:055016, 2013. [8](#)
- [32] Robert Foot, Archil Kobakhidze, Kristian L. McDonald, and Raymond R. Volkas. Poincaré protection for a natural electroweak scale. *Phys. Rev. D*, 89(11):115018, 2014. [9](#), [63](#)
- [33] A.D. Linde. Eternally existing self-reproducing chaotic inflationary universe. *Physics Letters B*, 175(4):395–400, 1986. [10](#)

- [34] B. L. Spokoiny. INFLATION AND GENERATION OF PERTURBATIONS IN BROKEN SYMMETRIC THEORY OF GRAVITY. *Phys. Lett. B*, 147:39–43, 1984. [10](#)
- [35] T. Futamase and Kei-ichi Maeda. Chaotic Inflationary Scenario in Models Having Nonminimal Coupling With Curvature. *Phys. Rev. D*, 39:399–404, 1989.
- [36] D. S. Salopek, J. R. Bond, and James M. Bardeen. Designing Density Fluctuation Spectra in Inflation. *Phys. Rev. D*, 40:1753, 1989.
- [37] R. Fakir and W. G. Unruh. Improvement on cosmological chaotic inflation through nonminimal coupling. *Phys. Rev. D*, 41:1783–1791, 1990. [10](#)
- [38] Y. Akrami et al. Planck 2018 results. X. Constraints on inflation. *Astron. Astrophys.*, 641:A10, 2020. [10](#), [18](#), [23](#), [42](#), [59](#), [60](#), [62](#)
- [39] Kazunori Nakayama and Masahiro Takimoto. Higgs inflation and suppression of axion isocurvature perturbation. *Phys. Lett. B*, 748:108–112, 2015. [13](#), [54](#), [59](#)
- [40] Gian F. Giudice and Hyun Min Lee. Unitarizing Higgs Inflation. *Phys. Lett. B*, 694:294–300, 2011. [13](#), [63](#)
- [41] J. L. F. Barbon, J. A. Casas, J. Elias-Miro, and J. R. Espinosa. Higgs Inflation as a Mirage. *JHEP*, 09:027, 2015. [13](#), [63](#)
- [42] N. Aghanim et al. Planck 2018 results. VI. Cosmological parameters. *Astron. Astrophys.*, 641:A6, 2020. [Erratum: *Astron. Astrophys.* 652, C4 (2021)]. [18](#), [20](#), [21](#), [22](#), [23](#), [26](#), [42](#), [59](#), [60](#), [62](#)
- [43] P. A. R. Ade et al. Improved Constraints on Primordial Gravitational Waves using Planck, WMAP, and BICEP/Keck Observations through the 2018 Observing Season. *Phys. Rev. Lett.*, 127(15):151301, 2021. [18](#), [20](#), [21](#), [22](#), [23](#), [42](#), [60](#), [62](#)
- [44] Marc Kamionkowski and Ely D. Kovetz. The Quest for B Modes from Inflationary Gravitational Waves. *Ann. Rev. Astron. Astrophys.*, 54:227–269, 2016. [19](#)
- [45] Andrew R Liddle and Samuel M Leach. How long before the end of inflation were observable perturbations produced? *Phys. Rev. D*, 68:103503, 2003. [19](#), [21](#)
- [46] Andreas Ringwald and Carlos Tamarit. Revealing the Cosmic History with Gravitational Waves. *arXiv e-prints*, page arXiv:2203.00621, March 2022. [20](#)
- [47] Daniel G. Figueroa and Francisco Torrenti. Gravitational wave production from preheating: parameter dependence. *JCAP*, 10:057, 2017. [20](#)
- [48] Andreas Ringwald, Ken’ichi Saikawa, and Carlos Tamarit. Primordial gravitational waves in a minimal model of particle physics and cosmology. *JCAP*, 02:046, 2021. [20](#), [21](#)
- [49] P.A. Zyla et al. Review of Particle Physics. *PTEP*, 2020(8):083C01, 2020. [21](#), [28](#), [29](#), [32](#), [35](#), [36](#), [37](#), [38](#)
- [50] Andrew R. Liddle and David H. Lyth. The Cold dark matter density perturbation. *Phys. Rept.*, 231:1–105, 1993. [21](#)

- [51] Jackson D. Clarke, Robert Foot, and Raymond R. Volkas. Natural leptogenesis and neutrino masses with two Higgs doublets. *Phys. Rev. D*, 92(3):033006, 2015. [25](#)
- [52] Wilfried Buchmuller and Michael Plumacher. Matter antimatter asymmetry and neutrino properties. *Phys. Rept.*, 320:329–339, 1999. [25](#)
- [53] W. Buchmuller, P. Di Bari, and M. Plumacher. Leptogenesis for pedestrians. *Annals Phys.*, 315:305–351, 2005.
- [54] Laura Covi, Esteban Roulet, and Francesco Vissani. CP violating decays in leptogenesis scenarios. *Phys. Lett. B*, 384:169–174, 1996.
- [55] Sacha Davidson and Alejandro Ibarra. A Lower bound on the right-handed neutrino mass from leptogenesis. *Phys. Lett. B*, 535:25–32, 2002. [25](#), [26](#)
- [56] J. A. Casas and A. Ibarra. Oscillating neutrinos and $\mu \rightarrow e, \gamma$. *Nucl. Phys. B*, 618:171–204, 2001. [26](#)
- [57] P. F. de Salas, D. V. Forero, S. Gariazzo, P. Martínez-Miravé, O. Mena, C. A. Ternes, M. Tórtola, and J. W. F. Valle. 2020 global reassessment of the neutrino oscillation picture. *JHEP*, 02:071, 2021. [26](#)
- [58] Nabarun Chakrabarty, Ujjal Kumar Dey, and Biswarup Mukhopadhyaya. High-scale validity of a two-Higgs doublet scenario: a study including LHC data. *JHEP*, 12:166, 2014. [28](#)
- [59] Joel Oredsson and Johan Rathsman. \mathbb{Z}_2 breaking effects in 2-loop RG evolution of 2HDM. *JHEP*, 02:152, 2019. [28](#), [39](#)
- [60] Satsuki Oda, Yutaro Shoji, and Dai-Suke Takahashi. High Scale Validity of the DFSZ Axion Model with Precision. *JHEP*, 03:011, 2020. [28](#), [37](#)
- [61] Erick J. Weinberg. *Radiative corrections as the origin of spontaneous symmetry breaking*. PhD thesis, Harvard U., 1973. [33](#), [65](#)
- [62] Florian Staub. SARAH 4 : A tool for (not only SUSY) model builders. *Comput. Phys. Commun.*, 185:1773–1790, 2014. [37](#)
- [63] Werner Porod. SPheno, a program for calculating supersymmetric spectra, SUSY particle decays and SUSY particle production at $e^+ e^-$ colliders. *Comput. Phys. Commun.*, 153:275–315, 2003. [37](#)
- [64] Philip Bechtle, Sven Heinemeyer, Oscar Stål, Tim Stefaniak, and Georg Weiglein. *HiggsSignals*: Confronting arbitrary Higgs sectors with measurements at the Tevatron and the LHC. *Eur. Phys. J. C*, 74(2):2711, 2014. [37](#), [39](#)
- [65] Philip Bechtle, Daniel Dercks, Sven Heinemeyer, Tobias Klingl, Tim Stefaniak, Georg Weiglein, and Jonas Wittbrodt. HiggsBounds-5: Testing Higgs Sectors in the LHC 13 TeV Era. *Eur. Phys. J. C*, 80(12):1211, 2020. [37](#), [39](#)
- [66] J. P. Lees et al. Precision Measurement of the $B \rightarrow X_s \gamma$ Photon Energy Spectrum, Branching Fraction, and Direct CP Asymmetry $A_{CP}(B \rightarrow X_{s+d} \gamma)$. *Phys. Rev. Lett.*, 109:191801, 2012. [38](#)

- [67] M. Misiak, Abdur Rehman, and Matthias Steinhauser. Towards $\overline{B} \rightarrow X_s \gamma$ at the NNLO in QCD without interpolation in m_c . *JHEP*, 06:175, 2020. [38](#)
- [68] H. Bahl, P. Bechtle, S. Heinemeyer, S. Liebler, T. Stefaniak, and G. Weiglein. HL-LHC and ILC sensitivities in the hunt for heavy Higgs bosons. *Eur. Phys. J. C*, 80(10):916, 2020. [39](#)
- [69] Daniele Lombardi. The DFSZ axion: analysis and generalization. Laurea thesis, U. Bologna, DIFA, 2018. [46](#), [47](#)
- [70] Georg G. Raffelt. Astrophysical axion bounds. *Lect. Notes Phys.*, 741:51–71, 2008. [49](#)
- [71] Pierluca Carenza, Tobias Fischer, Maurizio Giannotti, Gang Guo, Gabriel Martínez-Pinedo, and Alessandro Mirizzi. Improved axion emissivity from a supernova via nucleon-nucleon bremsstrahlung. *JCAP*, 10(10):016, 2019. [Erratum: *JCAP* 05, E01 (2020)]. [49](#)
- [72] Pierluca Carenza, Bryce Fore, Maurizio Giannotti, Alessandro Mirizzi, and Sanjay Reddy. Enhanced Supernova Axion Emission and its Implications. *Phys. Rev. Lett.*, 126(7):071102, 2021. [49](#)
- [73] Richard Lynn Davis. Cosmic Axions from Cosmic Strings. *Phys. Lett. B*, 180:225–230, 1986. [49](#)
- [74] David H. Lyth. Estimates of the cosmological axion density. *Phys. Lett. B*, 275:279–283, 1992. [49](#)
- [75] Ya. B. Zeldovich, I. Yu. Kobzarev, and L. B. Okun. Cosmological Consequences of the Spontaneous Breakdown of Discrete Symmetry. *Zh. Eksp. Teor. Fiz.*, 67:3–11, 1974. [49](#)
- [76] P. Sikivie. Of Axions, Domain Walls and the Early Universe. *Phys. Rev. Lett.*, 48:1156–1159, 1982. [49](#)
- [77] Richard Holman, Stephen D. H. Hsu, Thomas W. Kephart, Edward W. Kolb, Richard Watkins, and Lawrence M. Widrow. Solutions to the strong CP problem in a world with gravity. *Phys. Lett. B*, 282:132–136, 1992. [49](#)
- [78] Marc Kamionkowski and John March-Russell. Planck scale physics and the Peccei-Quinn mechanism. *Phys. Lett. B*, 282:137–141, 1992.
- [79] Stephen M. Barr and D. Seckel. Planck scale corrections to axion models. *Phys. Rev. D*, 46:539–549, 1992.
- [80] S. Ghigna, Maurizio Lusignoli, and M. Roncadelli. Instability of the invisible axion. *Phys. Lett. B*, 283:278–281, 1992. [49](#)
- [81] Howard M. Georgi, Lawrence J. Hall, and Mark B. Wise. Grand Unified Models With an Automatic Peccei-Quinn Symmetry. *Nucl. Phys. B*, 192:409–416, 1981. [49](#)
- [82] Alex G. Dias, V. Pleitez, and M. D. Tonasse. Naturally light invisible axion and local $Z(13) \times Z(3)$ symmetries. *Phys. Rev. D*, 69:015007, 2004. [49](#)

- [83] Alex G. Dias, V. Pleitez, and M. D. Tonasse. Naturally light invisible axion in models with large local discrete symmetries. *Phys. Rev. D*, 67:095008, 2003.
- [84] Alex G. Dias and V. Pleitez. Stabilizing the invisible axion in 3-3-1 models. *Phys. Rev. D*, 69:077702, 2004.
- [85] Linda M. Carpenter, Michael Dine, and Guido Festuccia. Dynamics of the Peccei Quinn Scale. *Phys. Rev. D*, 80:125017, 2009.
- [86] Keisuke Harigaya, Masahiro Ibe, Kai Schmitz, and Tsutomu T. Yanagida. Peccei-Quinn symmetry from a gauged discrete R symmetry. *Phys. Rev. D*, 88(7):075022, 2013.
- [87] A. G. Dias, A. C. B. Machado, C. C. Nishi, A. Ringwald, and P. Vaudrevange. The Quest for an Intermediate-Scale Accidental Axion and Further ALPs. *JHEP*, 06:037, 2014.
- [88] Andreas Ringwald and Ken’ichi Saikawa. Axion dark matter in the post-inflationary Peccei-Quinn symmetry breaking scenario. *Phys. Rev. D*, 93(8):085031, 2016. [Addendum: *Phys.Rev.D* 94, 049908 (2016)]. [49](#)
- [89] E. Armengaud et al. Physics potential of the International Axion Observatory (IAXO). *JCAP*, 06:047, 2019. [49](#)
- [90] Konstantin A. Beyer and Subir Sarkar. Ruling out light axions: the writing is on the wall. *SciPost Phys.*, 15:003, 2023. [49](#)
- [91] Kristjan Kannike. Vacuum Stability Conditions From Copositivity Criteria. *Eur. Phys. J. C*, 72:2093, 2012. [50](#), [51](#)
- [92] Kristjan Kannike. Vacuum Stability of a General Scalar Potential of a Few Fields. *Eur. Phys. J. C*, 76(6):324, 2016. [Erratum: *Eur.Phys.J.C* 78, 355 (2018)]. [50](#), [51](#)
- [93] Margarete Muhlleitner, Marco O. P. Sampaio, Rui Santos, and Jonas Wittbrodt. The N2HDM under Theoretical and Experimental Scrutiny. *JHEP*, 03:094, 2017. [51](#)
- [94] J. Horejsi and M. Kladiva. Tree-unitarity bounds for THDM Higgs masses revisited. *Eur. Phys. J. C*, 46:81–91, 2006. [51](#)
- [95] Margarete Mühlleitner, Marco O. P. Sampaio, Rui Santos, and Jonas Wittbrodt. ScannerS: Parameter Scans in Extended Scalar Sectors. 7 2020. [51](#), [52](#)
- [96] Shinya Kanemura, Takahiro Kubota, and Eiichi Takasugi. Lee-Quigg-Thacker bounds for Higgs boson masses in a two doublet model. *Phys. Lett. B*, 313:155–160, 1993. [52](#)
- [97] Jinn-Ouk Gong, Hyun Min Lee, and Sin Kyu Kang. Inflation and dark matter in two Higgs doublet models. *JHEP*, 04:128, 2012. [54](#), [55](#), [56](#), [59](#)
- [98] Sandhya Choubey and Abhass Kumar. Inflation and Dark Matter in the Inert Doublet Model. *JHEP*, 11:080, 2017.

- [99] Tanmoy Modak and Kin-ya Oda. Echoes of 2HDM inflation at the collider experiments. *Eur. Phys. J. C*, 80(9):863, 2020. [Erratum: *Eur.Phys.J.C* 81, 518 (2021)]. [54](#), [59](#)
- [100] Alexei A. Starobinsky. A New Type of Isotropic Cosmological Models Without Singularity. *Phys. Lett. B*, 91:99–102, 1980. [62](#)
- [101] Viatcheslav F. Mukhanov and G. V. Chibisov. Quantum Fluctuations and a Non-singular Universe. *JETP Lett.*, 33:532–535, 1981.
- [102] Alexei A. Starobinsky. Dynamics of Phase Transition in the New Inflationary Universe Scenario and Generation of Perturbations. *Phys. Lett. B*, 117:175–178, 1982.
- [103] Dmitry Gorbunov and Anna Tokareva. R^2 -inflation with conformal SM Higgs field. *JCAP*, 12:021, 2013. [62](#)
- [104] J. L. F. Barbon and J. R. Espinosa. On the Naturalness of Higgs Inflation. *Phys. Rev. D*, 79:081302, 2009. [62](#)
- [105] C. P. Burgess, Hyun Min Lee, and Michael Trott. Comment on Higgs Inflation and Naturalness. *JHEP*, 07:007, 2010. [62](#)
- [106] Georgios K. Karananas, Mikhail Shaposhnikov, and Sebastian Zell. Field redefinitions, perturbative unitarity and Higgs inflation. *Journal of High Energy Physics*, 2022(6):132, June 2022. [62](#), [63](#)